

People's Democratic Republic of Algeria

Ministry of Higher Education and Scientific Research

Ecole Nationale Polytechnique



Algerian Qatari Steel



Department of Materials Engineering

End-of-Studies Project Report

For the attainment of the State Engineer's Diploma in Materials Engineering

**EFFECT OF ALUMINUM CONTENT ON THE
MICROSTRUCTURAL AND MECHANICAL PROPERTIES OF A
LOW ALLOYED STEEL**

Realized by

KHELIFA Menad Dhaiaeddine

KECHOUT Anes

Presented and publicly supported on: **June 29th, 2024**

In front of the jury composed of:

President	Mohammed CHITROUB	Professor	ENP
Examinator	Hamid SEDJAL	Lecturer	ENP
Promotor	Choayb BOUHAFS	Lecturer	ENP

ENP 2024

People's Democratic Republic of Algeria

Ministry of Higher Education and Scientific Research

Ecole Nationale Polytechnique



Algerian Qatari Steel



Department of Materials Engineering

End-of-Studies Project Report

For the attainment of the State Engineer's Diploma in Materials Engineering

**EFFECT OF ALUMINUM CONTENT ON THE
MICROSTRUCTURAL AND MECHANICAL PROPERTIES OF A
LOW ALLOYED STEEL**

Realized by

KHELIFA Menad Dhaiaeddine

KECHOUT Anes

Presented and publicly supported on: **June 29th, 2024**

In front of the jury composed of:

President	Mohammed CHITROUB	Professor	ENP
Examinator	Hamid SEDJAL	Lecturer	ENP
Promotor	Choayb BOUHAFS	Lecturer	ENP

ENP 2024

République Algérienne Démocratique et Populaire

Ministère de l'Enseignement Supérieur et de la Recherche Scientifique

Ecole Nationale Polytechnique



Algerian Qatari Steel



Département de Génie des Matériaux

Rapport du Projet de Fin d'Etudes

Pour l'obtention du diplôme d'ingénieur d'état en Génie des Matériaux

Effets du Contenu d'Aluminium sur les Propriétés Microstructurales et Mécaniques d'un Acier Faiblement Allié

Réalisé par

KHELIFA Menad Dhaiaeddine

KECHOUT Anes

Présenté et soutenu publiquement le: **29 juin 2024**

Devant le jury composé de :

Président	Mohammed CHITROUB	Professeur	ENP
Examineur	Hamid SEDJAL	Maître de conférence	ENP
Promoteur	Choayb BOUHAFS	Maître de conférence	ENP

ENP 2024



ACKNOWLEDGMENTS



باسم الله الرحمن الرحيم

First, for the beginning, we thank God Almighty for providing us with the strength and success necessary for the completion of the research and the work on this project, praying for more luck and help in our future projects.

Besides, according to the Prophet's (Peace Be Upon Him) words: "He who is not grateful to people, is not grateful to Allah"; we express thankfulness and gratitude to all those who helped us with the completion of this document, we mention:

- *Our parents and the members of our families for all their hard work with only one goal to achieve: our success in our personal lives. I, Khelifa, focus on this point by mentioning, besides my great parents, my grand-mother BOUNEGAB Hadjila, and my aunt KESSIRA Fatima for sacrificing a big part of their lives raising me and educating me to be what I am today; special THANKS FOR BOTH OF YOU;*
 - *My other aunt Kessira Nadjia for her hard effort during the preparation of the presentation*
 - *We also thank all those who spent their time to give us knowledge and to show us good manners, those are our humble teachers starting from elementary school up until our professors at National Polytechnics School. We mention on this point our promotor Choay BOUHAFS as well as the other teachers who shared their experience with us during the work period we spent at the materials engineering lab; ABADLI Kamel and KASSER Abdelmadjid; as well as all the members of the jury.*
 - *Special thanks to the materials engineering lab staff: the engineer Samia, and mister Abdenour for their useful help and patience.*
 - *All those who helped us during our internship in AQS; the staff of the complex: RAIS Achrafeddine, and MEDJERAB Aziz. As well as all the staff of the administration of the university residence Boubidi Mohamed Chrif Ibn El Mekki for their support.*
 - *Our friends who shared their strengths to help us to finish our work, we mention specially: OUCHENE Souhil for providing us with the numerical Python codes we attached to the indexes for the alternative way of numerical calculations; and OUCHENE Mohammed Erachid for his help in the realization of the presentation of this document.*
-



DEDICATIONS



I dedicate all my efforts in the realization of this project to everyone who helped me, whether physically or morally, and to all those who prayed to God Almighty for my success.

- ❖ *To my precious beloved grandmother Hadjila*
- ❖ *To my aunt Fatima*
- ❖ *To my hardworking parents Nouredine and Souad;*
- ❖ *To my greatest supporters, my cherished siblings Kossai, Ghofrane, and Ouaisse.*

I also dedicate this work to the pure souls of

- ❖ *My great uncle Kessira Lakhdar*
- ❖ *My two grandfathers, Kessira Menad and Khelifa Rabah Mbarek as well as my grandmother Khelifa Zhor;*

For all their profound impact on my heart; May God's mercy be upon them all.

Your faithful son;

-KHELIFA Menad Dhaiaeddine-



FOREWORD



Steel is one of the most common and significant materials due to its crucial importance for global industry. In Algeria, steel is primarily produced for construction purposes, with production handled by three large multinational factories: the El Hadjar group, the TOSYALI group, and the AQS group. Additionally, many smaller companies focus on transforming the semi-finished products from these three major factories into finished products for commercialization and use.

This document compiles all the information gathered from our four-month internship at the Algerian Qatari Steel Group, combined with bibliographic research and experimental testing. It is part of our end-of-studies project, which investigates the effects of aluminum traces on the microstructural and mechanical properties of low-carbon steel used for wire rod fabrication.

The experimental parts of this report were primarily conducted at the Algerian Qatari Steel Complex and the National Polytechnic School. This report presents all the obtained results, along with data analysis and interpretations supported by bibliographic research.

In conclusion, we hope that this document serves not just as a report, but as a reference for future students who wish to further this research, as well as for those who are eager to enter the industrial field and explore the vast world of metallurgy and the steel industry.

ABSTRACTS

الملخص:

تلعب العناصر المضافة للحديد خلال صناعته التحويلية إلى فولاذ صلب دورا هاما في التأثير على خصائصه الميكانيكية والبنية حتى ولو أضيفت بنسب ضئيلة جدا قد تصل إلى حد وصفها بالآثار. يهدف هذا المشروع إلى دراسة تأثيرات إضافة الألومنيوم بمقادير ضئيلة. تمت صناعة العينات المدروسة عبر مختلف وحدات الإنتاج المتواجدة على مستوى المؤسسة الجزائرية – القطرية للصلب، انطلاقا من صب كرات المادة الأولية في فرن القوس الكهربائي إلى غاية انتاج لفائف الفولاذ مرورا بوحدة الصب المستمر ووحدة الدرفلة.

استعملنا خلال إنجازنا لهذا المشروع ثلاث أنماط من الفولاذ تحمل كل منها كميات متباينة من الألومنيوم. العينات المدروسة أخذت بالتحديد من ألواح الفولاذ الناتجة عن وحدة الصب المستمر (والتي دُرِسَتْ فيما بعد في حالتها الابتدائية ثم بعد تعريضها لمعالجات حرارية تحت ظروف تجريبية مختلفة) كما أخذنا بعض العينات من لفائف الفولاذ المدرفلة. عرَّضنا العينات الابتدائية إلى تجربة الكشف الكيميائي للحصول على تركيبة الفولاذ، ثم استخدمنا المجهر الضوئي لتحديد بنية كل عينة تحت كل من الشروط التجريبية المطبقة، وعرضناهم أخيرا لتجربتي قياس الصلابة واختبار الشد. أثبتت النتائج التجريبية أن تأثيرات الألمنيوم تتمحور في الحقيقة في تشكيل تكتلات غير معدنية من مادتي الألومين ونتريدات الألمنيوم التي ترسب على حدود الحبوب البنيوية للفولاذ، أين تؤدي إلى تضيقها مما يساهم بشكل مباشر في تغيير خصائص العينات الميكانيكية. لاحظنا أن هذا التأثير زال كلية عند المعالجة الحرارية عند الدرجة 1100°م لمدة 6 ساعات متواصلة.

الكلمات المفتاحية: العناصر المضافة، آثار، ألمنيوم، الصناعة التحويلية، الكشف الكيميائي، المجهر الضوئي، الصلابة، اختبار الشد، المعالجة الحرارية، تكتلات غير معدنية، الحبوب البنيوية

Résumé:

Les éléments d'addition souvent ajoutés à l'acier pendant le processus d'élaboration jouent un rôle crucial sur la modification de ses propriétés microstructurales même si leurs présences sont limitées au niveau de traces. Dans ce projet, on s'intéresse à la détermination de l'effet des traces d'aluminium. Les échantillons étudiés ont été fabriqués par le processus industriel de l'entreprise AQS.

Le travail suit donc trois aciers différents avec une teneur variante en aluminium. Les échantillons ont été pris à partir des billettes produites au CCM, et à partir du fil machine laminé. Le premier type a été soumis à la caractérisation chimique par XRF, puis, différents recuits ont été appliqués sous différentes conditions. Ces échantillons, ainsi que ceux obtenus du fil machines sont soumis à la microscopie optique et au test de dureté. L'essai de traction n'est appliqué que sur les échantillons laminés. Les résultats montrent que l'aluminium forme des inclusions non-métalliques qui se précipitent sur les joints de grains conduisant ainsi au rétrécissement de leur taille. La microstructure est nettoyée de toute hétérogénéité quand elle subit le recuit de 1100°C pendant 6h. Les essais mécaniques montrent également que la variation de la taille de grain sous l'effet de l'aluminium influe légèrement les propriétés mécaniques de l'acier.

Mots clés : Élément d'addition ; traces ; aluminium ; processus d'élaboration ; caractérisation chimique ; microscopie optique ; dureté ; essai de traction ; recuit ; inclusions non-métalliques ; taille de grains.

Abstract:

The alloying elements that are added to steel during the steelmaking process have a crucial impact on its microstructural properties even when their presence is limited to only a few traces. In this project, the effects of aluminum traces were investigated. The studied samples have been elaborated in the AQS complex in the Steel Melt Shop and Rolling Machines units. The CDRI pellets were put into the electric arc furnace to be melted, additions were added in the ladle refining furnace and the billet was formed in the continuous casting machines.

Three heats of steel with different aluminum contents were submitted for testing. The study was carried out on samples taken from the steel billet and the wire rod. The steel billet samples were submitted to chemical characterization by XRF, and then received annealing treatments at different heating temperatures and holding times. Optical microscopy for microstructural analysis and hardness test were applied on each of them, while the wire rod samples received the OM, hardness, and tensile testing. Results showed that aluminum forms non-metallic inclusions in the form of alumina that precipitate on grain boundaries, which will cause a decrease in the grain size; however, the microstructure was completely cleaned at 1100°C, 6h annealing. Mechanical testing showed that this variation of the grain size could affect directly the mechanical properties of the samples.

Key words: Alloying elements; traces; aluminum; steelmaking process; SMS; CDRI; LRF; CCM; chemical characterization; optical microscopy; hardness; tensile test; annealing; NMI; grain size

TABLE OF CONTENTS

List of Tables

List of Figures

General Introduction	15
Chapter I	18
I.1 Initiation to the metallic materials.....	19
I.2 Fundamentals about steel.....	19
I.2.1 Iron – Carbon alloys.....	20
I.2.2 Alloying elements in steel.....	24
I.3 Solidification and nucleation.....	26
I.3.1 Nucleation.....	27
I.3.2 Growth.....	31
I.4 Heat treatments.....	34
I.4.1 Definition of heat treatments.....	34
I.4.2 Parameters affecting the heat treatments.....	35
I.4.3 Types of heat treatments.....	36
I.5 Rolling.....	38
I.5.1 Deformation coefficients.....	39
I.5.2 Effects of rolling on the steel structure.....	40
I.6 Conclusion.....	41
Chapter II	43
II.1 Effects on steelmaking process: Deoxidation agent.....	44
II.2 Effects on the machinery: Nozzle clogging at CCM.....	47
II.2.1 Definition of nozzle clogging.....	47
II.2.2 Mechanism of the formation of nozzle clogging.....	48
II.2.3 Solution to nozzle clogging.....	49
II.3 Effects on steel composition: Formation of inclusions.....	51

II.3.1	Types of inclusions related to aluminum	51
II.3.2	Mechanism of the formation of the alumina inclusions	52
II.3.3	Effects of inclusions	53
II.4	Effects on steel structure: Grain size control.....	54
II.4.1	Formation of grain boundaries.....	54
II.4.2	Precipitation of AlN inclusions	55
II.4.3	Consequences on grain size	56
II.5	Effects on steel mechanical properties	57
II.6	Bibliographic synthesis.....	58
Chapter III	60
III.1	Quality control of raw material	61
III.1.1	Physio-mechanical controls	61
III.1.2	Chemical controls: oxides determination.....	65
III.2	Elaboration process.....	66
III.2.1	Electric arc furnace (EAF)	66
III.2.2	Ladle refining furnace (LRF).....	69
III.2.3	Continuous casting machine (CCM).....	70
Chapter IV	74
IV.1	Test samples' manufacturing	75
IV.1.1	Specimens cutting and milling.....	75
IV.1.2	Heat treatments	76
IV.1.3	Grinding and polishing	77
IV.1.4	Chemical etching.....	79
IV.2	Characterization tests.....	82
IV.2.1	Chemical characterization.....	82
IV.2.2	Structural characterization	88
IV.2.3	Mechanical characterization.....	95
Chapter V	98
V.1	Chemical composition of the test specimens	99
V.2	Structural analysis.....	102
V.2.1	Observation before etching.....	103

V.2.2	Structure revelation.....	104
V.2.3	Heat treatment effect on steel microstructure	106
V.2.4	Effect of hot rolling on the microstructure.....	115
V.3	Mechanical properties	117
V.3.1	Harness test	117
V.3.2	Tensile test	120
General Conclusion.....		125
Indexes		127
Index A.....		128
Index B.....		141
Index C.....		150

LIST OF TABLES

TABLE I-1: Effects of common alloying elements on steel properties [1:4]	26
TABLE I-2: Kinetic models for diffusion-activated growth [1:7].....	32
TABLE I-3: Key parameters affecting each of the heat treatment stages	35
TABLE II-1*: Behavior of inclusions before and after rolling	53
TABLE III-1: Granulometry test results.....	64
TABLE III-2: Comparison between the blast furnace and the electric arc furnace [3:2,3]	67
TABLE IV-1: Heat treatments' conditions.....	76
TABLE IV-2: Common plain steel etchants and their functions [4:3,4].....	81
TABLE IV-3: Magnifications available on the laboratory microscope.....	90
TABLE IV-4: Methodology of micrographs analysis.....	90
TABLE IV-5: Grain size equivalence by the ASTM E112 norm [4:8].....	92
TABLE IV-6*: Most common indenters shape	96
TABLE V-1: Oxides determination on the raw material	99
TABLE V-2: Chemical composition of the studied steel samples.....	100
TABLE V-3: Theoretical calculation of the Al-contribution on recrystallization temperature.....	100
TABLE V-4: Grains sizes and areas calculations	102
TABLE V-5: Theoretical calculation of pearlite amount in steel.....	105
TABLE V-6: Synthesis of heat treatment effects on the microstructure	114
TABLE V-7: Numerical results for the hardness test.....	118

LIST OF FIGURES

FIGURE I-1* : Pictures showing some properties of pure iron.....	20
FIGURE I-2* : Pictures of some Carbon allotropes	21
FIGURE I-3* : Possible positions for alloying elements in solid solutions.....	22
FIGURE I-4* : Fe-Cementite phase diagram.....	23
FIGURE I-5* : Classification of steel.....	24
FIGURE I-6* : Qualitative variations of free Gibbs energy vs temperature.....	27
FIGURE I-7* : Qualitative representation of the free Gibbs energy variations vs nuclei radius.....	29
FIGURE I-8 : Comparison between the ideal nuclei formed by homogenous and heterogenous nucleation [1:5].....	30
FIGURE I-9* : Graphic comparison between energy barriers of homogenous and heterogenous modes of nucleation	31
FIGURE I-10* : Johnson-Mehl-Avrami curves in the original version of the formula (A), and the linear transformed version (B)	34
FIGURE I-11 : Heat treatment cycles of annealing (A) and quenching & tempering (B)	35
FIGURE I-12 : Schematic representation of the structural effects of different annealing processes.....	37
FIGURE I-13 : <i>Structures obtained after cooling at different environments</i> [1:9]	37
FIGURE I-14* : Cracks on a steel blade quenched but not tempered.....	38
FIGURE I-15 : <i>Dimensional change within rolling</i> [1:10].....	39
FIGURE I-16 : Continuous rolling through multiple cylinders [1:10]	40
FIGURE I-17* : Steel structure at hot and cold rolling conditions.....	41
FIGURE II-1 : Solubility of oxygen in molten iron [2:1]	45
FIGURE II-2 : Comparison between steel samples [2:1].....	45
FIGURE II-3 : Metallic oxides equilibrium in molten iron at 1600°C [2:1]	46
FIGURE II-4 : Schematic representation of a nozzle clogging within a CCM, vs an actual photograph of a severe clogging [2:3].....	47
FIGURE II-5 : Alumina dendrites [2:3]	48
FIGURE II-6 : Mechanism of nozzle clogging [2:5].....	49
FIGURE II-7 : Working principle of the calcium treatment	50
FIGURE II-8 : Calcia-Alumina (CaO-Al ₂ O ₃) phase diagram [2:6].....	50
FIGURE II-9 : Forms of aluminum inclusions found in steel [2:7]	51

FIGURE II-10: Mechanism of formation of inclusions [2:10]	52
FIGURE II-11: Micrography of cracks on rolled steel at different concentrations of inclusions [2:11]	54
FIGURE II-12*: Micrography of austenitic phase in steel where grain boundaries are clear	55
FIGURE II-13: Crystallin structure of AlN inclusions [2:12]	56
FIGURE II-14*: Aluminum nitrides at the grain boundaries are blocking its size growth	57
FIGURE III-1: Pellets at different stages of the DRI process	61
FIGURE III-2: Sampling of the CDRI	62
FIGURE III-3: Mechanical granulometry test (*for c)	63
FIGURE III-4: Pellets size distribution in function of their diameters	64
FIGURE III-5: Steel melt shop main steps [3:4]	66
FIGURE III-6*: Furnace unloading	69
FIGURE III-7: Different parts of continuous casting	71
FIGURE IV-1: Cutting and milling of test samples	76
FIGURE IV-2: Heat treatment curves for tests	77
FIGURE IV-3: Grinding (A) and polishing (B) machines	79
FIGURE IV-4: Revelation of grain phases etching mechanism	80
Figure IV-5*: Revelation of grain boundaries etching mechanism	80
FIGURE IV-6: Preparation of Nital etchant	81
FIGURE IV-7*: Atom excitation and deexcitation alongside with Siegbahn notation for specters	83
FIGURE IV-8*: Comparison between EDXRF and WDXRF work principle	84
FIGURE IV-9*: NDIR working principle	85
FIGURE IV-10*: TCD working principle	86
FIGURE IV-11: XRF test sample	87
FIGURE IV-12: Sample preparation for ELTRA ON 900 tests	88
FIGURE IV-13: Optical microscope components	89
FIGURE IV-14: Example of application of manual grain size determination	91
FIGURE IV-15: ImageJ software manipulation	93
Figure IV-16: Measurements taken on typical equiaxial structure (sketch)	93
FIGURE IV-17*: Stress-strain tensile test curve interpretation	95
FIGURE IV-18: Brinell indentation hardness test	97
FIGURE V-1: Microscopic observation before chemical etching, sample taken from billet (X100)	103
FIGURE V-2: Phase evolution during cooling of hypoeutectoid steel [5:4]	104
FIGURE V-3: Microstructure of billet sample before heat treating or rolling (X400)	105
Figure V-4: Mechanical analogy for heat treatment effect on the structure [5:5]	106

FIGURE V-5: Evolution of grain dimension depending on heating temperature (the curve)	107
FIGURE V-6: Evolution of grain dimension depending on heating temperature (micrography X100)	108
FIGURE V-7*: Sketch for grain size evolution during the heat treatments.....	110
FIGURE V-8: Evolution of heterogeneities density in function of heat treatment.....	110
FIGURE V-9: Comparison between inclusions density and distribution using SEM (X1000; 25kV)	111
FIGURE V-10: SEM/EDX focus on the composition of inclusions	112
FIGURE V-11: Evolution of grain dimension depending on holding time (micrography X100).....	113
FIGURE V-12: Evolution of grain dimension depending on holding time (the curve)	114
FIGURE V-13*: Forces applied during rolling of materials.....	115
FIGURE V-14: Microstructure of wire rod after the final pass of the process	116
FIGURE V-15: Graphic representation of hardness variations	118
FIGURE V-16: Most common types of 1 and 2D crystal imperfections [5:6].....	121
FIGURE V-17: Load-extension curves for the three specimens.....	123
FIGURE V-18: Measured variations of the critical values of the tensile strength in function of Al content	123

GENERAL INTRODUCTION

Aluminum is one of the common alloying elements added to steel due to its beneficial effects on strengthening the structure and enhancing mechanical properties. However, despite these benefits, aluminum has a high affinity for oxygen. This often results in the formation of alumina in the ladle furnace, leading to clogging of the mold nozzles in the continuous casting machine.

Numerous solutions have been proposed in the literature to address this issue. The most effective solutions include equipping the machine with specialized cleaning equipment, while other suggestions involve melting Ca-Si wires inside the furnace to alter the alumina inclusions from dendritic to spherical forms. Given the high cost of the first solution compared to the benefits, the AQS complex decided to adopt the second solution during the factory's initial phase. They opted to produce samples with minimal aluminum content, at trace levels, to reduce the density of harmful inclusions and thus improve the quality of their steel.

Even when this step was taken into consideration, inclusions (globally) of alumina (specifically) continued to appear on the steel microstructure. Industrials think that these inclusions have no effects on the properties, nevertheless, and as we were preparing for our internship, we found an article that claimed the opposite. In his article published in November 1995, in the Physics Journal, the author, J.J. Dufrane asked and answered a key question, that we consider as the driving force to direct our study. The question was: **“Why do we need to measure trace elements in steel?”**, where he started by giving a global answer before diving into details, he said [0:1]:

““ With the increase in performance requested by users in the last twenty years, steelmakers have had to improve their melting operations dramatically. Numerous chemical elements are now controlled or eliminated at levels of 50 ppm and below. Control of these substances has led to improvements in: - Mechanical characteristics at room and elevated temperatures, as well as creep resistance. - Toughness and fracture mechanics at low temperatures. - Practical weldability - Hot and cold formability - Corrosion resistance in numerous media.

In this context, and to verify if any effects of the aluminum trace amounts could be observed on the microstructural and mechanical properties of the steel produced by AQS, we conduct the following study to provide an answer to this question.

The methodology we followed for the construction of this document led us to divide it into five chapters, the starting two chapters briefly summarize the bibliography and introduce the most useful concepts we need for the continuation, while the last three chapters relate all the practical work we have done, the results we got and the interpretations we deduced. Here is a quick presentation of each chapter independently:

Chapter I. Fundamentals

Common important information about most of the phenomena related to steel was briefly introduced in this chapter, as we defined steel as an Iron – Carbon alloy, studied the nucleation and growth during the solidification to explain the mechanisms of the creation of the microstructure, defined and explained the effects of the different heat treatments that we could apply in the steel industry, and then we finished finally by an introduction to rolling and its working principle.

Chapter II. Effects of Aluminum

A list of the effects of aluminum on the properties of aluminum is established in this chapter. All the discussed effects were taken from the bibliography and published research articles. We ended this chapter with a synthesis that played a double role of closing to the bibliographic research and an introduction to the practical part.

Chapter III. Steelmaking Process

The first step in the practical part was the elaboration of steel and the extraction of samples. The chapter describes the quality controls we apply to the CDRI and the elaboration process within the SMS unit. Working principles of each division of the SMS have been established.

Chapter IV. Methodology and Experimental Procedure

All the main practical work and tests applied to the samples are detailed in this chapter. We described the process of the samples' preparation, and explained all the working principles of the chemical, structural, and mechanical characterization tests, with a step-by-step demonstration of their manipulations. We also explained the methodology we followed for the interpretation of the obtained results.

Chapter V. Results, Interpretation and Analysis

All the practical work results taken of the tests run during Chapter IV were mentioned in this chapter. Each result was analyzed by giving the constatations we noticed under

the varying conditions. Then, an interpretation is held to justify those constatations and link them with the theory we established in chapters I and II to either verify it or deny it.

Finally, the report is tailed with three complementary indexes to give further information about:

- (A) The Algerian Qatari Steel complex, in the form of general information for those who would like to visit it for internships or projects.
- (B) Some demonstrations related to the Classic Nucleation Theory (CNT), more specifically the equations of heterogeneous nucleation and the Johnson-Mehl-Avram formula.
- (C) Numerical codes as an alternative method to measure the grain size and the quantification of inclusion density on the microstructure.

Reference:

[0:1] J. Dufrane. "Why do we Need to Measure Trace Elements in Steel?". Journal de Physique IV Proceedings, 1995.

Chapter I.

Fundamentals

“Research is what I’m doing when I don’t
know what I’m doing

*Wernher Von Bron; a German-American
physicist and rocket engineer whose team
launched the first US satellite into space*

Introduction to the chapter:

Before starting the work on our project, it is necessary to give a preview of the most important concepts related to the solidification and manufacturing of steel, which match our practical work.

The main points of the study that we are willing to cover through our project concern the observation and examination of the microstructures in different stages of the steelmaking process at their bulk state, heat-treated (annealed) state, and rolled state. These microstructures will then have effects on the mechanical properties of the product.

In this chapter, we aim to present a synthesis of the bibliography related to each of the previous states in the form of fundamental knowledge for the rest of the study.

I.1 Initiation to the metallic materials

Today, the engineer has at his disposal a very wide range of materials to meet various industrial needs, so much so that a collection of around 50,000 different materials can be used for very precise and delicately tailored applications [1:1]. This highlights the importance of knowing materials and their different classifications.

From this wide range, metals represent a very broad family of materials because of their multiple applications in different fields, thanks to their varied properties. Practically, we have two possible ways to exploit metallic materials:

- (1) **In their pure form:** Meaning a state without any type of additions (not to be confounded with their natural form, where they are found in the form of oxides). A metal in its pure form is characterized by its conduction of heat and electricity. However, most of them are known to be malleable with very weak mechanical properties, making their uses very limited to some specified applications.
- (2) **In the form of alloys:** To rectify the weakness of pure metals, it was practically found that mixing them with some additions can sometimes enhance their properties to very high levels, making them more efficient for much more varied applications in more fields.

However, it is very important to note that adding elements to a pure metal to transform it into an alloy with specified properties can't be done randomly. Metallurgists make very profound studies about materials selection to optimize all the combinations that can be possibly done and evaluate their usefulness. Sometimes, some specific elements need to be added at a very precise rate, because opposite and unwanted results can be obtained if the necessary quantity is missing or exceeded.

Steel is a fundamental example of metallic alloys where many metallic and non-metallic additions are used based on their application.

I.2 Fundamentals about steel

In daily life, we usually see people confound between steel and pure iron, even though the two elements have very different properties. In fact, in most of the cases, we deal with steel rather than iron. In metallurgy science, steel is defined as an iron-carbon alloy with many other additional elements (called also: alloying elements) that enhance its structural and mechanical properties.

I.2.1 Iron – Carbon alloys

a) Iron:

Most of the iron on our planet is locked away in Earth's hot, molten core. However, this element is widely found in rocks worldwide, and almost 2.5 billion tons of iron is purified every year. Mineral ores rich in iron include pyrite (FeS_2) and/or chalcopyrite (FeS). Other ores, including hematite (iron III oxides, Fe_2O_3), are used to extract pure iron in a process called smelting or direct reduction (deoxygenation). [1:2]

Unlike what people think in their common sense, iron has very weak mechanical and chemical properties, it is known to be:

- Soft and malleable: It can easily be shaped or molded, it can also be bent or flattened without breaking.
- Ductile: Makes a big elongation when subjected to tensile test compared to other brittle materials.
- Magnetic: Being a ferromagnetic element, it shows big reactions when put into magnetic fields.
- Chemically active element: It oxidizes rapidly in moist air and water, forming Fe_2O_3 leading to corrosion and degradation of mechanical pieces.

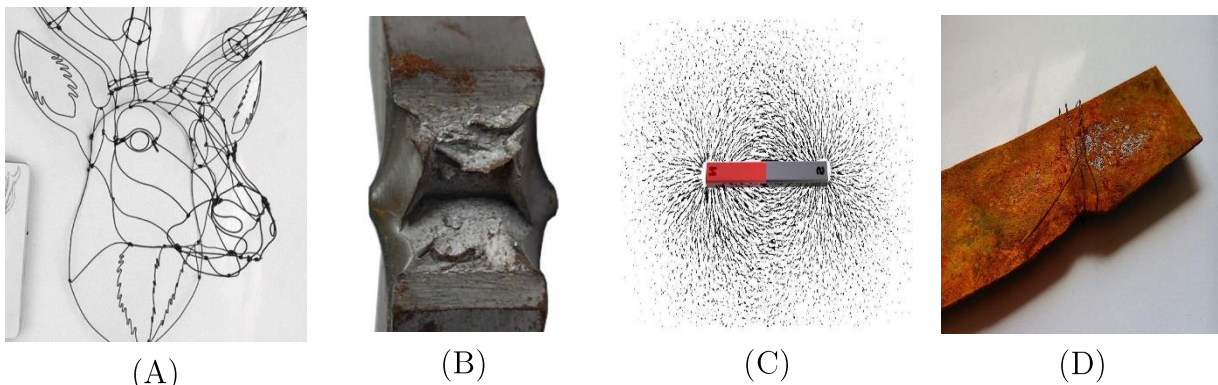
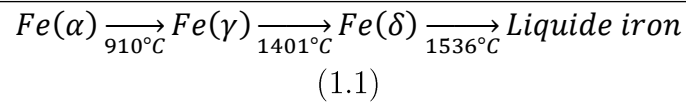


FIGURE I-1*: Pictures showing some properties of pure iron

A- Beautiful piece of art made of iron wire, thanks to its malleability, B- Iron bar under Charpy test showing its ductility, C- Visualizing the magnetic field of a magnet using iron filings, showing its magnetic properties, D- Rust formed on an iron bar due to corrosion

Additionally, iron has one other property that is very important. It's its allotropic phases. Meaning that it can change its crystalline structure according to the range of temperature it is submitted to. For pure iron case, we distinguish the following chain of reactions (assuming we are heating from ambient temperature into the liquidus temperature):



Where: Fe(α) and Fe(δ) have a centered cubic (CC) structure, while Fe(γ) has a face-centered cubic structure (FCC). The difference between the α and the δ structures lies in their lattice parameter.

b) Carbon:

Carbon is a chemical element with an atomic number of 6. It is a non-metallic element that is essential for life as we know it, forming the basis of organic chemistry and serving as a building block for all known life on Earth. Carbon compounds are abundant in nature and have diverse uses, ranging from fuels (such as coal and petroleum) to pharmaceuticals, plastics, and electronics. Carbon's ability to form stable covalent bonds with other elements and with itself allows for the vast array of compounds and materials that are vital to modern society.

Carbon can be found in nature in many different forms, each of them having properties that are different than the others. Few examples of the better-known types of this element:

- Graphite: A soft, black, crystalline form of carbon with a layered structure, known for its lubricating properties, electrical conductivity, and use in pencils and lubricants.
- Coal: A combustible black or brownish-black sedimentary rock, primarily composed of carbon and various other elements, formed from fossilized plant matter, and used as a fuel source for electricity generation and heat production.
- Graphene: A single layer of carbon atoms arranged in a two-dimensional honeycomb lattice, known for its exceptional strength, electrical conductivity, and versatility in various applications, including electronics, energy storage, and composite materials.
- Diamond: A naturally occurring allotrope of carbon, characterized by its transparent, colorless appearance and exceptional hardness, making it the hardest known natural material. It has high thermal conductivity and is often used in jewelry, cutting tools, and industrial applications requiring abrasion resistance.



(A)



(B)



(C)



(D)

FIGURE I-2*: Pictures of some Carbon allotropes

c) Solid solutions Fe-C

In the metallurgy of alloys, it is known that the secondary (alloying) element can be introduced into the lattice of the primary (main) element through one of two possible mechanics. Let's consider the simplest example of a binary alloy, and let it be A-B (A is the main element, and B is the alloying element). In this case, B-atoms can enter the lattice:

- (1) Either by **substitution**, which means that they take away an A-atom, and replace it, which is the case of large atoms, respecting the conditions imposed by the Hume-Rothery rules [1:3]:
 - A and B atoms should have nearly the same radius (no more than 15% difference)
 - A and B substances should have the same crystalline structure
 - A and B atoms have nearly the same electronegativity
 - A and B atoms should have nearly the same valance.
- (2) Or, in the case of smaller atoms, by occupying **interstitial** positions, which means that they slightly push A-atoms from their initial positions, to fit in between them. There are two types of these interstitial positions in a cubic structure, according to the number of A-atoms that surround B-atoms:
 - *Tetrahedral* sites, where four A-atoms surround each B-atom. We count 12 of these in a CC structure, and 8 in an FCC structure.
 - *Octahedral* sites, where six A-atoms surround each B-atom. We count 6 of them in a CC structure, and 4 in an FCC structure.

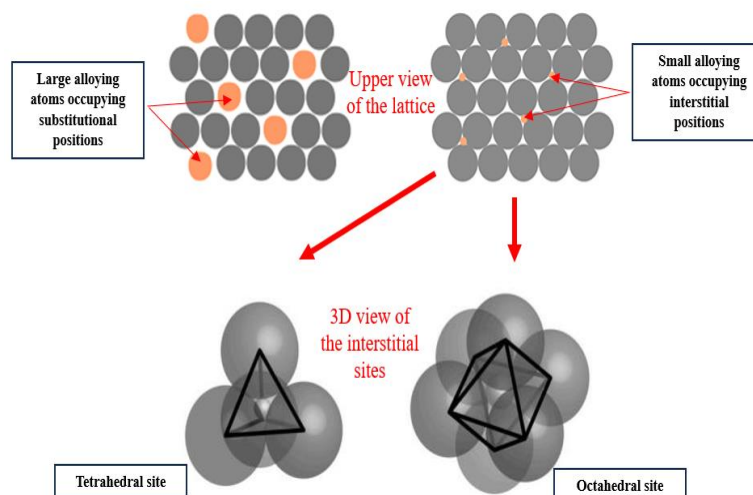
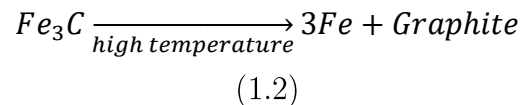


FIGURE I-3*: Possible positions for alloying elements in solid solutions

In an iron-carbon solid solution, carbon (being a small atom compared to iron) is found in the interstitial position, with a high solubility depending on the type of carbon used (reaching the value of 100% for the case of graphite). Once in the iron's structure, according to the quantity of carbon dissolved and to the range of the temperature imposed on the mixture, many equilibrium phases can be defined between them, from these we count:

- Ferrite: produced when carbon is dissolved in ferritic iron, symbolized as Fe(α) previously. It can hold up to 0.022%C at a maximum temperature of 727°C.
- Austenite: produced when carbon is dissolved in Fe(γ). It can hold a maximum of 2.1%C at a temperature of 1147°C.
- Cementite: a chemically defined component with a formula of Fe₃C. It is an unstable element that decomposes at high temperatures into iron and carbon following the chemical reaction:



- Perlite: a eutectoid element composed of a mixture of ferrite (88.9%) and cementite (11.1%) that forms at a temperature of 727°C from cooling an austenitic phase.

On the other hand, two types of iron-carbon alloys might be had depending on the quantity of the alloying element present in the solid solution: *Steel* when %C < 2.1% or *Cast iron* when %C > 2.1%.

The following equilibrium diagram gives a synthesis of the possible phases and the domains of steel and cast iron and all their types:

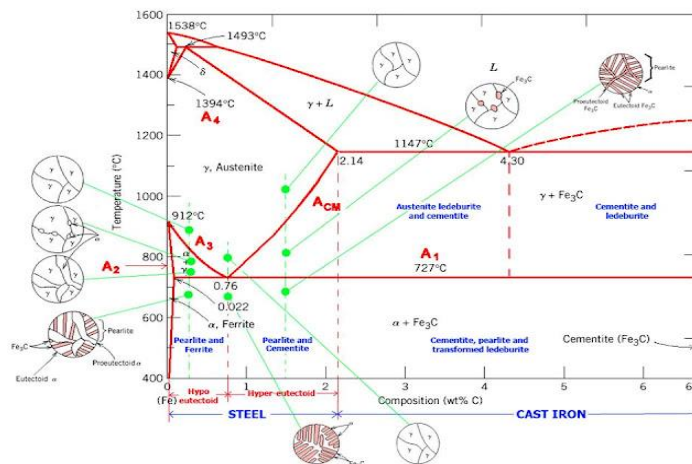


FIGURE I-4*: Fe-Cementite phase diagram

I.2.2 Alloying elements in steel

a) Classification of steel

Practically, it has been proven that the quantity of carbon added to a steel grade affects directly its properties, however, it leads sometimes to unwanted results or it is just not enough to reach the requirements of a specified application.

So, besides carbon, many other elements can be added to the mixture to get satisfactory results, such as silicon, manganese, chromium, nickel, and many others. Moreover, some elements are present by default and can't be deleted such as oxygen, sulfur, and phosphorous (with these elements considered as impurities that need to be minimized, due to their negative effects).

According to the quantity of the alloying elements, we distinguish many classes of steel, as shown in the following diagram:

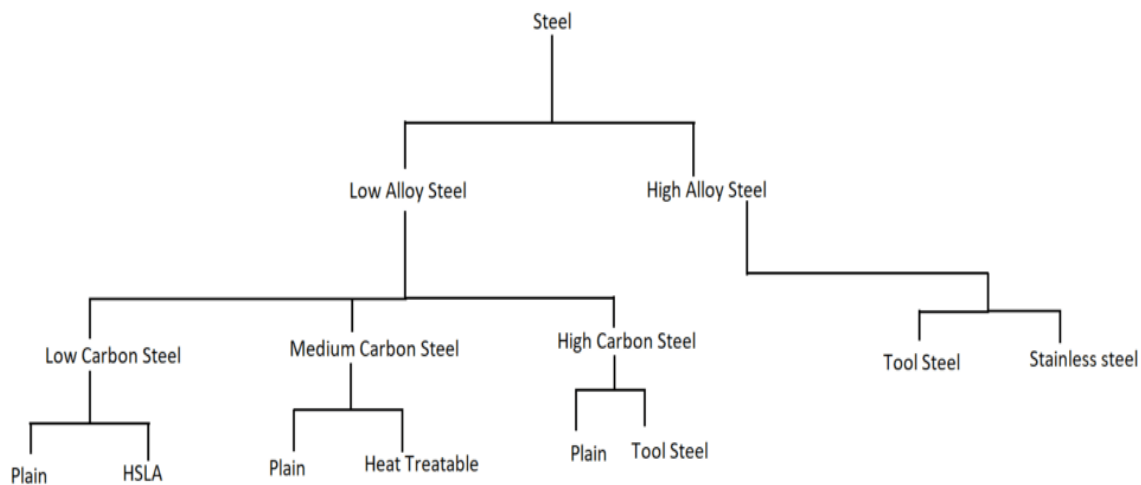


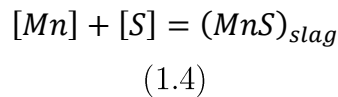
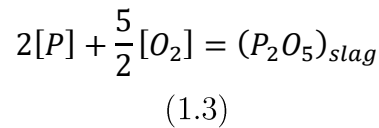
FIGURE I-5*: *Classification of steel*

b) Effects of the alloying elements on the steel properties

When added to the steel structure, every alloying element is meant to have a role in affecting steel properties such as its purity, density, mechanical properties, microstructure, and so on. These effects have been widely explored, and a large amount of information can be found in all the sources of documentation. In the following paragraph, we present a brief synthesis of some of the most common and the major effects of the elements used frequently in the manufacturing of low alloy low carbon steel (Note that we didn't mention the effects of Aluminum in this section because its possible effects will be explored with more details in the next chapter, where we state the causes and the consequences of its utilization in the steel making process):

(1) Phosphorous and sulfur:

Both of these elements are considered impurities for their detrimental effects on the properties of steel as they lead to dangerous fragilizations of the structure by forming unwanted inclusions. So, it is of a big concern to reduce their quantity as much as possible so their presence would be reduced in trace rate. For this reason, dephosphorization and desulfurization treatments should be done by adding oxygen and manganese respectively, to form elements that would rise into the slag following the chemical equations:

**(2) Oxygen:**

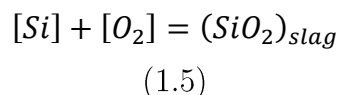
Oxygen is added, as shown in the previous chemical equation for the dephosphorization treatment. It also has the role of the control of carbon quantity that needs to be dissolved in the steel, as it reacts with oxygen to form carbon (di)oxide. However, it can have a reverse effect if it is present in quantities more than it should be, as it could lead to the creation of defects in the steel structure and to the formation of the inclusions.

(3) Manganese:

It is used mainly for the desulfurization treatment as shown in the previous equation. Besides that, manganese is often added to improve hardenability, which is the ability of steel to develop hardness through heat treatment. It also acts as a deoxidizer, helping to remove oxygen during steelmaking, which enhances the steel's cleanliness and reduces brittleness. Manganese can also increase strength and toughness, improving the overall mechanical properties of the steel.

(4) Silicon:

Silicon is primarily used as a deoxidizer and to improve the steel's strength and hardness. It also aids in enhancing the steel's resistance to oxidation and scaling at elevated temperatures, within the following chemical equation:



More elements can be added for specified applications, such as nickel, chromium, molybdenum, vanadium, and others. In the *following table*, Paul Kah et al. [1:4] summarize the effects of the alloying elements:

TABLE I-1: *Effects of common alloying elements on steel properties* [1:4]

Beneficial effects for low-temperature service steels	Harmful effects for low-temperature service steels
Elements that help to decrease the grain size (Al, Ni, V, Nb, Ti, N)	High carbon content
Metals with FCC crystal structure (Ni, Ca, Al, Cu)	Impurities, especially P and S
Rare earth elements (Ce)	Gases (O, N, H)
Metals with hexagonal close-packed structure (Ti, Zr)	
Deoxidizers (Al, Ca, Ce, Si)	
Boron (for quenched and tempered steels)	

I.3 Solidification and nucleation

Solidification is a clue phenomenon when studying the microstructures of steel samples. It is defined as a physical transformation of a substance from a liquid state into a solid state, at a special temperature, called melting temperature (T_m).

$$T = T_m: \text{Liquid} \rightarrow \text{Solid} + \text{Heat energy} \quad (1.6)$$

In this case, some changes in the properties could be observed. For the example of iron (if we accept its approach to the steel), a fall in viscosity of the material is trivially remarked, as the molten iron has a viscosity near to the one of water, while solid iron has a high resistance to shear forces. Also, the diffusion is easier in molten steel and is by far simpler than in solid steel (as it is a thermally activated mechanism).

So, for this equation to be possible, the solid state must become more equilibrated than the molten state by having less intern energy, which is transformed into heat and liberated into the environment. This translates thermodynamically by the free energy approach (Gibbs energy) following the inequation:

$$T \leq T_m \Leftrightarrow (G_s = H_s - TS_s) \leq (G_L = H_L - TS_L) \quad (1.7)$$

Where: T: temperature, H: enthalpy, G: free (or Gibbs), S: entropy

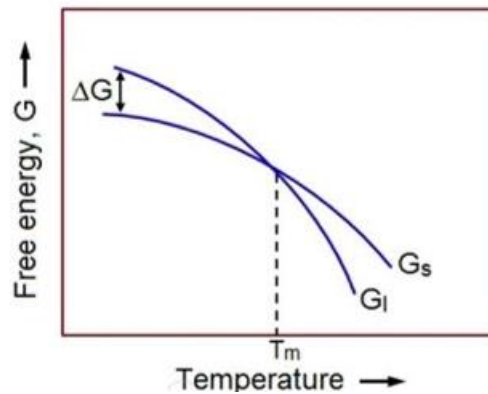


FIGURE I-6*: *Qualitative variations of free Gibbs energy vs temperature*

We can see for $T < T_m$ the solid-state energy is less, and thus more equilibrated, than the liquid-state energy

Also thermodynamically, the theory after the solidification is explained by the nucleation and growth mechanisms. The nucleation is responsible for the precipitation of steel embryos, that will grow and transform into steel grains and/or crystals.

I.3.1 Nucleation

The process of the transformation of liquid iron atoms into embryos and nuclei is related to the nucleation mechanism. Two models of this process are referenced in the bibliography [1:5,6]:

- An ideal case model, where all the necessary conditions (the absence of all types of impurities) are verified. In this case, typically spherical-shaped nuclei are expected to form within what's known as **homogenous** nucleation. This model is (obviously) unreal and serves only for academic and comparison purposes.
- A realistic model, where the impurities are considered to have an actual effect on the solidification process, which has a significant role in shaping the formed nuclei, and thus the obtained grains won't have the same typical spheric shape but rather some irregular forms. This model is known as the **heterogenous** nucleation. This latter model is then proved thermodynamically to be more stable than the ideal one as we will state later, and that's why it is the favored way of solidification.

a) Homogenous nucleation

In this typical model, we consider the hypothesis where the conditions to obtain nuclei typically spherical-shaped are verified. In this case, and to form these nuclei from the molten iron, two types of energies need to be implied:

- (1) A volume energy because as the solidification occurs, we can note a difference in the volume occupied before and after the transformation (atoms are more attached). In the equation, this is then represented by a negative term as it represents the difference between the free Gibbs energy of the solid and molten states.

$$\Delta G_v = V \cdot (G_s - G_L) = \frac{4}{3} \pi r^3 (G_s - G_L) < 0 \quad (1.8)$$

Where: V: average nuclei volume, r: average nuclei radius,

ΔG_v : volume energy

- (2) The other type is the surface energy as boundary layers covering the nuclei are formed during the transformation. In the equation, it is represented by a positive term, since the creation of the surface requires a gain of energy.

$$\Delta G_s = S \cdot \gamma_{sl} = 4\pi r^2 \cdot \gamma_{sl} \quad (1.9)$$

Where: A: average surface area of nuclei, γ_{sl} : superficial tension energy,

ΔG_s : surface energy

So, by adding up the two terms, we obtain the overall homogenous nucleation mechanism energy equation given as:

$$\Delta G = \Delta G_v + \Delta G_s = \frac{4}{3} \pi r^3 (G_s - G_L) + 4\pi r^2 \gamma_{sl} \quad (1.10)$$

The following curve shows the variation of each term of the equation in function of the nuclei radius:

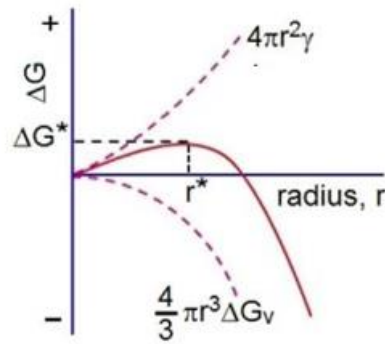


FIGURE I-7*: Qualitative representation of the free Gibbs energy variations vs nuclei radius

In the previous curve, we can see that actually the free energy required for the homogenous nucleation passes through a critical value for a critical nuclei radius. This radius can easily be determined by derivation and nulling the last stated equation, and so we obtain:

$$\left. \frac{d(\Delta G)}{dr} \right|_{r=r^*} = 0 \Rightarrow r^* = -\frac{2\gamma_{sl}}{G_s - G_L} \quad (1.11)$$

And:

$$\Delta G^* = \Delta G(r = r^*) = \frac{16\pi\gamma_{sl}^3}{3(G_s - G_L)^2} \quad (1.12)$$

A thermodynamical discussion based on mathematics can be then discussed, by following the slope of the graph, as we note two regions on it:

- First, for $r < r^*$ we note that $d(\Delta G) > 0$, and thus the system is destabilized. The nuclei which have a radius less than the critical value required are self-destroyed and cannot proceed into the growth step.
- Second, for $r > r^*$ we note that $d(\Delta G) < 0$, and thus the system is stabilized. This means that nuclei with higher radius than the critical value required do proceed into the growth step to transform into grown grains.

As a synthesis of this model, we can say that the theory of the homogenous nucleation mechanism requires the system to attend to a certain energy barrier. The barrier is set up by a volume energy that stimulates it, and a surface energy that delays it.

b) Heterogenous nucleation

In the real state of the molten iron mixture, impurities and defects (grain boundaries, inclusions, attachment to the mold or furnace limits...) are always present and cannot be avoided. In such a case the nucleation will favorize to occur near these sites.

As this happens, the geometry of the formed nuclei will be different than the one supposed in the previous model, as shown in the **FIGURE I-8**:

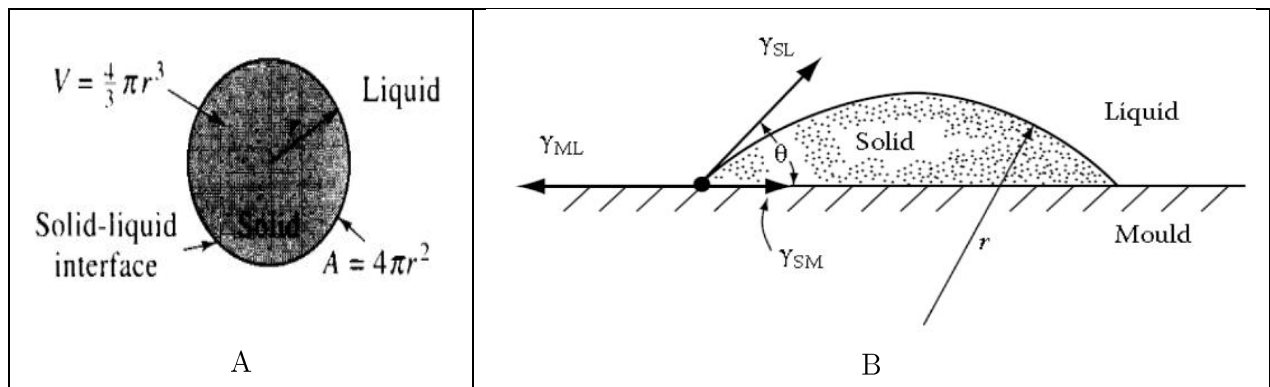


FIGURE I-8: Comparison between the ideal nuclei formed by homogenous and heterogenous nucleation [1:5]

Note that even the model of the heterogenous nucleation doesn't represent the exact reality since it has also some suppositions and hypotheses about the shape of the nuclei

From the figure above, we notice that the nuclei formed by the heterogenous nucleation process are shifted from the wall surface by a driving angle θ . The heterogeneous nucleation model suggests that this angle matches the free Gibbs energy required for the formation of the nuclei by the following equation:¹

$$\Delta G_{het}^* = f(\theta) \cdot \Delta G_{hom}^* \quad (1.13)$$

With:

$$f(\theta) = \frac{1}{4} (2 + \cos(\theta))(1 - \cos(\theta))^2 < 1; \forall \theta \quad (1.14)$$

So, this model states that the barrier of energy set by the heterogenous model is lower by the perfectionist homogenous model, and thus it is easier to get through it than

¹ See demonstrations in the index B.

to reach a higher level, which explains then why the heterogenous model is realistic and more descriptive to the actual events happening in the inner structure of the material.

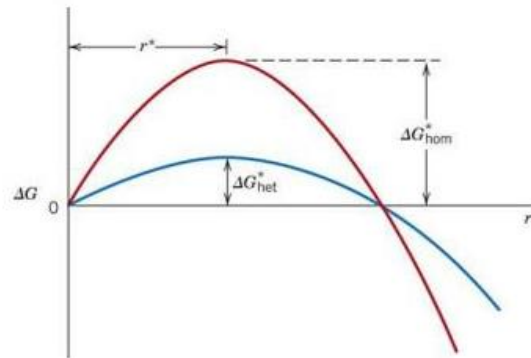


FIGURE I-9*: *Graphic comparison between energy barriers of homogenous and heterogenous modes of nucleation*

I.3.2 Growth

a) Growth mechanisms

When the nuclei are formed and have a radius above the critical value, the free Gibbs energy tends to fall in both homogenous and heterogenous nucleation. At this stage, they will proceed into their next step to transform into grains by a growth mechanism. Two main ways of growth are stated in the bibliography:

(1) Growth induced by diffusion mechanism:

This way is activated at high temperature, when the gradient of concentration is high. At this case, the elements required for the growth of the nuclei enter its structure by bypassing the vacancies in its boundaries until they reach the inner positions, following the famous laws of Fick:

$$\begin{cases} 1^{st} Law: J = -D \cdot \frac{dC}{dx} \\ 2^{nd} Law: \frac{dC}{dt} = D \cdot \frac{d^2C}{dx^2} \end{cases} \quad (1.15)$$

Where: J: diffusion flux, i.e. the amount of the substance that will flow through a unit area during a unit of time interval,

D: diffusion coefficient, given as a function of energy and temperature with an Arrhenius-type formula,

C: the concentration of the substance in function of position and time,

t: time, x: position

(2) Growth induced by the capture at the interface:

Which is the case of a low gradient of concentration between the two phases (depending on the studied case, phases might be liquid \rightarrow solid in a solidification process, or oversaturated \rightarrow saturated state in a precipitation process). In this case, the boundary of the nucleus will absorb the required elements to its interior and so they are added to its structure and thus it grows. As stated before, this happens when the concentration gradient is low, which and so this way generally appears after the end of the diffusion mechanism.

b) Growth kinetics

During the second half of the previous century, many works established by several scientists tried to give approximative models to describe the kinetics of the growth mechanism within the diffusion-activated method. Dr. S. Bensaada [1:7] stated the proposed models by those scientists, the *following table* summarizes some of the given results:

TABLE I-2: Kinetic models for diffusion-activated growth [1:7]

Model	Description	Equation	Equation terms
Zener	The growth rate is controlled by the volume diffusion coefficient (D_v).	$D_v = \frac{0.5X_0}{X_0 - X_e} VL$ (1.16)	X_0 : Initial oversaturated concentration of the matrix X_e : Equilibrium concentration of impoverished matrix V: Growth rate L: interlamellar distance
Turnbull	Adapted the Zener model, but considered however that the growth is driven rather by the interfacial diffusion (D_i) coefficient than by a volume one.	$\lambda D_i = \frac{X_0}{X_0 - X_e} VL^2$ (1.17)	λ : Reaction front thickness

Aaronson et Liu	Considered the terms present in the previous model are wrong, and found that the interfacial diffusion coefficient is related also to the concentration of the formed β phase (X_β) during the reaction.	$\lambda D_I = \frac{1 X_\beta - X_0}{4 X_\beta - X_e} V L^2 \quad //$ (1.18)	
Cahn	The diffusion coefficient is also proportional to the speed of the advance of the reaction frontal.	$\lambda D_I = \frac{\partial X_I^2}{\partial z^2} + V(X_0 - X_\alpha)$ (1.19)	X _I : Interfacial concentration z: Reaction front position

Another approximation to the study of the growth kinetics is to take into consideration the fraction of the matter transformed from phase 1 into phase 2. The most famous bibliographic approach to this concept is expressed by the equation of Johnson-Mehl-Avrami obtained by considering some idealistic hypotheses²:

$$Y(t) = 1 - \exp [-Kt^n] \quad (1.20)$$

Where: Y(t): fraction of the formed phase- β in the volume, i.e. $Y=V_\beta/V$,

K, n: constants

In fact, despite that this approach has been established by considering many idealistic conditions, however, the experience showed that the real case isn't very different from it, with the only noted differences were on the values of the constants K and n, which made it necessary to determine them experimentally. The previous equation can be rewritten as:

$$\ln \left(\ln \left(\frac{1}{1-Y(t)} \right) \right) = \ln(K) + n \ln(t) \quad (1.21)$$

And so, the method consists of measuring the fraction Y in function of the necessary time taken for the transformation, and then draw the curve: $\ln \left(\ln \left(\frac{1}{1-Y(t)} \right) \right) = f(t)$, which will have a linear form. The slop gives the value of n, and the intersection with the y-axes will lead to the deduction of the value of K.

² These hypotheses are stated and justified within the demonstration of this formula. Check index B.

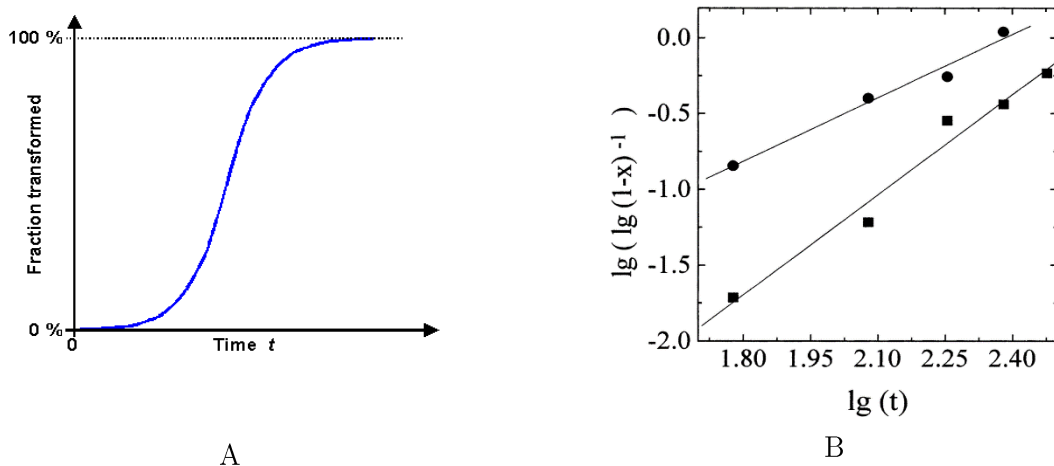


FIGURE I-10*: *Johnson-Mehl-Avrami curves in the original version of the formula (A), and the linear transformed version (B)*

I.4 Heat treatments

In most cases, only adding alloying elements is not sufficient for the obtention of the characteristics that are attended, as most of them require thermal conditions to be fixed in the steel structure.

Historically speaking, humanity discovered this fact at very early ages, since this fact is as old as the necessity for the hunt to obtain food. In the Middle Ages, the manufacturing of weapons such as swords and knives required the blacksmiths (people who forge steel) to heat the metal to a temperature near its melting point, subject it to deformation (forging), and then drown it into water for cooling during few seconds. This process was noticed to be extremely beneficial, and highly necessary to enhance the mechanical properties of the produced steel, as it gave it a great hardness and a good resistance to deformation.

This set of steps (heating, holding, cooling) is defined in metallurgy science as heat treatments, which proved to have important effects on the structure and the properties of steel.

I.4.1 Definition of heat treatments

Heat treatments consist of applying a series (sets) of thermal cycles on a material (such as steel) before, during, or after a shaping process to give it enhanced mechanical properties (such as hardness, toughness, and resilience...), eliminating residual stresses present inside the material's structure, and/or facilitate the processing. [1:8]

All the heat treatments are divided into three steps: heating, holding, and cooling. Each of these steps is related to some factors that can affect it significantly. According to the durations and the succession of these steps, three types of heat treatments can be defined: annealing, quenching, and tempering.

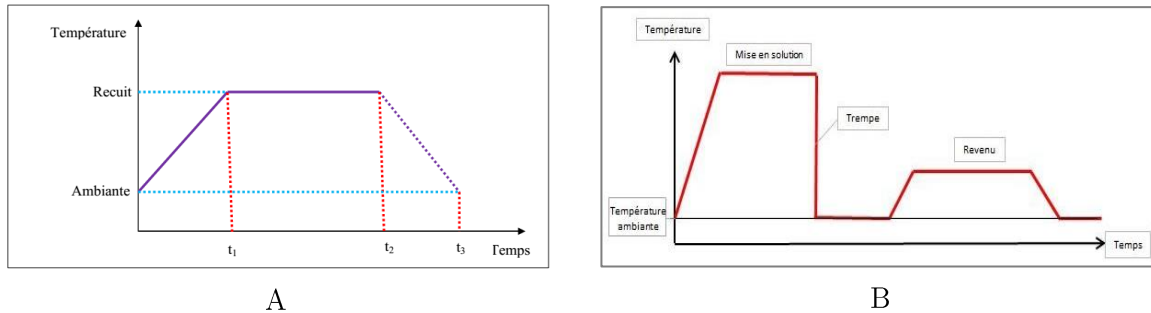


FIGURE I-11: Heat treatment cycles of annealing (A) and quenching & tempering (B)

I.4.2 Parameters affecting the heat treatments

As stated above, a heat treatment is applied within steps. Each of them is submitted to parameters that could affect the treatment quality, the structure of the product, and the mechanical properties. The following table summarizes some of the clue parameters and their effects:

TABLE I-3: Key parameters affecting each of the heat treatment stages

Stage	Parameter	Justification
Heating	Atmosphere	The gases present in the atmosphere can interact with the steel components at high temperatures. For example, an oxidized atmosphere enhances corrosion.
	Equipment	The power of the equipment's energy transfer can affect the heating time.
	Chemical composition of steel	To determine the necessary temperature for heating, the chemical composition of the steel interferes. When heating, the Ac_1 and Ac_3 temperatures are must-knows, however, they are linked to the steel's composition by Andrew's relation. For example, for hypo eutectoid steels:
		$Ac_1 = 723 - 10.7Mn - 16.9Ni + 29.1Si + 16.9Cr + 6.38W + 290As$ (1.22)
Holding	Geometry	The heat transfer rate isn't equal in all three dimensions in the steel structure, and it depends on the geometry, so it is safe to consider that complex geometries require more holding time than the simple ones.

	Time	Helps the heat to reach the core of the treated piece, and so the treatment is homogenous in all the structure.
Cooling	Medium	Controls the cooling speed. High cooling speeds can lead to a shock of the structure and the formation of hard structures, while slow speeds give enough time for the structure to follow the equilibrium phases, and thus, soft phases are obtained.

I.4.3 Types of heat treatments

a) Annealing

Annealing is the most common heat treatment cycle, where the metal the metal is heated by two processes:

- (1) Heat transmission from an external source, by one of the transfer modes: conduction, convection, or radiation.
- (2) Heat generation, by creating a heat flux within the material by induction or by electric energy.

After the holding time, the sample is then cooled slowly to the ambient temperature.

According to the heating temperature and the holding time alongside the objective of the treatment, many types of annealing processes can be defined, the following types are the most common in concern to the structural and mechanical properties of the material:

- *Homogenization annealing*: used generally before shaping processes, it gives the grains in the structure a homogenous form, which will minimize the strains that can be possibly present due to the impurities and defects.
- *Softening annealing*: in case of the presence of extremely hard phases that can lead to the fragilization of the structure, and so the steel is heated into an austenite phase and then it is left to cool calmly, where all the metastable phases turn into the stable ones.
- *Recrystallization annealing*: applied on steels with a deformed structure (failed rolling or forging), and so the initial structure is reestablished.

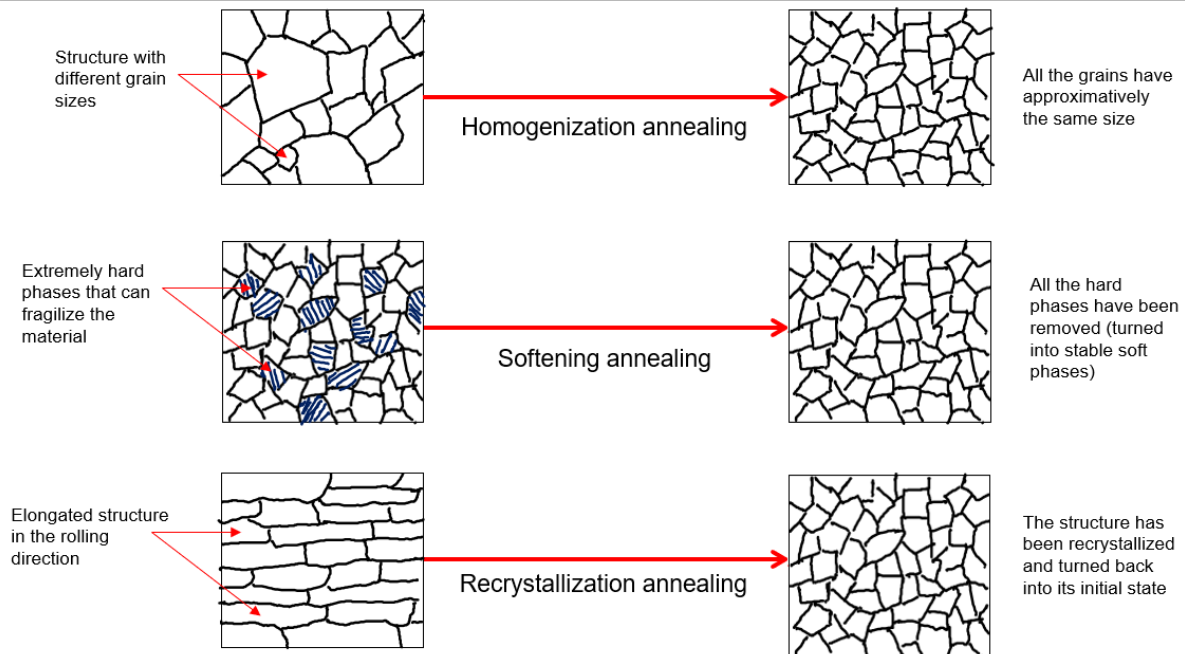


FIGURE I-12: Schematic representation of the structural effects of different annealing processes

b) Quenching

Quenching consists of heating the structure into the austenitic phase and then cooling it at a very high speed, with a large temperature gap (sample at around $T > 1000^\circ\text{C}$ is cooled into ambient temperature within few seconds). This will cause a shock in the metal structure, which will no longer follow the equilibrium phase diagram. In this case, very hard structures could appear, depending on the quenching fluid (hence the quenching speed). Two types of quenching can be applied:

- Oil quenching: the sample is quickly drawn in oil. A bainitic structure is formed in its structure.
- Water quenching: the sample is drawn into water, which has an extremely high heat absorption, the structure is shocked at a high rate and forms the hardest possible structure which is the martensite.

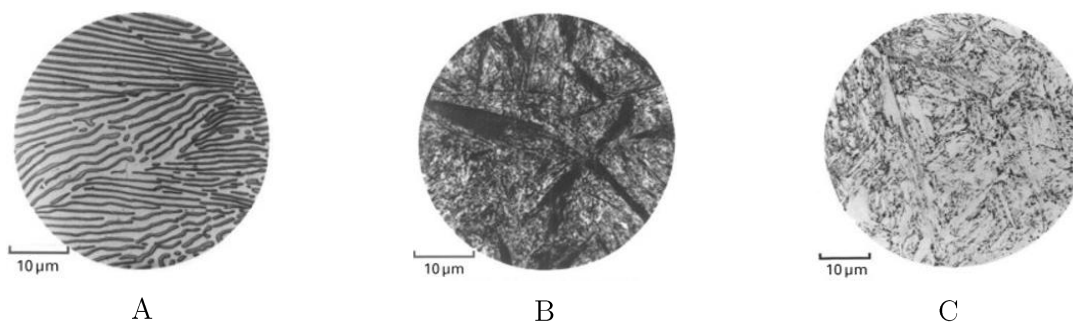


FIGURE I-13: Structures obtained after cooling at different environments [1.9]

Slow cooling at ambient air gives a pearlitic structure (A), Medium speed cooling in oil gives a bainitic structure (B), and High-speed cooling in water gives a martensitic structure (C)

c) Tempering

As the quenching process is applied, sometimes the big shock of the structure leads to a higher than the wished value of hardness. Also, a lot of residual stresses are generated especially in water quenching, because of the crystalline structure of the martensite. This can lead to the formation of cracks in the product (**FIGURE I-14**).



FIGURE I-14*: *Cracks on a steel blade quenched but not tempered*

So, tempering is considered as a secondary treatment applied after quenching to cure to problem. The material is heated at a temperature below the one applied before quenching, held for a shorter time, and then cooled slowly at ambient air.

I.5 Rolling

Rolling is the most important shaping process of steel by plastic deformation found in the industry. It helps to transform thick steel billets into thin, but long steel products such as wire rods or rebar. Practically, it consists of passing the steel billet between two rolling cylinders separated by a gap that is thinner than the billet's height. As the cylinders turn around themselves, they induce a shear stress that forces the metal to pass through it, which will automatically result in a reduction of the billet's thickness. [1:10]

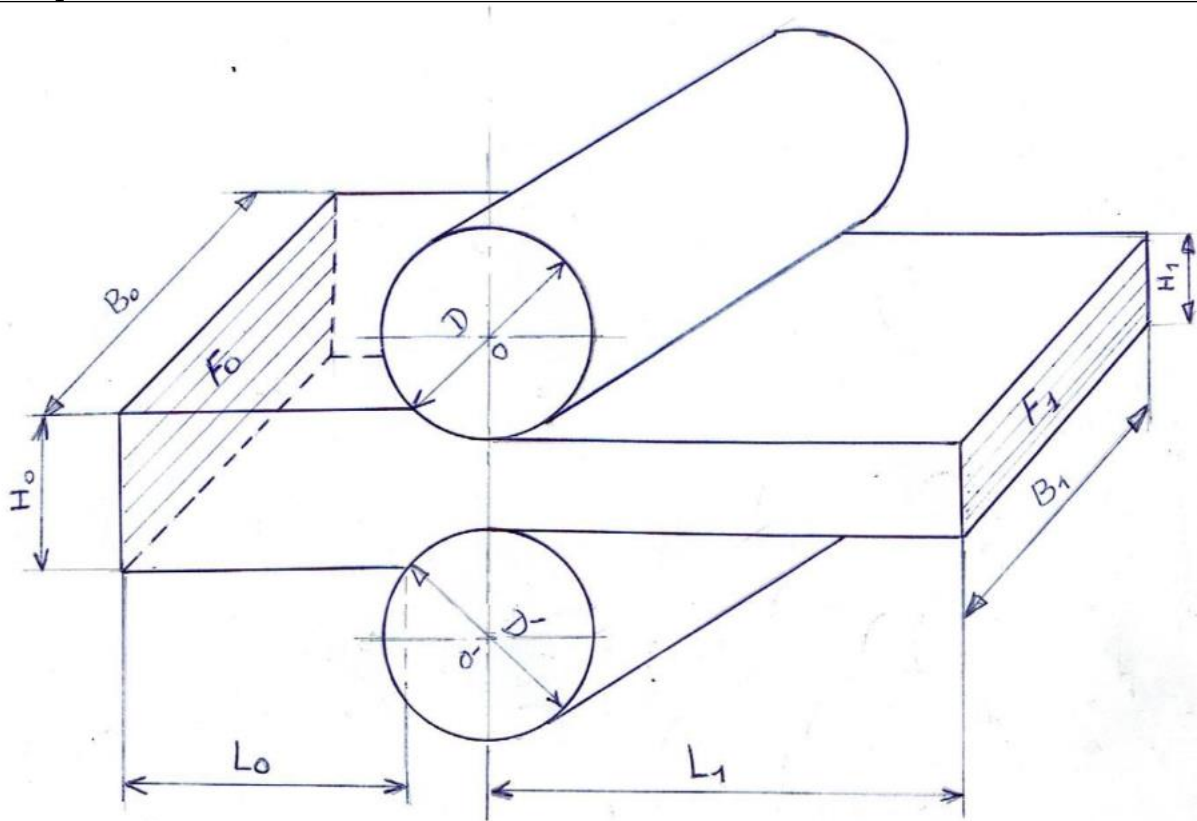


FIGURE I-15: Dimensional change within rolling [1:10]

I.5.1 Deformation coefficients

Let's consider the example of a steel bar, that has its initial dimensions stated as: $H_0 \times B_0 \times L_0$ (in a format of Height x Width x Length) before passing through the gap between the two rolling cylinders. After the deformation, we can notice that its dimensions changed to become (for example) $H_1 \times B_1 \times L_1$. Visually, a reduction in height and an augmentation in both width and length directions are observed. This will lead us to define the following deformation coefficients according to each of the directions:

$$\gamma = \frac{H_1}{H_0} < 1 ; \quad \mu = \frac{L_1}{L_0} > 1 ; \quad \lambda = \frac{B_1}{B_0} > 1$$

(1.23)

These parameters can be linked to each other using the volume conservation formula. Actually, as we are dealing with a material full with matter inside, and which is continuous, it is logical then that the volume before and after the deformation is remained constant, and thus we can write:

$$V_1 = V_0 \Rightarrow H_1 B_1 L_1 = H_0 B_0 L_0 \Rightarrow \frac{H_1 B_1 L_1}{H_0 B_0 L_0} = 1 \Rightarrow \gamma \lambda \mu = 1$$

(1.24)

Practically, it is just not enough for the material to only pass through one pair of cylinders. A successive rolling is used in industry, and the billets pass through multiple pairs of cylinders (**FIGURE I-16**).

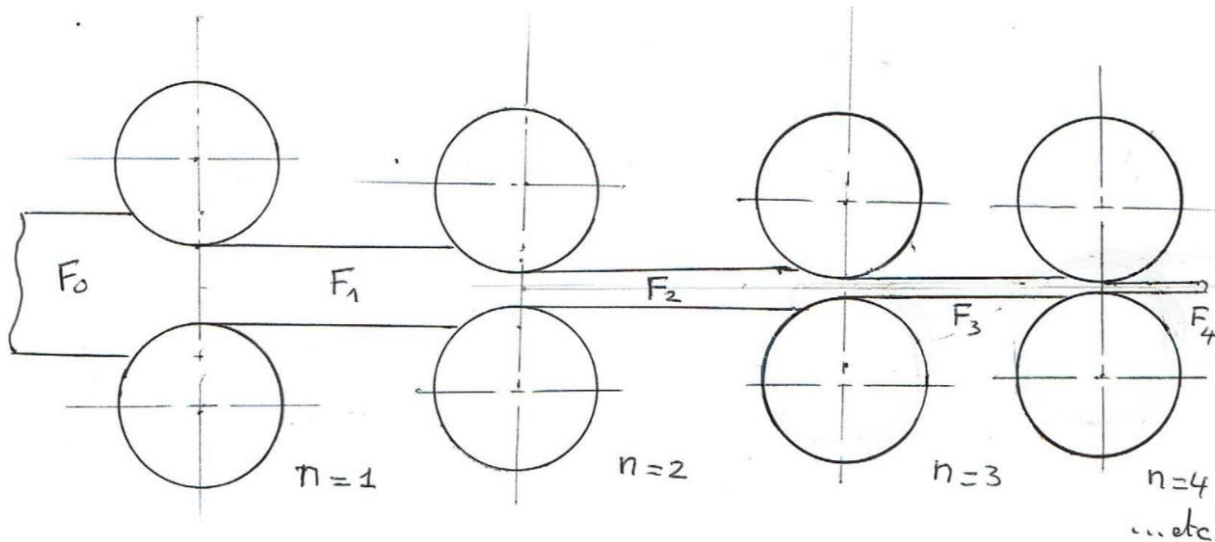


FIGURE I-16: Continuous rolling through multiple cylinders [1:10]

In this case, overall and average expansion coefficients are defined, such as:

$$\left\{ \begin{array}{l} \mu_{\Sigma} = \frac{L_n}{L_0} = \frac{L_1}{L_0} \cdot \frac{L_2}{L_1} \cdot \dots \cdot \frac{L_n}{L_{n-1}} = \prod_{i=1}^n \mu_i \\ \mu_m = \sqrt[n]{\mu_{\Sigma}} \end{array} \right.$$

(1.25)

Based on these equations, we can derive a formula that matches between the number of passes, the final and initial lengths and the average expansion coefficient, given as:

$$n = \frac{\log(L_n) - \log(L_0)}{\log(\mu_m)}$$

(1.26)

I.5.2 Effects of rolling on the steel structure

The plastic deformation induced by the rolling process is explained by the variation in the shape of the grains in the steel structure. According to the conditions of deformation (hot or cold), the following effects can be observed:

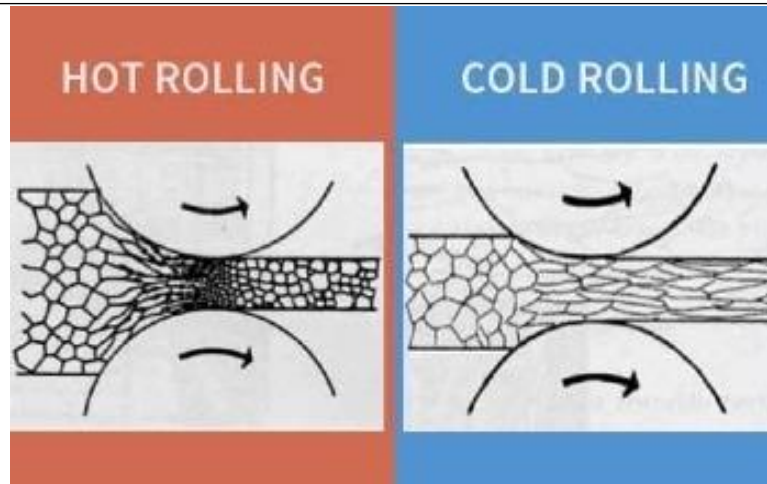


FIGURE I-17*: *Steel structure at hot and cold rolling conditions*

For the cold rolling, we note that the grains are deformed permanently far from the rolling site, following the deformation direction (horizontal direction on the *figure above*), while during the hot rolling more structures are distinguished simultaneously:

- Zone before rolling has an equiaxial structure.
- The zone between the cylinders has longitudinally expanded grains.
- Far from the rolling site, the grains reestablish another structure as they proceed into dynamic recrystallization activated by the high work temperature.

I.6 Conclusion

Steel is one of the most common and the most used materials in different industrial fields. Many people who use it in their daily lives confound it by mistake with pure iron, ignoring the fact that it is a solid solution between iron, carbon, and many other alloying elements. These alloying elements are responsible for giving steel the properties that make it useful. Each of them has its effect on the structure, the manufacturing processing, and characteristics.

For these elements to enter the steel's structure, they need to be added into it during the steelmaking process, so they can integrate the structure during the solidification. This latter is enhanced by a heterogeneous nucleation mechanism to form steel nuclei that will evolve into steel grains by a growth mechanism. At the end of these two processes, the bulk steel structure is obtained, however it can contain many defects.

These defects must be cured by heating cycles called heat treatments. Controlling the parameters of these treatments leads to a complete control of the steel properties.

Finally, the last step before the produced steel can be destined for normal usage, a shaping process is required. Shaping is done by applying plastic deformation on the steel such as rolling or forging. These processes can affect the steel grain shapes in the microstructure, and thus lead to a modification of its properties.

References:

- [1:1] Michael F. ASHBY, David R.H. JONES. *Matériaux 4^{ème} édition*. DUNOD, Paris, 2013
- [1:2] Tom JACKSON. *The periodic table book, a visual encyclopedia of the elements*. Dorling Kindersley, 2017. p-60.
- [1:3] Livio Battezzati. *Solid Solutions in Metals: from Hume-Rothery's Rules to High Entropy Alloys*.
- [1:4] Paul Kah, Pavel Layus, Jukka Martikainen. *Influence of alloying elements on the low-temperature properties of steel*.
- [1:5] Fateh Hellal. *Solidification chapters I to III*. ENP. 2023.
- [1:6] Abadli. *Germination et croissance*. ENP. 2023.
- [1:7] S. BENZAADA. *Mécanismes de germination, croissance et coalescence dans les alliages binaires*. Biskra university.
- [1:8] Abadli. *Traitements thermiques des aciers de construction*. ENP. 2023.
- [1:9] Jean-Christophe Hell. *Aciers bainitiques sans carbure*. Autre. Université Paul Verlaine- Metz, 2011.
- [1:10] Kasser. *Transformation des métaux par déformation chapitre III: Laminage*. ENP. 2024.

Note: All the pictures and tables with a (*) mark are taken from open sources found on the internet.

Effects of Aluminum

“Research is seeing what everybody else has seen and thinking what nobody else has thought

Albert Szent-Györgyi; a Hungarian pharmacologist known for his work on vitamins and oxidation. He was awarded the Nobel Prize in Physiology or Medicine in 1937.

Introduction to the chapter:

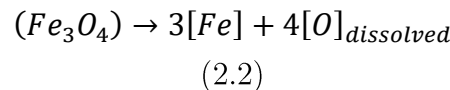
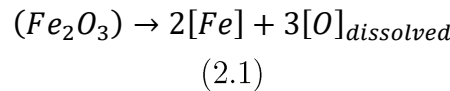
Aluminum is an element of the third group of the Mendeleev classification with atomic number 13. In the industrial field, it is very famous for its lightweight. That is why it is widely used in aeronautics. It is also known to be ductile and corrosion-resistant because it quickly (or even instantly) forms a layer of aluminum oxide on the surface when exposed to an oxidizing environment. In addition, it has excellent thermal and electrical conductivity.

When added during the elaboration process, aluminum grants steel some of its characteristics, and helps for the control of its grain size. In this chapter, we aim to list and present all the aluminum effects that could be faced either in the industrial field or during the study, based on what was reported in the bibliography from previous research.

II.1 Effects on steelmaking process: Deoxidation agent

During the steelmaking process, oxygen can be introduced into the molten metal from many sources, such as:

- (1) The CDRI: Being made of iron oxide (Fe_2O_3 or Fe_3O_4), and even after the reduction process at the DRI unit, it has been found that it is impossible to reduce all the iron in the raw material, leading to having some residuals of the previous species which can then be reduced in the EAF during the steelmaking process, according to the reactions:



- (2) Scrap Metal: Scrap metal is often used as a secondary raw material in steelmaking. It can contain surface oxides or rust, which may introduce oxygen into the molten metal when melted down in the steelmaking furnace.
- (3) Oxygen Injection: Oxygen can be injected during the steelmaking process, directly into the EAF in case of an excessive addition of carbon. This will cause the carbon to form CO_2 . Most of this substance evacuates into the air, however, a small part of it can still and decompose again leading to the addition of the amount of oxygen in the mixture.
- (4) Reactions with Alloying Elements: Some alloying elements used in steelmaking, such as manganese and silicon, can react with atmospheric oxygen during the melting and refining processes. These reactions may contribute to the overall oxygen content in the molten metal.
- (5) Ambient Air: During the handling and processing of molten metal, exposure to ambient air can introduce oxygen into the metal. This can occur during tapping from furnaces, pouring into molds, or during other handling operations.

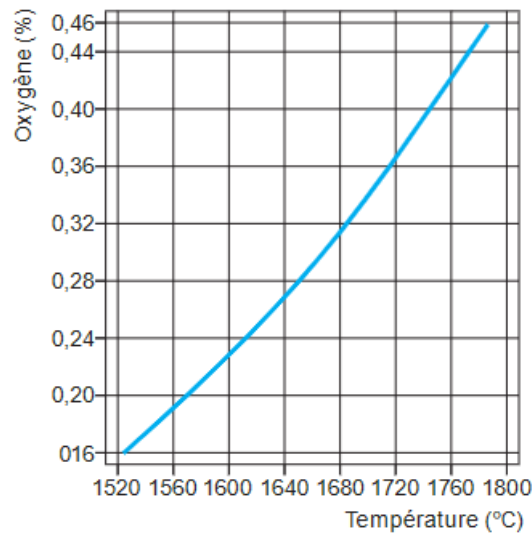


FIGURE II-1: *Solubility of oxygen in molten iron [2:1]*

The quantity of oxygen provided from the previous sources can lead to many problems concerning the quality of the final product. It can react with the alloying elements added during the secondary refining leading them to rise in the slag instead, which will affect the overall chemical composition of the fabricated steel. Moreover, some unwanted non-metallic inclusions (**FIGURE II-2**) may introduce the final structure decreasing its mechanical properties and leading to a weakness of the product. Another major problem of the presence of oxygen in the metal is its potential to form interior unseen cavities containing gases, leading to the most dangerous corrosion forms (pitting and blowholes) causing rapid degradation of the material.

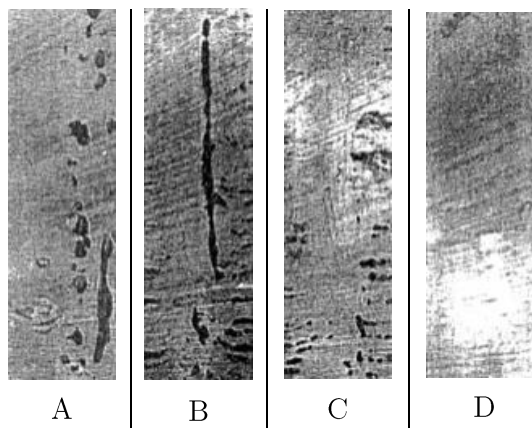
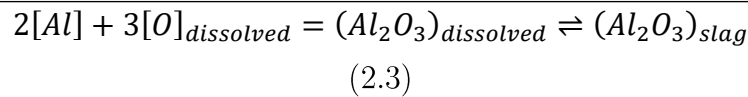


FIGURE II-2: *Comparison between steel samples [2:1]*

A- and B- no aluminum added, C- Al added at 150g/t, D- Al added at 1000g/t. We see that the density of oxides on the structure decreases when we use more Al to kill the steel

So, the primary role of aluminum being added in the mixture is acting as a deoxidation agent following the chemical equilibrium equation:



This process is known in the industrial field by the term “Aluminum killing of steel”. The following diagram given by Jean Marcel in [2:1] compares the deoxidation power of several elements based on the metallic oxides’ equilibrium curves.

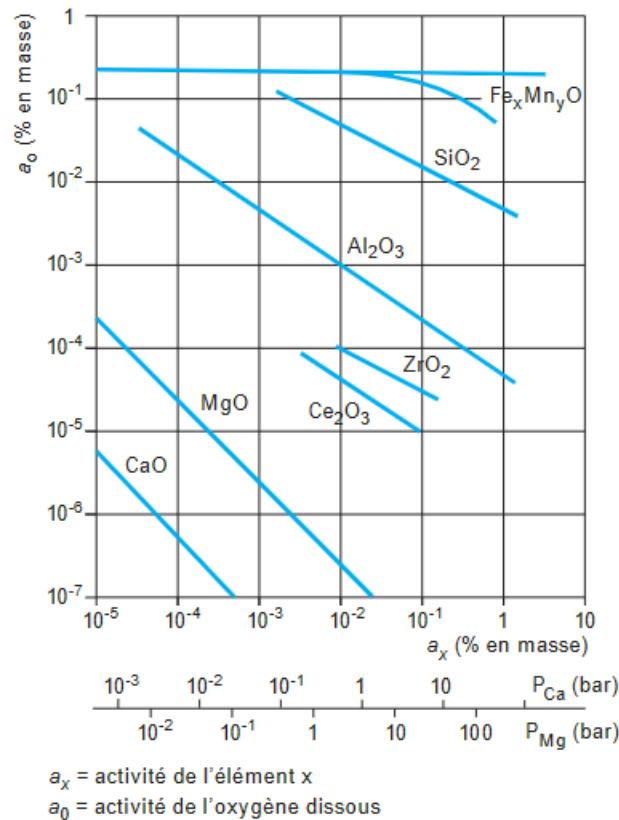
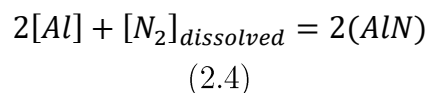


FIGURE II-3: *Metallic oxides equilibrium in molten iron at 1600°C [2:1]*

(average temperature of EAF)

In such a curve, an element represented by a line with the lowest ending point is considered to be more deoxidant than the higher ones because this means that it can reduce even the smallest proportions of oxygen. With this being said, we can notice in the figure above that Al has a higher deoxidant power than Si. However, many other substances such as Mg or Ca seem to be more effective in that case. The selection is also dependent on many other factors, like the cost and the effect of the substance on the manufacturing of the metal. According to Mirwafjanova et al., the choice of aluminum is justified for its contribution to eliminating other gases like nitrogen [2:2], within the chemical reaction:



II.2 Effects on the machinery: Nozzle clogging at CCM

II.2.1 Definition of nozzle clogging

Clogging in continuous casting nozzles is the buildup of material in the flow passage between the tundish and mold [2:3].

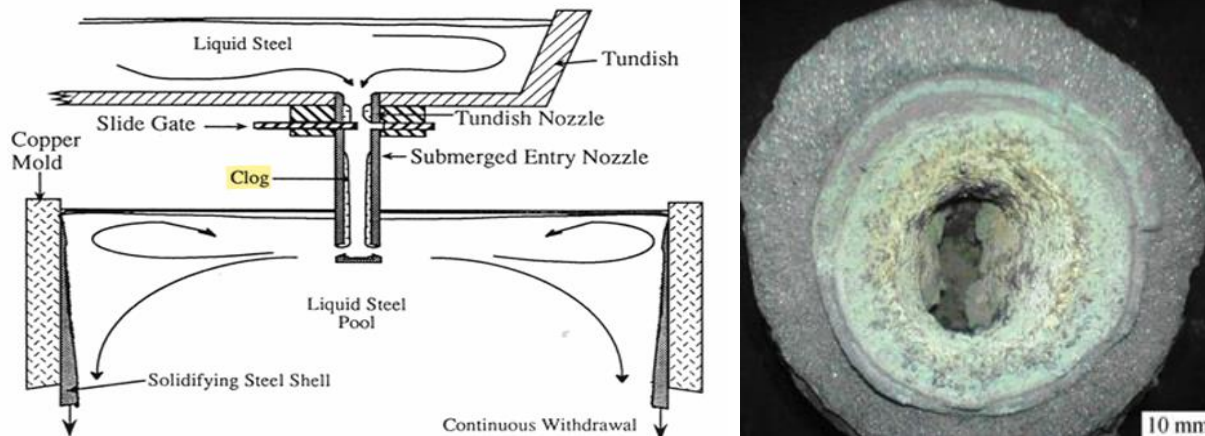


FIGURE II-4: Schematic representation of a nozzle clogging within a CCM, as an actual photograph of a severe clogging [2:3]

This can lead to many serious industrial problems, such as:

➤ Decreased productivity:

To compensate for clogging, the flow control device (e.g., slide gate) must be further opened. If the clogging becomes sufficiently severe, the flow control device will no longer be able to compensate and then either a decrease in casting speed or replacement of the nozzle must result. These events reduce the net casting throughput and thereby reduce productivity. Haers et al. [2:4] reported that the clogging reduced the number of heats (290 tons each) they produced from 12 to just 6 resulting in a huge productivity gap. A similar remark has been given to us at AQS where we were told that the number of heats they produced daily went down from an average of 32 heats per day (120 tons each) to only around 13 heats per day as the clogging happened.

➤ Decreased quality:

Nonmetallic particles can become dislodged from the clog buildup and result in unacceptable cleanliness defects in the product, especially when oxides are required to be minimized.

➤ Increased cost:

The happening of nozzle clogging in CCM can lead to a cost increase in two possible ways. First, the reduction of the flow rate will automatically decrease productivity, thus fewer steel will be sold and then the gain will decrease too. Second, a severe clogging will lead to a complete block of the nozzle, and at this stage, a change of this component is necessary inducing additional fees to the cost of the process, besides the need to stop the process which is hugely unwanted for its various implications on the CCM and the other services.

II.2.2 Mechanism of the formation of nozzle clogging

Alumina is one of the most common elements that can be found in the nozzle clogging of a continuous casting machine. As we mentioned before, most of this substance rises into the slag, but some of it is still in the mixture.

During the CCM process, the work is done at around 1580°C which is far from the melting point of alumina, evaluated at 2072°C. This means that the remaining substance in the mixture will be in a solid state while the mixture is in a liquid state. As a result, Alumina powder, which has a dendritic form (**FIGURE II-5**), will precipitate in the solution.

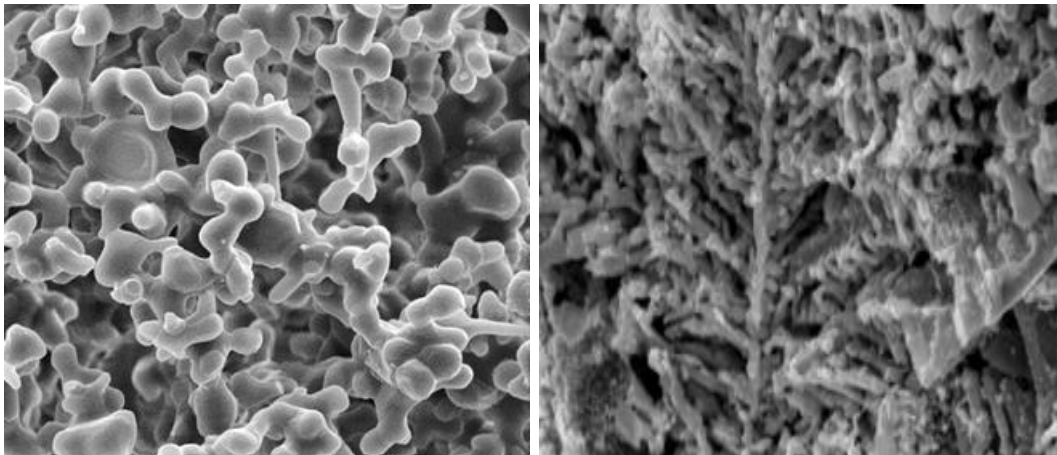


FIGURE II-5: *Alumina dendrites* [2:3]

As the solution flows through the nozzle, the precipitates of alumina will be subjected to a high pressure (resulted from the weight of the liquid) and to a high temperature. This will cause the first layer of them to sinter to the wall of the nozzle (**FIGURE II-6. A**). Since the process is continuous, alumina particles will continuously pass through that layer, and their dendritic form will allow them to adhere to each other, and compact under the pressure, forming a web (**FIGURE II-6. B**) that will transform

little by little into a clog, as shown in the simulation presented by Wen Yang et al. (FIGURE II-6. C), in an overall process of agglomeration. [2:5]

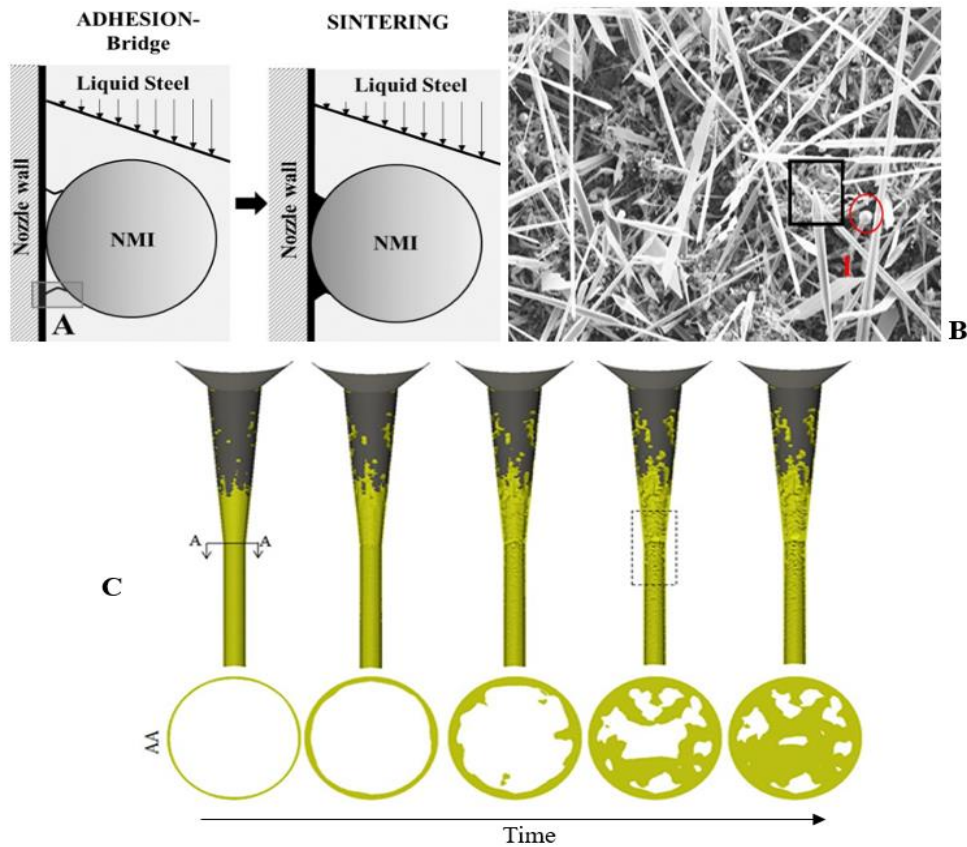
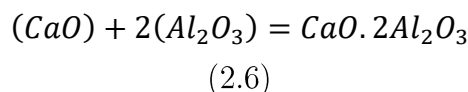
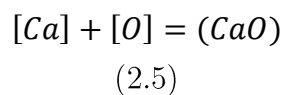


FIGURE II-6: Mechanism of nozzle clogging [2:5]

II.2.3 Solution to nozzle clogging

In the industrial field, calcium treatment is a common solution to reduce the effect of nozzle clogging (we say reduce since it is inevitable).

This treatment consists of adding some Ca-Si wire to the solution. In this case, calcium will react with oxygen to form calcium oxide, which will then react with alumina, following the equations (2.5) and (2.6) below [2:3]



The CaO reacting with alumina will complete the gaps of the dendritic form of the powder and make a substance ($CaO \cdot 2Al_2O_3$) with a pseudo spherical shape, which is much less likely to compact, in the opposite of the previous dendritic form, leading it to slide easily through the nozzle.

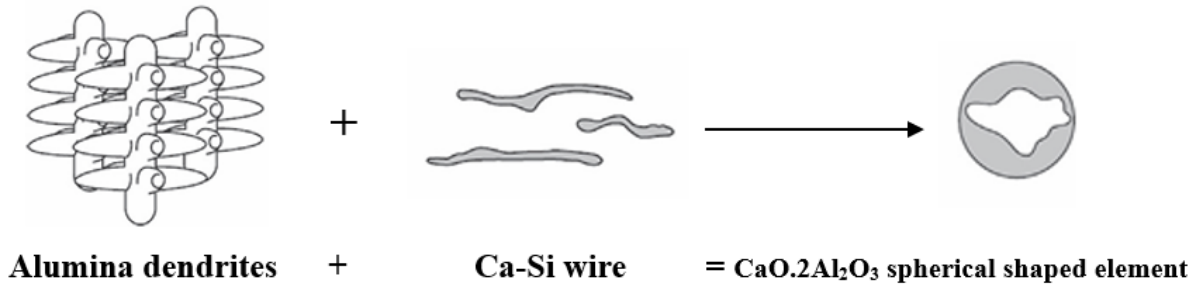


FIGURE II-7: Working principle of the calcium treatment

However, operators must be careful of two possible problems:

- (1) The quantity of the Ca-Si wire must be adequate for the alumina present in the solution. Insufficient amounts will force the CaO to catch more alumina molecules forming a $\text{CaO} \cdot 6\text{Al}_2\text{O}_3$, which will have the reverse effect of the original treatment, leading to speeding up the formation of the clog. For this reason, operators can refer to the calcia-alumina phase diagram (**FIGURE II-8**) or the works done by Roney Eduardo et al. to determine the right amounts of Ca-Si according to the aluminum rate [2:6]

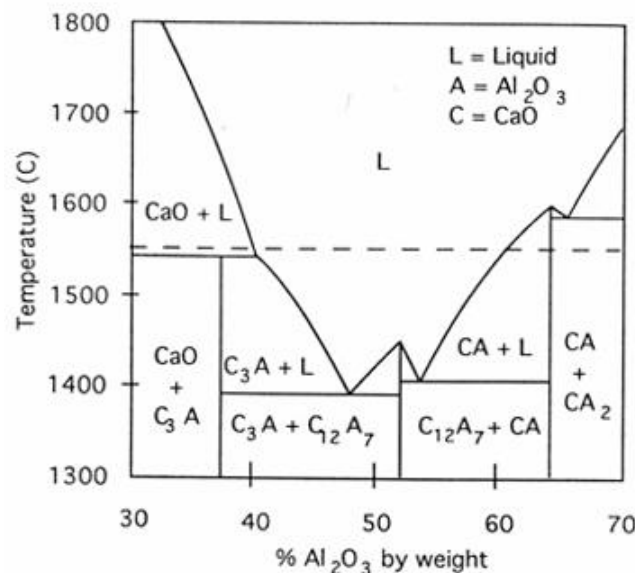


FIGURE II-8: Calcia-Alumina ($\text{CaO}-\text{Al}_2\text{O}_3$) phase diagram [2:6]

The dashed line represents the typical work temperature for the CCM (1560°C to 1580°C)

- (2) This solution cannot be applied to steels with high amounts of sulfur, because in this case, calcium will preferably react with it instead of oxygen of alumina.

II.3 Effects on steel composition: Formation of inclusions

II.3.1 Types of inclusions related to aluminum

According to the chemical composition of steel and whether it has been treated with a Ca-Si wire, we can distinguish many types of inclusions in the steel structure. Since our work holds on low alloying steel the main types are:

- (1) Alumina inclusions: in case of the unuse of the Ca-Si wire, and since alumina is supposed to be homogeneously distributed in the solution (because it is mixed with argon during the process), the precipitates that don't enter in friction with the wall or the accumulating clogging layers will then slip and pass into the steel structure. Using a microscope, we can see them as some black discontinued lines (**FIGURE II-9. A**).
- (2) Calcium-treated alumina: in this case, the spherical-shaped inclusions will be observed in the steel structure (**FIGURE II-9. B**). The stoichiometric numbers between the CaO and the Al_2O_3 depend on the weight percentage of calcium and aluminum molten in steel. Results are given by Xiaobao LI et al. at a temperature of 1873K (1600°C) in the following graph (**FIGURE II-9. C**). [2:7]
- (3) Aluminum nitrides: when cooling the metal as it solidifies, aluminum tends to react with the dissolved nitrogen and form AlN inclusions, which tend to precipitate in the grain boundaries of the structure. The creation of these inclusions can be further favored during the heat treatment processes that could be done later in practice.

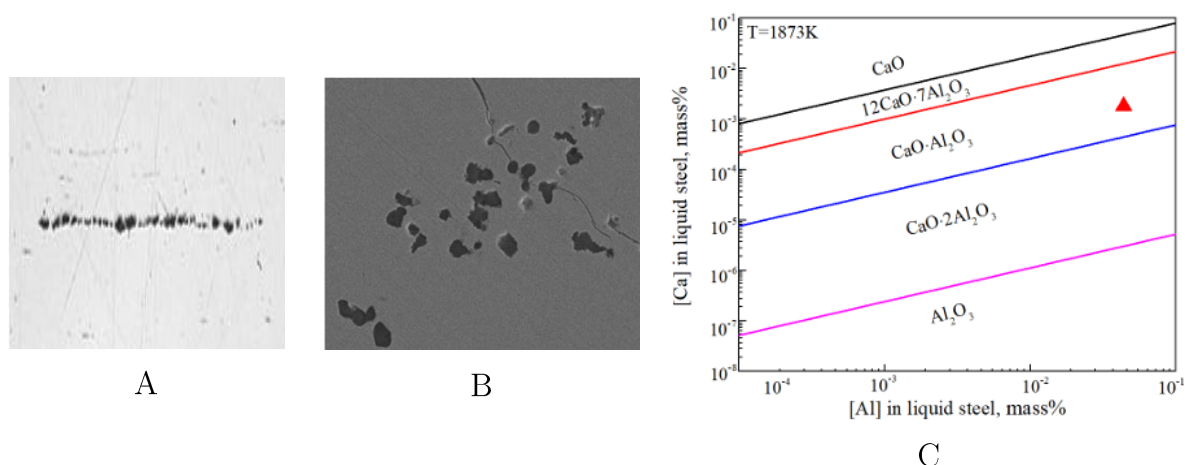


FIGURE II-9: Forms of aluminum inclusions found in steel [2:7]

II.3.2 Mechanism of the formation of the alumina inclusions

Up until now in this chapter, we have been talking repeatedly about the alumina inclusions, and we noted that they are produced according to the chemical equation (2.3). However, in this subsection, we will describe the mechanism behind their creation.

According to the documentation [2:8,9], the creation of the alumina inclusions starts early in the steelmaking process.

When iron pellets are put into the EAF, and as the temperature starts to augment, iron forms at an early stage some FeO inclusions already, they are called primary inclusions. When aluminum is added to the mixture to deoxidize it, solid aluminum favors to locate near those inclusions because of its oxygen affinity, creating an oversaturated area. At a higher stage of the temperature, the aluminum is liquid and englobing the FeO inclusion, reaching a level where the iron is molten, and then the oxygen atoms are freed, yet caught again by the aluminum, forming the alumina. The melting point of this substance is extremely above the temperature of the mixture at this level (2027°C vs 1620°C), meaning that this substance will solidify by a nucleation mechanism. This means that the quantity of free aluminum and oxygen decreases (as the reaction advances directly), while the quantity of alumina increases, which leads to a point where this position isn't over-saturated anymore, and then the nucleation stops starting the second step of growth, fueled by the diffusion of the elements (Al and O) through the liquid steel. When big enough, the oxide particles tend to separate from liquid metal and agglomerate, transforming into the actual dendritic formed shape shown before in this chapter.

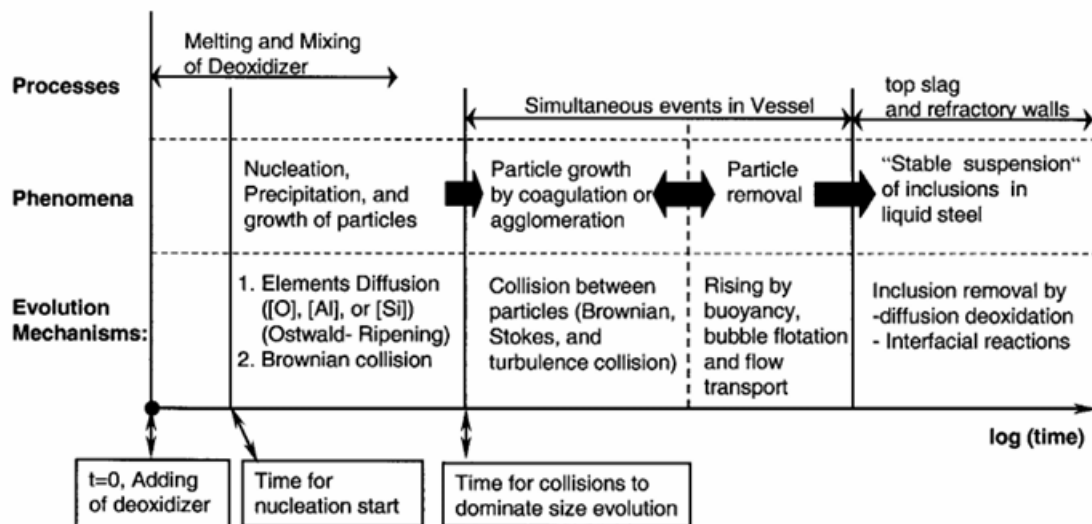












FIGURE II-10: Mechanism of formation of inclusions [2:10]

II.3.3 Effects of inclusions

When involved in the steelmaking industry, the cleanness of steel is a term frequently said to refer to a product with the minimum of inclusions (since they are impossible to avoid) in its structure. These inclusions can have a very bad effect in function of their diameter.

The *following table* resumes the possible results that might be obtained in the structure of the final steel product after rolling:

TABLE II-1*: *Behavior of inclusions before and after rolling*

Type	Description	Before rolling	After rolling
(a)	A hard inclusion under rolling conditions		
(b)	A hard crystalline inclusion broken during rolling		
(c)	A hard inclusion cluster strung out during rolling		
(d)	An inclusion composed of hard crystals dispersed in a soft matrix		
(e)	A soft inclusion under rolling conditions		

As we can see in the *table above*, the types of aluminum inclusions mentioned earlier are matched to the cases (a) for the Ca-Si treated type and (c) for the non-treated type (where the shape resembles **FIGURE II-9-A**).

The hard inclusions aren't deformable. They break and create a gap between the fragments; moreover, they detach from the metal, leaving two sharp-shaped voids on either side of the inclusion. Even small (on the order of a few micrometers), they can cause internal chevron-shaped cracks during wire drawing. If their quantity is very high, the cavities caused by the a-type inclusions after rolling can develop into cracks in the final structure, as shown in the *figure below*:

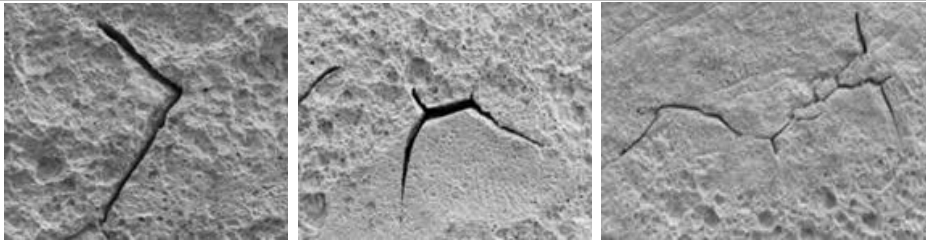


FIGURE II-11: *Micrography of cracks on rolled steel at different concentrations of inclusions [2:11]*

This is why, when the analysis of the chemical composition of the steel shows a high concentration of non-metallic inclusions, the rolling isn't processed, and the steel billet is considered as failed and reused as scrap in future heats.

II.4 Effects on steel structure: Grain size control

II.4.1 Formation of grain boundaries

As the solidification of steel starts, it is launched by a nucleation mechanism. Thermodynamically, two types of nucleation are distinguished:

- *Homogenous:* This is the case where there are no impurities in the liquid steel. It is always considered as the perfect case, where all conditions are optimized.
- *Heterogenous:* This is the case of the presence of impurities. It reflects what happens in reality, where conditions might be slightly or highly different than the perfect conditions.

When they are created, the solidified nucleus will augment in volume within a diffusion mechanism to become steel grains, characterized by having crystallin directions. However, since the nucleation appears to be a random phenomenon (which means even the same substances in the same conditions wouldn't react the same way), the grains of steel will thus have all different directions. When all the steel is finally solidified, and grains are all put beside each other, limits between those with different crystalline directions can be seen, they are called grain boundaries (**FIGURE II-12**).

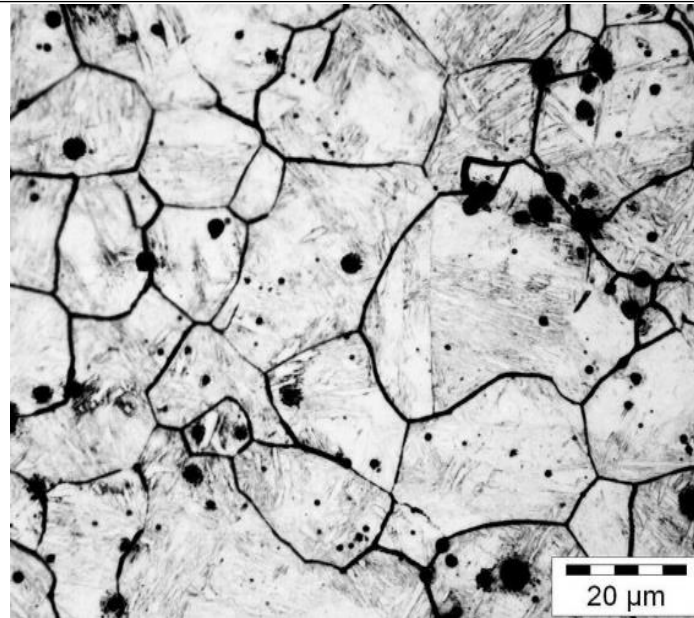


FIGURE II-12*: *Micrography of austenitic phase in steel where grain boundaries are clear*

According to this, we can deduce that grain boundaries are the limits of grains. The expansion or the shrinking of these grains is then defined by their ability to push these boundaries. The difficulty of this task is directly related to the composition of these limits.

II.4.2 Precipitation of AlN inclusions

When they are formed in steel, aluminum nitride inclusions tend to precipitate at the grain boundaries for two major reasons:

- (1) Crystallin structure of the metal:

The AlN inclusions have a hexagonal structure [2:12] while the austenite (the first steel phase that forms when cooling from liquidus) has a face-centered cubic structure. As the inclusions have a significant size, their only way to form a solid solution with the metal is through occupying substitutional sites. However, we mentioned before in the fundamentals chapter that according to Hume-Rothery, two substances can form a substitutional solid solution only if they respond to some conditions, and one of them is to have the same crystalline structure.

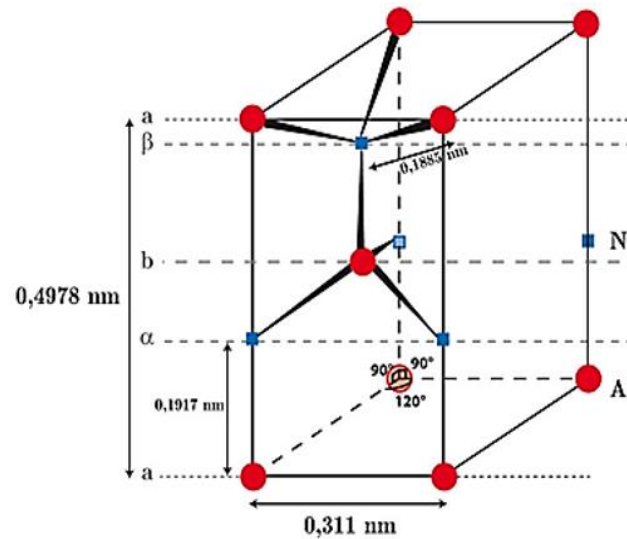


FIGURE II-13: *Crystalline structure of AlN inclusions [2:12]*

With this being said, as the solidification and the precipitation proceed, AlN inclusions are pushed into the grain boundaries.

(2) Thermodynamics of the grain boundaries

The grain boundaries have a bunch of characteristics that are suitable for the processing of heterogeneous nucleation (since this mechanism is activated through the presence of impurities as we mentioned before). Consequently, the intergranular diffusion coefficient becomes significantly higher than the volume diffusion coefficient, allowing segregated atoms to migrate rapidly toward any critical second-phase nucleus within a grain boundary. High intergranular segregation leads to the saturation of the grain boundary with solute atoms, facilitating the formation of precipitates. Additionally, grain boundaries serve as regions of high crystallographic disorder with high vacancy concentrations, areas richer in foreign atoms, and regions of high-stress concentrations. These conditions promote the preferential nucleation and growth of aluminum nitrides along the grain boundaries rather than within the bulk steel structure. [2:13]

II.4.3 Consequences on grain size

The aluminum nitride inclusions precipitate in the grain boundaries, they will strengthen them, leading to an increase of the difficulty of the change of the grain size. As a result, when the mixture is solidifying (the time when liquid atoms are supposed to transform into grains), the grains' growth is restricted since their limits cannot be pushed forward, thus they'll remain in a small size (**FIGURE II-14**). With all this being said, we can synthesize by saying that aluminum reduces the grain size.

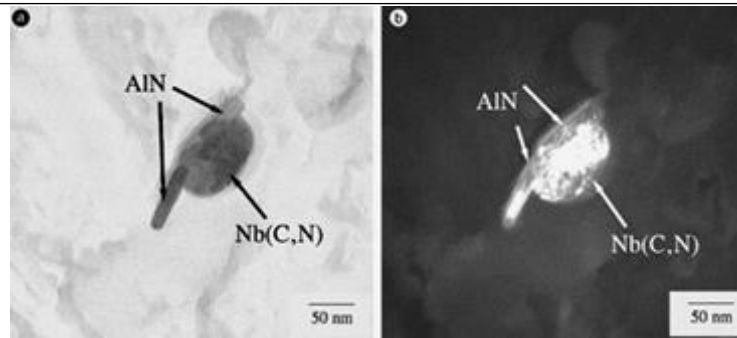


FIGURE II-14*: Aluminum nitrides at the grain boundaries are blocking its size growth

II.5 Effects on steel mechanical properties

The mechanical properties of materials are defined in metallurgy as their behavior under the application of loads to cause a deformation in them. On the macroscopic scale, a deformation is observed as the geometric form of the material changes (rupture, torsion, flexion...). Deep inside the structure of the material at a microscopic scale, a deformation is justified by the creation of the displacement of the defects (vacancies-1D, dislocations-2D, and/or grain boundaries-3D). As a result, it is logical then to deduce that the effects on the mechanical properties of steel are just reflections of the effects on the grain size.

Previously, we have shown that aluminum leads to refining the grains in steel, i.e., reducing the average grain size. This can have several significant effects on its mechanical properties, such as:

- Strength improvement: By reducing the grain size, both the yield strength and tensile strength of the steel tend to increase. This is due to a greater density of grain boundaries, which act as obstacles to plastic deformation and strengthen the material.
- Increased hardness: Grain refinement also increases the hardness of the steel. The greater number and tighter spacing of grain boundaries impede plastic deformation, making the material more resistant to penetration or indentation.
- Toughness enhancement: While hardness increases with grain refinement, the toughness of the steel can also improve. The small grain size can reduce the size of crack propagation zones, making the material less prone to brittle fracture and more capable of absorbing energy before fracture.

- *Ductility improvement:* In some cases, grain refinement can also enhance the ductility of the steel, i.e., its ability to deform plastically without fracturing. Smaller grains facilitate plastic deformation by allowing more uniform material deformation.

II.6 Bibliographic synthesis

Through this bibliographical chapter, we have mentioned much of the fundamental information about the various aluminum effects on the steel structure. These effects can be observed in multiple stages, starting from the steelmaking process itself where aluminum is added as a deoxidation agent to reduce the potential defects caused by oxygen, however, we saw that it can lead to a clogging appearance at the continuous casting machine nozzles (cured by adding Ca-Si wire), into the modification of the steel properties through the formation of alumina and aluminum nitrides inclusions.

Meanwhile, a lot of documentation sources cover the possible effects of aluminum on steel, it is of high importance to note that these effects are directly linked to the steel grade and the quantity of aluminum in each of the respective studies. With this being said, the principal difficulty that we faced during the research phase is that none of these bibliographic references cared to test the effects of as small amounts of aluminum as 0.005%, such a small amount that it is usually judged to have little to no effects at all, in the opposite way, the least amount we could find in any of the studies we found was around 0.05% which is ten times higher than the amounts we are expecting on our studies.

Aside from the effects on the processing (deoxidation and the nozzle blocking) since we verified them directly through our internship in AQS, a question about the remaining effects stated in the bibliography must be asked: “Do trace amounts of aluminum really affect the properties of the steel? And if they do, what’s the scale of this affection? Is it even measurable?”

It is the objective of this work to test the validity of the various effects of aluminum on steel properties to answer the previous questions.

References:

- [2:1] Techniques de l'ingénieur. M3624. Link : [Élaboration de l'acier moulé - Analyse des processus métallurgiques : Dossier complet | Techniques de l'Ingénieur \(arn.dz\)](#). p14-17.
- [2:2] Mirzadjanova S.B., Yusupkhodjayevev A.A., Saidova M.S., Matkarimov S.T., Khatamkulov V.X. *Research of the Possibility of Upgrading of the Melted Steel Pumping Out Process*.
- [2:3] Rackers, K., and B.G. Thomas. 78th *Steelmaking Conference Proceedings*, Nashville, TN, April 2, 1995, Iron and Steel Society, Warrendale, PA, Vol. 78, 1995, pp. 723-734.
- [2:4] F. Haers et. al., "First Experience in Using the Caster Tube Change Device (TCD90)", Fourth International Conference on Continuous Casting, 1988.
- [2:5] Wen Yang, Lifeng Zhang, Ying Ren, Wei Chen, Fenggang Liu. *Formation and Prevention of Nozzle Clogging during the Continuous Casting of Steels: A Review*. 2023
- [2:6] Roney Eduardo et al. *Influence of the chemical composition on steel casting performance*.
- [2:7] Xiaobao LI, Nan WANG, Min CHEN and Zhiqiang. *Effect of Molten Steel Composition on Inclusion Modification by Calcium Treatment in Al-Killed Tinplate Steel*. 2022
- [2:8] [Soudage aluminothermique des rails de chemins de fer : Dossier complet | Techniques de l'Ingénieur \(arn.dz\)](#) p.6-7
- [2:9] [Inclusions non métalliques dans l'acier : Dossier complet | Techniques de l'Ingénieur \(arn.dz\)](#) p.8-11
- [2:10] Lifeng et al. *NUCLEATION AND GROWTH OF ALUMINA INCLUSIONS DURING STEEL DEOXIDATION*. P.464
- [2:11] Heng Cui, Kaitian Zhang, Zheng Wang, Bin Chen, Baisong Liu, Jing Qing and Zhijun Li. *Formation of Surface Depression during Continuous Casting of High-Al TRIP Steel*.
- [2:12] Guillaume JEANMAIRE. *Précipitation des nitrures d'aluminium AlN dans un acier maraging à très faible teneur en azote*. 2015. P. 13-43
- [2 :13] L. Priester. *Physico-chimie des joints de grains: ségrégation- precipitation*. 2009.

Note: All the pictures and tables with a (*) mark are taken from open sources found on the internet.

Chapter III.

Steelmaking Process

“Observation is a passive science,
experimentation an active science.

*Claude Bernard; a French physiologist and
considered one of the founders of
experimental medicine.*

Introduction to the chapter:

The first step in the realization of all the practical work that will lead us to the verification of the theoretical effects of aluminum is simply the elaboration of the test steel samples. This work has been done on the Algerian Qatari Steel complex at Bellara, Jijel. The entire elaboration process is done within a sequence: a bench of successive steps that are all dependent on each other; thus, any problem at any step during the process will block the chain and all the sections will turn into a maintenance mode.

As we stated briefly on index A about the definition of the complex, the main work passes through three fundamental production units: The DRI unit specialized in the transformation of raw material extracted from ores into a substance called CDRI, which is transported to be used in the next unit. The second step is the SMS unit, responsible for the fabrication of steel billets using the CDRI, the scrap, and, obviously, the alloying additions. Finally, the produced billets are transformed into the RM unit where they are rolled to make rebar and wire rods.

This chapter will then detail the process, starting from the quality control of the used CDRI (the elaborated steel was destined for exportation, so imported and maximally purified CDRI has been used, so we didn't follow the process of the direct reduction, also it is out of our subject so we wouldn't dive too much into it), and passing through the SMS main divisions: EAF, LRF, and CCM, finishing with the rolling operation.

III.1 Quality control of raw material

Before the introduction of any CDRI (imported or locally manufactured) into the steelmaking process, it needs to pass the quality control tests where its purity, properties, and high quality are subjected to examination. This is done to ensure that the used portions will not cause any form of trouble during the process that could stop the entire sequence, or that could reduce the lifetime of the machinery.

The tests are divided into two categories: physical controls where physical and mechanical properties are verified such as granulometry and resistance to compression; and chemical controls that serve for the determination of the composition of the CDRI, besides the detection and the quantification of all sorts of impurities.

III.1.1 Physio-mechanical controls

The samples are first subjected to the physical control methods. These tests aim to the determination of the mechanical properties as well as the preparation of the samples for chemical testing (since the CDRI pellets need to be transformed into powders so the tests can be applied).

a) Visual observations and sampling

In their as-received form, raw materials pellets have a reddish color characteristic of the iron oxide (III) Fe_2O_3 ; after the DRI process with the reduction of most of the oxide, the pellets are purified and contain a high quantity of iron in a deoxidized form, giving it a sort of a grey color (**FIGURE III-1**).

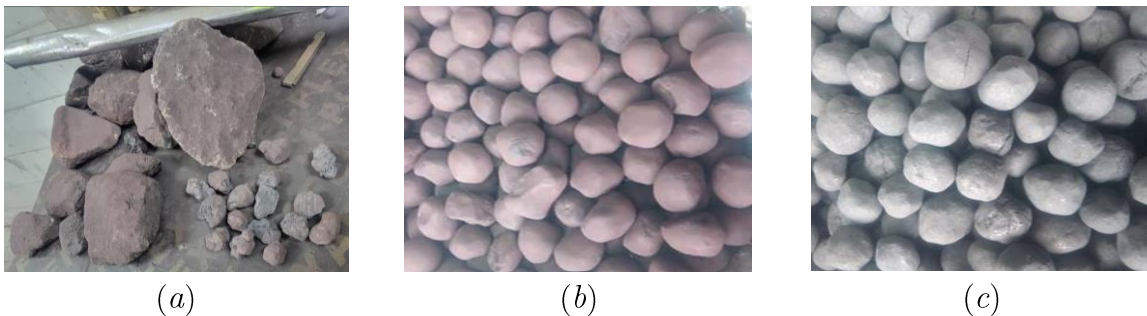


FIGURE III-1: Pellets at different stages of the DRI process

In its natural form, iron is present in the form of rocks rich in iron oxide III (a); they are then transformed into reddish pellets (b) which are then turned into CDRI for industrial use (c)

As, obviously, we cannot test all the tons of CDRI we are going to use, we need to extract a few samples out of the total quantity, however, the selected samples need to be chosen carefully so they can be representative of the overall pellets. Imported CDRI is received in bags, the operator selects randomly a few of them and takes small amounts

of each one. The quantity taken is mixed in using a dedicated manual machine. Finally, a quantity of about 2kg is taken for testing



FIGURE III-2: *Sampling of the CDRI*

b) Humidity test

The first physical test is the determination of the humidity rate in the CDRI, samples are put inside a furnace and heated to a temperature above 100°C (generally under 120°C) for 4 hours.

Initial and final masses of the sample are measured, so the humidity ration could be calculated using the formula:

$$\text{Humidity (\%)} = 100 \cdot \frac{M_0 - M_1}{M_0} \quad (3.1)$$

c) Granulometry

To avoid the suffocation of the EAF, large CDRI pellets cannot be used during the elaboration process. Thus, a granulometry test should be applied to determine the diameters of the pellets. The dedicated machine is composed of several meshes with different opening sizes, scaled from the widest placed on the top to the thinnest placed on the bottom. CDRI samples are placed above the first mesh and are mechanically vibrated for a short duration under a specific frequency.

At the end of the testing period, each mesh will block a quantity and will let the rest pass through it. The **ISO 4701:2019** regulation followed in the complex specifies that the average diameter of the samples must not be above 16mm nor under 9.5mm with 90% of the sample having diameters within this range. If this condition isn't verified, the CDRI is disqualified and a complaint paper is sent to the exporter (if it is exported), or it is redirected to the DRI unit for amelioration (if it is local).

The average diameter of the pellets can be calculated if we measure the masses of the pellets blocked at each mesh respectively, we define then the mass ratio of the blocked quantity, and use the following formula for calculations [3:1]:

$$\overline{\phi}_m = O_1 X_1 + \left(\sum_{i=2}^n \left(\frac{O_{i-1} + O_i}{2} \cdot X_i \right) \right) + \frac{O_n}{2} X_p \quad (2.2)$$

Where: O_i is the diameter of the opening of the mesh ranked I;

X_i is the mass fraction of the pellets blocked by the mesh ranked I, defined as:

$$X_i = \frac{m_i}{M} \quad (2.3)$$

m_i is the mass of the pellets blocked at this step, and M is the total mass of the sample;

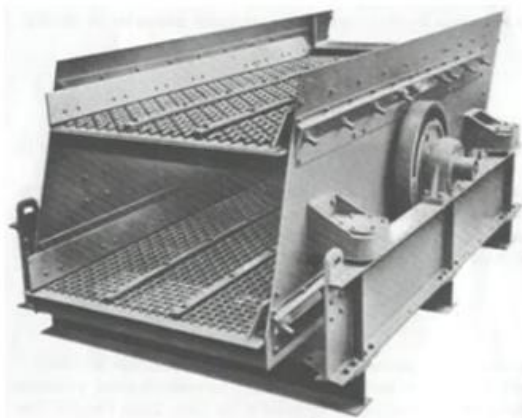
X_p is the mass fraction of pellets that fell into the plate.



(a)



(b)



(c)

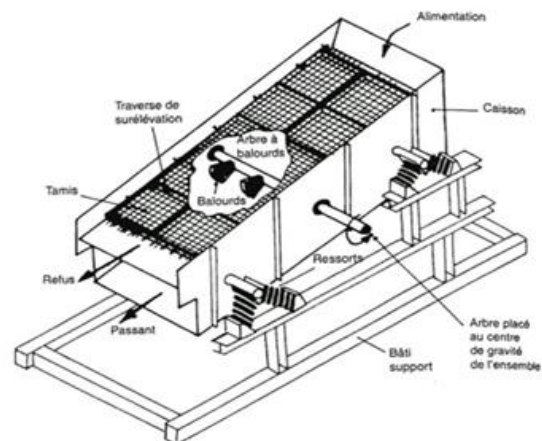


FIGURE III-3: Mechanical granulometry test (*for c)

The test could be applied using manual meshes or automatic ones. The ones represented in images (a) and (b) are only used for quality control purposes. Generally, pellets out of the previously specified range are taken out of the quantity, the granulometry in this case requires a bigger machine to deal with all the tons (c)

The samples of the used CDRI gave the following results when submitted to the granulometry test:

TABLE III-1: Granulometry test results

Diameter, d [mm]	19.0	16.0	12.5	9.5	6.3	3.3	<3.3	[9.5; 16[
Ratio, X [%]	0	9	58.51	31.5	0.75	0.03	0.2	90.01

These values can be represented graphically on the following curve which corresponds to the theoretical Gaussian bell (representative of normal distribution in statistics).

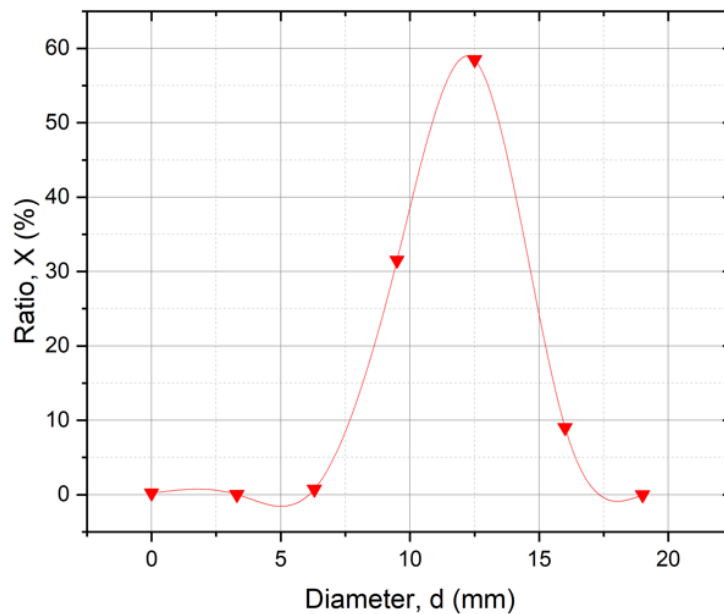


FIGURE III-4: Pellets size distribution in function of their diameters

d) Compression crushing test

To ensure good resistance to crushing and according to the ISO4700 standard, at least 60 pellets per bulk sample of the raw material with sizes ranging from 9.5 to 16 mm are tested. The operation consists of applying a progressive force through a hydraulic press and measuring the resistance in Kg/pellet.

This test is very important to avoid any sort of block that could reduce the efficiency of the EAF or even damage it. The accepted pellets should have a crushing resistance of at least 250 kg/pellet. If most pellets don't conform to this criterion, directions are sent to the DRI unit to adjust the parameters of the reduction process, which include: temperature, reducing gases flux, cooling gases flux, and the charging/discharging speed.

III.1.2 Chemical controls: oxides determination

In contradiction to the mechanical controls, chemical ones deal with CDRI in the form of powder instead of pellets. The transformation is done following the international standards for the succession of steps: drying, crushing, pulverization, and granulometry.

The first test to be applied is the XRF analysis to determine the overall composition, which will then be followed by oxide determination tests.

The working principle of the detection and the quantification of oxides in the CDRI samples is quite simple with some knowledge of chemistry science. The work starts with the preparation of the test solutions, following the following steps:

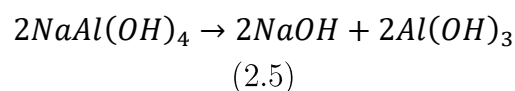
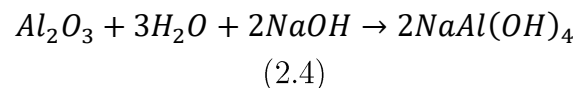
Step 1. The CDRI powder is dissolved into a combination of acids (most commonly HCl and HNO₃) to dissolve it. In this case, other oxides (impurities) will precipitate in the mixture.

Step 2. The dissolution operation is done on a heater at temperatures between 70 to 90°C (under the boiling point of water), so the nitric gases would evaporate, with the addition of HClO₄ acid.

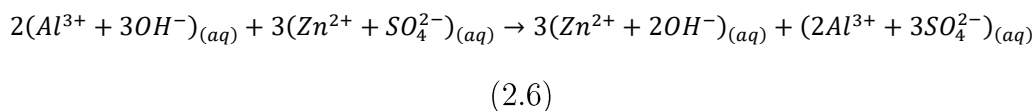
Step 3. The solution obtained is filtered in a membrane and the oxides are recovered (SiO₂, Al₂O₃, Cr₂O₇, P₂O₅, ...).

Then, the obtained precipitate is dissolved in water, mixed, and divided into portions of 25mL each. For each portion, coherent reactive is added to quantify the respective oxide. As our project focuses on aluminum and alumina, we will take this substance as an example.

In the case of alumina, a solution of NaOH (50% purity) is added to the portion, forming aluminum hydroxide according to the chemical reactions chain:



We add a color indicator to the mixture (the xylenol orange), and a color-based titration is applied using sulfates of zinc (ZnSO₄) solution. The titration chemical equation can be written as:



The determination of pH and volume added at the equilibrium phase will help determine the initial quantity of alumina.

Results of this test as well as those for the rest of the oxides will be mentioned and discussed in the last chapter (V) in the chemical characterization.

III.2 Elaboration process

The steelmaking process, or elaboration process is the term that describes the sequence which will lead us at the end to the obtention of the steel samples. In our project, we will treat only the steel melt shop (SMS) unit, since this was the location of our internship. The other units of the sequence are the DRI (direct reduction of iron unit) and the RM (rolling machines unit).

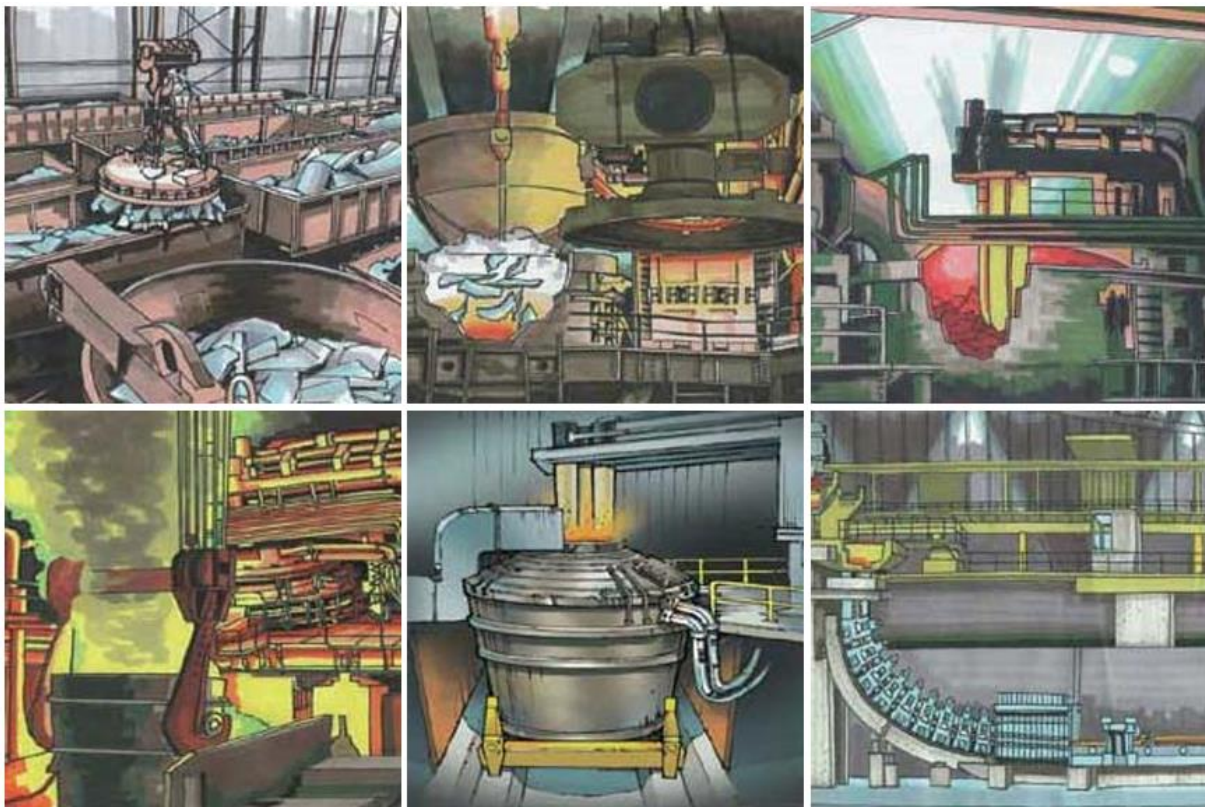


FIGURE III-5: *Steel melt shop main steps* [3:4]

III.2.1 Electric arc furnace (EAF)

Today, the metallurgy of steel elaboration has widely evolved from its historical ancient image. Modern large steel complexes use either the blast furnace or the electric arc furnace for their productions.

Being more recent, the EAF presents some good qualities that make it a better choice than its competitor, the BF, as shown in the following comparison *table*:

TABLE III-2: Comparison between the blast furnace and the electric arc furnace
[3:2,3]

	Blast furnace	EAF
Raw material	Iron ore only	Iron ore, scrap, recycled metal
Energy source (Cost*)	Coke is the main source (Expensive)	Methane gas, chemical reactions (Economic)
Environmental impact	Harmful (Coke reaction leads to the creation of CO)	Environment friendly (Methan releases CO ₂)
Productivity	Around 1h30min or more for 120T of steel	38-47min per heats of 120-140T
Efficiency	60 to 70%	Up to 95%

***Note:** The cost is judged economic for the EAF regarding the abundance of natural gases in Algeria, this could be different at foreign locations.

The secret behind the good stats we get for the use of the EAF lies behind its advanced working principle that is evolving since the creation of the process lately in the 19th century by Paul Héroult. The work is done following the steps presented below. [3:4]

a) Furnace loading

Two modes of furnace loading can be selected according to the nature and composition of the raw material we use. The two methods are:

- (1) **Bulk loading** for loads that contain less than 20% of CDRI pellets which means that this mode is favored in the cases where scrap metal constitutes the majority of the load. All the charge is added at once to the furnace.
- (2) **Continuous loading** for loads that contain more than 20% of CDRI. The load is introduced continuously to the furnace so at the end of the process it will all be added. For example, if we have to load 120T of raw material, and the overall process duration is capped at 48min, then the selected flow will be calculated as 120T/48min, equal to 2.5T/min.

b) Creation of heat energy

The temperature inside the furnace must be high enough to melt iron. It is generally recommended by the industrials to raise it up to levels of 1620 to 1640°C. Three modes of energy supply are implied in this operation:

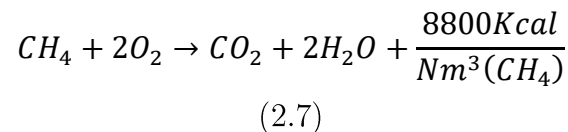
- (1) **Short circuit** mode, ensured by the three electrodes attached to the furnace. A high electric current passes through them, and the electric circuit is closed by the

electric conductivity of the charge. High temperatures are generated. (We use three electrodes to create an energetic whirl in the CDRI and create a heat flux in a larger area).

Table 2-3: *Influence of electrodes' length [3:4]*

Long Arc	Short Arc
Low electrode consumption	High electrode consumption
Melts scrap away from the electrode	Melts scrap under the electrode
Will cause greater refractory wear rate	Will cause less refractory wear rate
Might be dangerous for water-cooled panels if arc is excessively long	Provides adequate protection for water-cooled panels

- (2) Although the first mode can be enough by itself to melt all the quantity, in this case, it would be very consuming and expensive, so industrials just prefer to use a secondary mode which is less costly, that is the **burner mode**. Methane is combusted creating additional energy to push the temperature into higher levels, following the chemical reaction:



- (3) The last heating mode is more automatic and natural, which is the **exothermic chemical reactions** that will release automatically more heat in the mixture. An intuitive example of this mode is the combustion of the carbon content in the raw material producing CO₂.

c) Composition control

If the operator starts the process directly when all the load is added, the resulting steel will not have an adequate composition. So, the latter needs to be adjusted. In this first step, we focus more on the adjustment of the carbon content, as in most cases, we either need to increase it or decrease it. For the first purpose, we must add a calculated carbon flow to the mixture while we need to introduce an oxygen flow for the second purpose.

At this step, most of the oxides we found earlier during the quality control will rise in the mixture due to density difference, forming the slag. In contradiction to the common sense of people, slag plays a very beneficial role in the process, since it:

- Absorbs the arc radiation,
- Increases the stability of the electric arcs, leading to less power losses,
- Decreases the hydrogen and nitrogen (harmful gases for the process) levels in the bath,
- Reduces the electrical disturbances and noise,

- Lowers the consumption rate of electrodes

d) Furnace unloading

At the end of the time duration, the upper layer of the EAF content is mainly the slag, the furnace is equipped with a high exit so the slag will automatically leave when its quantity is too excessive. The molten metal is unloaded into a ladle and directed to the next step of the process. The EAF is equipped with and put on giant gears that give it the rotation ability. The operator gives then the command, and the EAF rotates at around 20° unloading its content in the ladle.

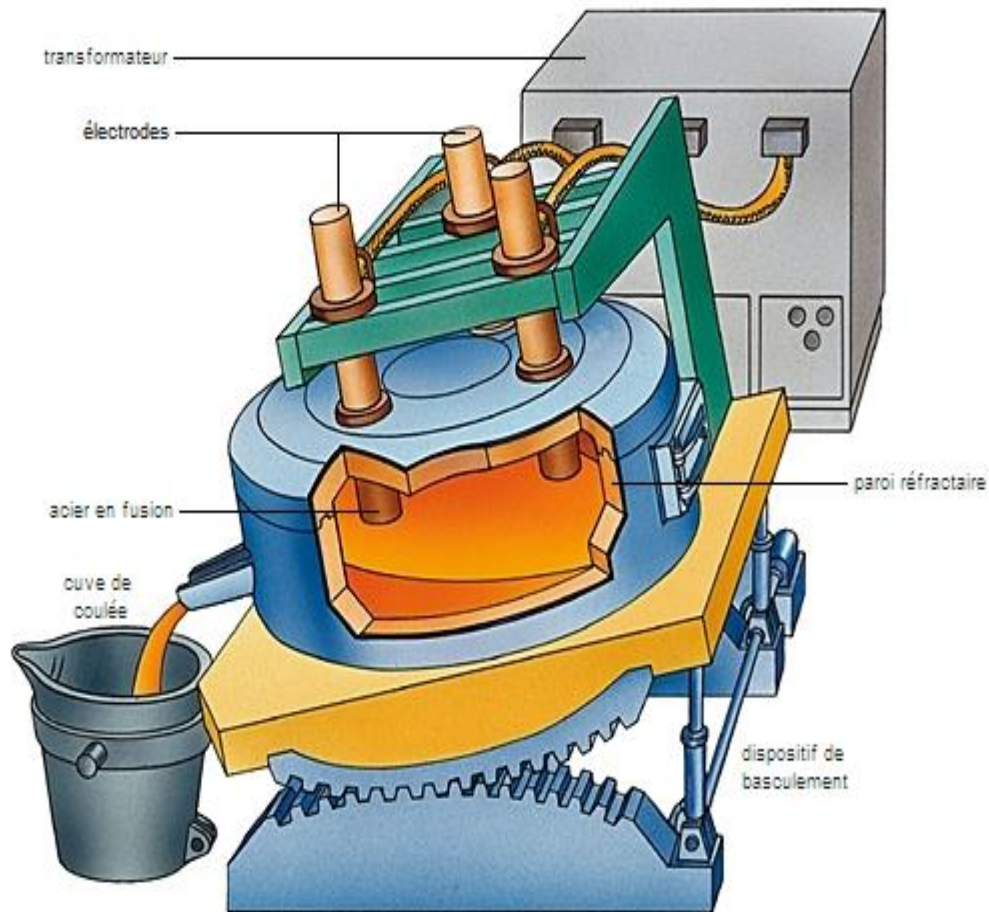


FIGURE III-6*: *Furnace unloading*

III.2.2 Ladle refining furnace (LRF)

The second step in the process is the LRF, also commonly known as the secondary refining (since this step is generally optional for steel complexes; those that don't do it just transfer its tasks to the EAF).

Basically, the LRF is just a small EAF, with technically the same working principle, of whom the objective is to adjust exactly the chemical composition.

At this level, chemical additions are added. At different times, a sample is taken from the mixture, sent to the quality control laboratory, and submitted to the XRF test for the verification of the composition. If it is not adequate, it must be either less or higher than the necessary level. In the first case, additional quantities are added, while in the second, the ladle content is split into two ladles, and the content of the next heat is added to the actual one, and they are both treated together. At the end, another sample is sent for the XRF test for verification.

Although this step is quite simple, and doesn't take too much time (around 10 to 15 minutes only), it is actually very important, since the composition, and yet all the future properties of the elaborated steel rely on its accuracy.

Two additional operations that are crucial and which can be held at the LRF are the desulfurization and dephosphorization, by the introduction of manganese and oxygen respectively, since the two elements are considered impurities when present in steel (see chapter I).

Besides, even though the slag formation happens automatically, it can be favored by the addition of slagging agents such as lime and dololime. This step is important to reduce the amount of any excessive non-metallic inclusions.

At the end of the LRF process, the ladle is transported to the last and final step of the steel melt shop.

III.2.3 Continuous casting machine (CCM)

The CCM is the dedicated machine for the fabrication and the obtention of the steel billets.

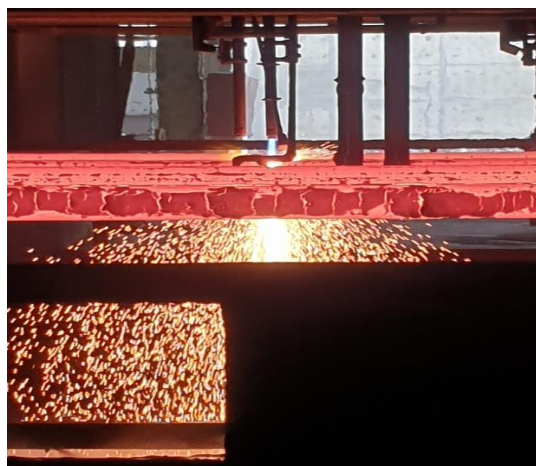
The ladle holding the molten metal with adjusted chemical composition is placed on the top of the machine. Gravitational power will do its part of the work, and the liquid falls into a tundish; container equipped with five exits, linked to five independent molds, making it possible to elaborate five billets simultaneously (note that the SMS of the AQS complex is equipped with 2 EAFs, 2 LRFs and 2 CCMs, making it possible for 10 billets to be produced in the same time).



(a) *The ladle is placed above the CCM; its content is unloaded in the tundish by gravitational forces*



(b) *The bending curve in the machine; billets have a soggy composition being solid in the interior and solid on the exterior*



(c) *A laser is programmed to cut the billets every 12m*

FIGURE III-7: *Different parts of continuous casting*

Each heat has an average weight of 120T, while one single billet weights around 2T, so, sixty billets are produced per heat, when produced in groups of five, this makes them distributed into 12 groups per heat, each takes an average duration of 3min, so the CCM process takes a duration of 36min, added to the average 12min of the LRF and 48min of the EAF, it takes then 1h36min (96min) for 120 tons of CDRI pellets to be transformed completely into billets (to be compared with the 1h30 duration of only the blast furnace, without counting the duration of casting).

The CCM available in the AQS is the bent type, which means that it transforms from a vertical to a horizontal direction during casting. This operation requires precise control of the solidification of the steel, because if it solidifies earlier than the bending spot it will not be able to change its direction and will block the sequence, and if doesn't solidify just at the ending point of the curve, the laser cutter risks to cut the external surface and molten liquid metal will spread causing great damages. So, the solidification is ensured by a water spray and air convection. The water spray is applied in different zones with different flows that need to be precisely calculated to avoid the previous problems.

During the work, and before arriving at the laser cutter, the billet has three different zones:

- (1) **Liquid zone** before the curvy part of the machine,
- (2) **Soggy zone** at the curvy part. This zone is characterized by being solid at its external surface, while it is still liquid in its interior. This property gives the billet the ability and the softness required to change its direction.
- (3) **Solid zone** after complete solidification at the leaving point of the curvy part.

The machine is also equipped with rollers that direct it all along the path.

Further away, a laser cutter is programmed by the operator to cut every measured 12 meters, forming the billets.

On the demand of the next unit, the recently produced billets can be directly transported to be rolled in the next unit, as this would save time and energy (it doesn't require to be re-heated to the hot working temperature of 1150°C). Otherwise, heat ID is labeled and the billets are transported into the inventory to be either sold, cold rolled into rebar, or hot rolled into wire rod.

References:

[3:1] A. Kasser. [Chapitre II] Caractérisation qualitative des matériaux en poudre. 2024.

[3:2] Thomas Hay et al. A Review of Mathematical Process Models for the ElectricArc Furnace Process. 2021.

[3:3] KINTEK tech team. What is the difference between a blast furnace and an EAF?. Last check date: 08-06-2024. Link: [What Is The Difference Between A Blast Furnace And An Eaf? - Kintek Solution \(kindle-tech.com\)](https://www.kindle-tech.com/what-is-the-difference-between-a-blast-furnace-and-an-eaf/)

[3:4] Amir Mishriky. The melt shop process. Al Ezz Rebar company. 2005. 38p.

Note: All the pictures and tables with a (*) mark are taken from open sources found on the internet.

Chapter IV.

Methodology & Experimental Procedure

“It is a capital mistake to theorize before one has data.

Arthur Conan Doyle; a British crime writer and creator of the legendary Sherlock Holmes, master of deduction.

Introduction to the chapter:

In the last chapter, we checked the bibliography about the possible effects of aluminum quantities on steel properties. As we also said, most of those effects were observed at quantities of aluminum that are at least ten times higher than the rates we normally would deal with in our project. We then asked a question about how many of those properties could still be effective at trace levels.

Ultimately, the effects of aluminum on the steel structure could be summarized according to what we saw before in the following five points: Deoxidation of the molten steel mixture; Formation of nozzle clogging in the continuous casting machine; Formation of inclusions; Grain size reduction; Improvement of the mechanical properties.

As the first two points can be checked directly during the steelmaking process, they can be trivially verified, since the aluminum's affinity to oxygen is commonly known in materials science, and the nozzle clogging has been spotted and pictured during the elaboration of samples.

With this in mind, the three remaining properties still need to be verified experimentally through tests. In this chapter, we aim to describe the work done to verify these properties.

IV.1 Test samples' manufacturing

Before we engage in the processing of the experiments, test samples should be manufactured to make them compatible with the standards required by the testing machinery.

For our study, the specimens that we are using are taken from two steps of the steelmaking process, we have samples from the steel billets and from the wire rod obtained by hot rolling. The obtention of these samples is acquired while the elaboration is going through. Thus, the form and the outer surface of the as-obtained specimens will be irregular and inadequate for testing, which will make it necessary to proceed with some preparation before running the tests.

These preparations include shaping the specimens to make their forms as regular as possible, heat treatments as we aim to verify the effect of the aluminum on heat-treated samples too, surface cleaning through grinding and polishing, and finally chemical etching (before the use of the optical microscope).

IV.1.1 Specimens cutting and milling

In their initial form, specimens were obtained as cuts from billets and wire rods. Smaller samples need to be taken out of them. For this purpose, we follow the following path to make them suitable for experiments:

- (1) Using a caliper, we measure and draw boundaries for the coherent dimensions of our specimens.
- (2) A semi-automatic hydraulic hacksaw is used to cold-cut the samples under a flow of special oil lubrication according to the dimensioning applied in the previous step. As the saw works with a material tearing-off principle, we apply our cut a little bit further than the suitable position to avoid the obtention of samples that are smaller than we aim for.
- (3) At the end of the cutting operation, and as we intentionally cut samples at higher dimensions, also due to the softness of the samples, their form will not be perfectly shaped, needing then a correction to adjust it. For this purpose, samples are exposed to milling.
- (4) To facilitate the manipulation, small rolling samples receive also mounting using a polymeric resin powder. Hot-mounting involves enclosing the sample in a polymeric powder that melts at about 200°C, with pressure applied to ensure a high-quality, porosity-free mold. This method ensures intimate contact between the sample and polymer, unlike cold mounting, which can suffer from porosity and etchant seepage issues. Thus, hot-mounting is preferred if resources allow and the sample is heat-resistant. [4:1]



(A)



(B)

FIGURE IV-1: *Cutting and milling of test samples*

As we will deal with three heats of steel with different rates of aluminum, and since we will apply different conditions on samples of the same steel, we need to produce eight samples for each grade six from steel billets and two from wire rods, making then a total of twenty-one (7x3) test sample that is going to be manipulated throughout our study.

IV.1.2 Heat treatments

a) Description of the applied heat treatments

To study the effect of heat treatment (annealing) conditions on the structure of these steel grades, and determine whether aluminum enhances or reduces its efficacy, samples should be subjected to heat at different temperatures and different holding times. Through this phase, we apply the following treatments on each of the three grades of the billets:

TABLE IV-1: *Heat treatments' conditions*

Code	Heat temperature (°C)	Holding time (h)
HT 1	800	3
HT 2	1000	3
HT 3	1100	3
HT 4	1100	6

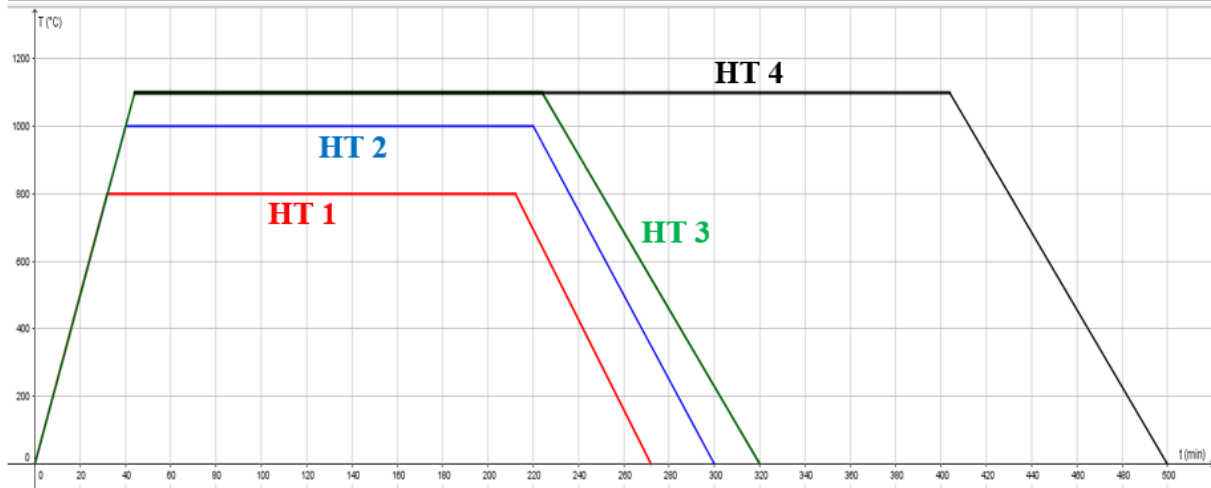


FIGURE IV-2: Heat treatment curves for tests

We use HT 1, HT 2, and HT 3 to determine the effect of heating temperature on the structure, while HT 3 and HT 4 are also used to determine the effect of the holding time on the structure.

b) Operating the heat treatments

Heat treatments were applied using a dedicated programmable furnace. Operating includes the following steps:

- (1) We select one sample from each steel grade for the specific heat treatment and put them in the furnace. The furnace used works with the heat induction principle, where resistance is electrically heated and transfers the heat to the substance by convection.
- (2) The next step is to adapt to the heating conditions. First, the heating temperature is introduced. Then the heating rate is selected. In our condition, the selected rate is 25°C/min. And finally, the holding time is defined.
- (3) At the end of the holding time, the furnace is automatically shut down, and the cooling phase starts. The operator has the choice to cool the samples inside the furnace for extra-low cooling speed, cool in ambient air atmosphere for moderate speed, or apply a quench in oil or water for harder substances. In our treatments, the first choice is taken.

IV.1.3 Grinding and polishing

After cutting, milling and/or heat treating, the samples present unclean surfaces that can hold many imperfections such as scratches, raids, corrosion, and other problems that can be disruptive to the microscopic observations of specimens. So, it is very necessary to clean these surfaces to get coherent and good observations. The cleaning process is done by grinding and polishing the faces of the substances designated for the microscopy test.

a) Mechanical grinding

This operation is mainly used to reduce the damage caused by previously done sectioning. Generally speaking, this means reducing the size of the particles in such a way that the surface of the material is ready for polishing. In this step, it is necessary to be cautious in order not to produce greater damage than the one caused by cutting [4:2].

In our test, we used for this step silicon carbide papers of different grades, which mainly are: 120, 240, 400, 600, 800, 1000, and 1200 grades. We occasionally used the 80-grade paper especially for heat-treated samples since they have got a calamine layer on their surface that is a little bit harder to remove. Also, 180, 320, and 500-grade papers were sometimes used for a smoother transition from one paper to another in cases where the surface was highly damaged or if excessive pressure was applied during the polishing using the previous paper.

The operation of this step is done by maintaining the sample constant on the paper that turns on with a speed of 150 to 300 rounds per minute, under a sufficient water flow to reduce the heat resulting from the shear forces, and to clean the paper from the residues of the steel and the paper's grains they are detached due to the friction. We use each grade of paper for around three to five minutes per sample, and then we move to the next grade with a rotation of the sample by 90° from its previous position. In this case, we should see at each step that there are no clear surface defects, but only stripes can be seen, and they must be all directed in the same direction for the same grinding paper. From a paper grade to the following, we must observe that stripes are getting finer and finer until they are hardly seen on 1200 paper.

b) Final polishing

At the end of the previous step, and if all goes well concerning the direction and the size of stripes, we move to the final polishing step where a mirror-like surface must be obtained, totally exempt of stripes and scratches. For this purpose, we use a special polishing cloth on the polishing machine and move the samples in the opposite way of the rotating direction of the disc. At this step, lubrication is done with fine alumina solution, with a grain size of 9 microns, instead of water. At this stage, stripes cannot be visually seen and can be detected only on microscope images. The final suppression is done using a diamond spray with a grain size of 1 micron, and only after this, stripes are completely removed and cannot be detected even by the microscope.



FIGURE IV-3: Grinding (A) and polishing (B) machines

IV.1.4 Chemical etching

After all the grinding and polishing steps, we need to apply etching to obtain microscope images of the present phases on the sample (called micrography). For this reason, etching needs to be applied.

For steel, etchant solutions are generally combinations of acids and alcohols. Commonly, Nital solutions are used with different concentrations and different holding times in the etching solution.

a) Chemical etching work principle

When applying the etching on the steel, we can notice that it reveals the grain boundaries as well as the present phases. The mechanisms behind these revelations are quite different, as the first relies on electrochemical properties, while the second relies on light refraction.

(1) Revelation of grain phases

The etching mechanism of a multiphase structure is based on its electrochemical properties. When the sample reacts with the etchant, a potential difference arises between the different phases. The phase with the higher electropositive potential acts as a positive electrode and begins to dissolve during etching. Conversely, the other phase, acting as a negative electrode (cathode), remains unchanged. To prevent over-etching, the concentration of the etching solution and the duration of the process must be optimized. As the positively charged phase dissolves, it creates craters. During microscopic analysis, these craters appear dark because light cannot reflect off these regions. In contrast, the negatively charged phase reflects light, resulting in a bright appearance.

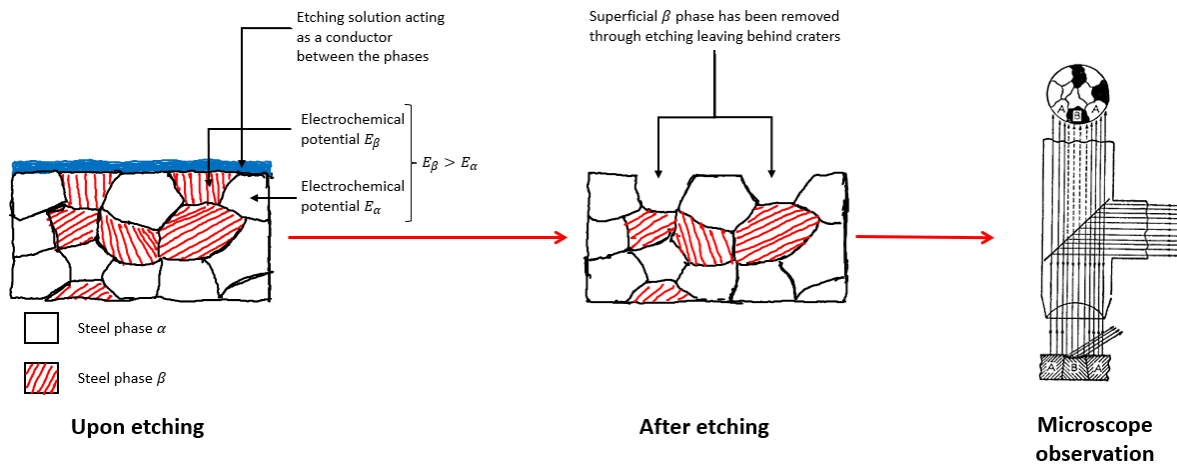


FIGURE IV-4: Revelation of grain phases etching mechanism

(2) Revelation of grain boundaries

In this case, the etching mechanism relies on an electropositive process because the potential difference between the matrix material and inclusions, or between the bulk material and grain boundaries, is so small that detecting any differences is highly challenging. The goal is to observe differentiation in the grains based on their dissolution rates. Grains with the same orientation exhibit the same brightness when viewed under an optical microscope, a phenomenon known as "oriented grain brightness." This difference becomes particularly noticeable during long etching processes. Grain boundaries, having higher energy compared to the bulk material, preferentially dissolve upon contact with the etchant, resulting in the formation of cracks along the valleys.

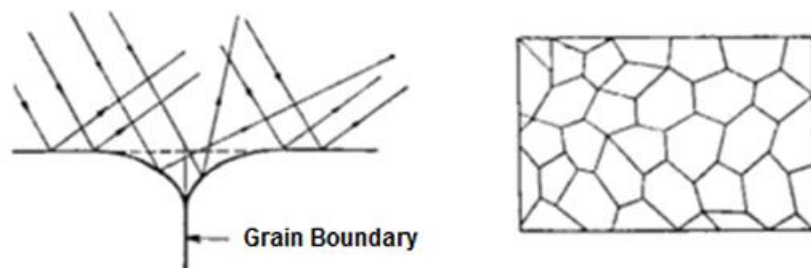


Figure IV-5*: Revelation of grain boundaries etching mechanism

b) How to select the coherent etchant

The chemical etching agent is selected through a large variety of etchants according to the nature of the studied material and the objective of the operation. The bibliography [4:3,4] provides a large documentation rich of data that helps the metallurgist to make a good choice corresponding to the purpose of the study. The *following table* lists the most commonly used etchants for steel alloys and their functions.

TABLE IV-2: Common plain steel etchants and their functions [4:3,4]

Etchant	Materials	Composition/use	Notes
Nital	Plain-carbon and low-alloy steels	1–5 ml HNO ₃ in 100 ml of ethanol or methanol. Immerse sample for several seconds	General microstructure for most steel welds. Develops good contrast of ferrite at prior austenite grain boundaries
Picral	Plain-carbon and low-alloy steels	4% (saturated) solution of picric acid in ethanol or methanol. Immerse sample for several seconds	General microstructure for most steel welds. Provides better detail of fine structure than nital
Super picral	Alloy steels	Same solution as above, but with a few drops of HCl. Immerse sample for several seconds	This etchant is often used for heat-treated microstructures
Vilella's	Alloy steels	5 ml HCl, 1 g picric acid, and 100 ml ethanol or methanol. Immerse sample for several seconds	Used for alloys steels containing chromium. Reveals prior austenite grain boundaries in martensitic and bainitic microstructures
Macroetching	All steels	2–25% HCl in ethanol. Immerse for several minutes to reveal general structure	Reveals overall weld outline and is used for procedure development. Sample surface should be ground to an approximate 240 grit condition for best contrast

As we deal with ferritic steel and we aim to check over the microstructure, we chose for our study to use a 4% Nital solution (i.e. for a volume of 100mL of etchant, we mix 4mL of nitric acid with 96mL of ethanol), with a holding time between 7 to 10 seconds.

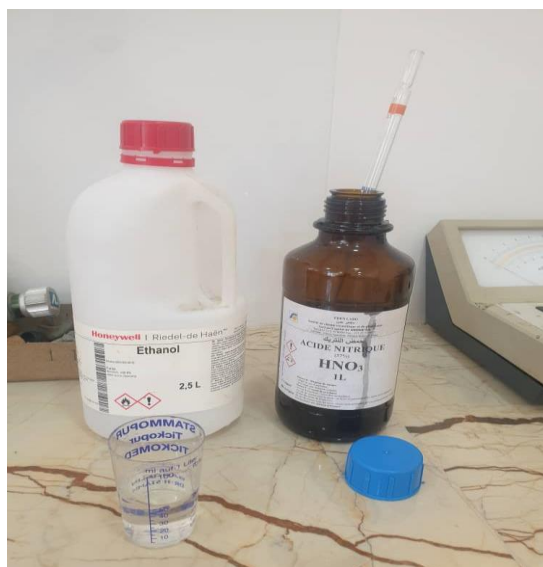


FIGURE IV-6: Preparation of Nital etchant

IV.2 Characterization tests

Materials characterization is key field in materials science and engineering that involves the analysis and measurement of a material's structure, properties and performance. This process is very important to understand the behavior of materials under various conditions. These types of tests will lead us to detect the effects of the additions on the properties of the steel for the validation of bibliography.

In our work, we will amplify tests of characterization of different types: chemically to determine the exact composition of steel, structurally to determine the present phases and the variations of the grain sizes and mechanically to check if these changes would affect the practical properties of the materials.

IV.2.1 Chemical characterization

The chemical characterization of the steel samples is applied to determine the exact compositions of the steel samples. For this purpose, an X-rays fluorescence (XRF) analysis alongside with elementary analysis through ELTRA O-N 900 machine are run on the specimens obtained from the CCM's mold. The first test will then give us the ratios of the alloying elements in the specimen, while the second test will give us information about the total oxygen and total nitrogen inside them.

a) XRF working principle [4:5,6]

The XRF analysis works following a spectroscopic principle. The work is mainly done by subjecting the sample to a powerful light providing a photonic energy. If sufficient energy is supplied, it will interact with the atom's inertial electrons from the K orbital causing them to be kicked out. Almost immediately, a relaxation process takes place, with an electron from upper orbitales will go down to fill in the gap left by the leaving of the previous one. This operation is accompanied with an energy release in form of photons, known as specter which will spread in form of a wave.

The dimension of the specter and the energy of the released will then depend on the previous position of the deexcited electron. Specters are named following the initial and final positions of the deexcited electrons according to the Siegbahn notation, as shown below:

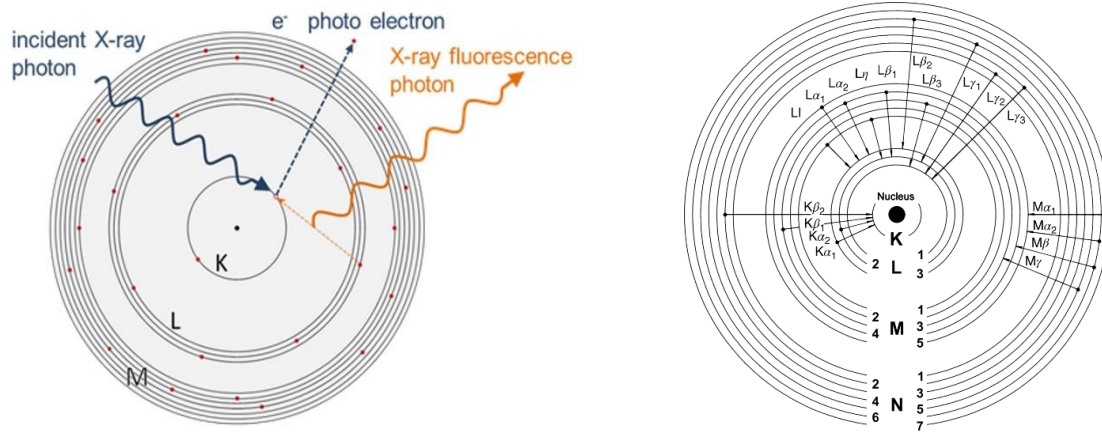


FIGURE IV-7*: Atom excitation and deexcitation alongside with Siegbahn notation for specters

The energy released by this process is actually the kinetic energy of the resulting photons. It can be expressed as:

$$E = \Delta W = W_{down} - W_{up} = h\nu = \frac{hc}{\lambda} \quad (3.1)$$

Where: h: Planck's constant, ν : frequency, c: light celerity,

λ : wave length of the fluorescence photon

With this in mind, we notice that the equation contains a couple of varying parameters: the wave length and the energy. Thus, the basics behind the XRF, is controlling one of them and then measuring the response on the other:

- In the case where the energy is the input and the wave length is the output, the process is called EDXRF. In this case, an X-ray tube emits light beams with controlled energy that hit the sample and reflect into a detector (**FIGURE IV-8-A**). This process gives fast results with a low cost, but results are less accurate compared to those obtained in the second case (**FIGURE IV-8-C**).
- The second type is known as WDXRF. In this case, the wave length is the input and it is controlled by changing the light intensity of the incident beams, while the energy is the output. For this test, an analyzing crystal is added between the sample and the detector (**FIGURE IV-8-B**). This test is certainly more accurate, but presents otherwise an expensive cost and a slow processing.

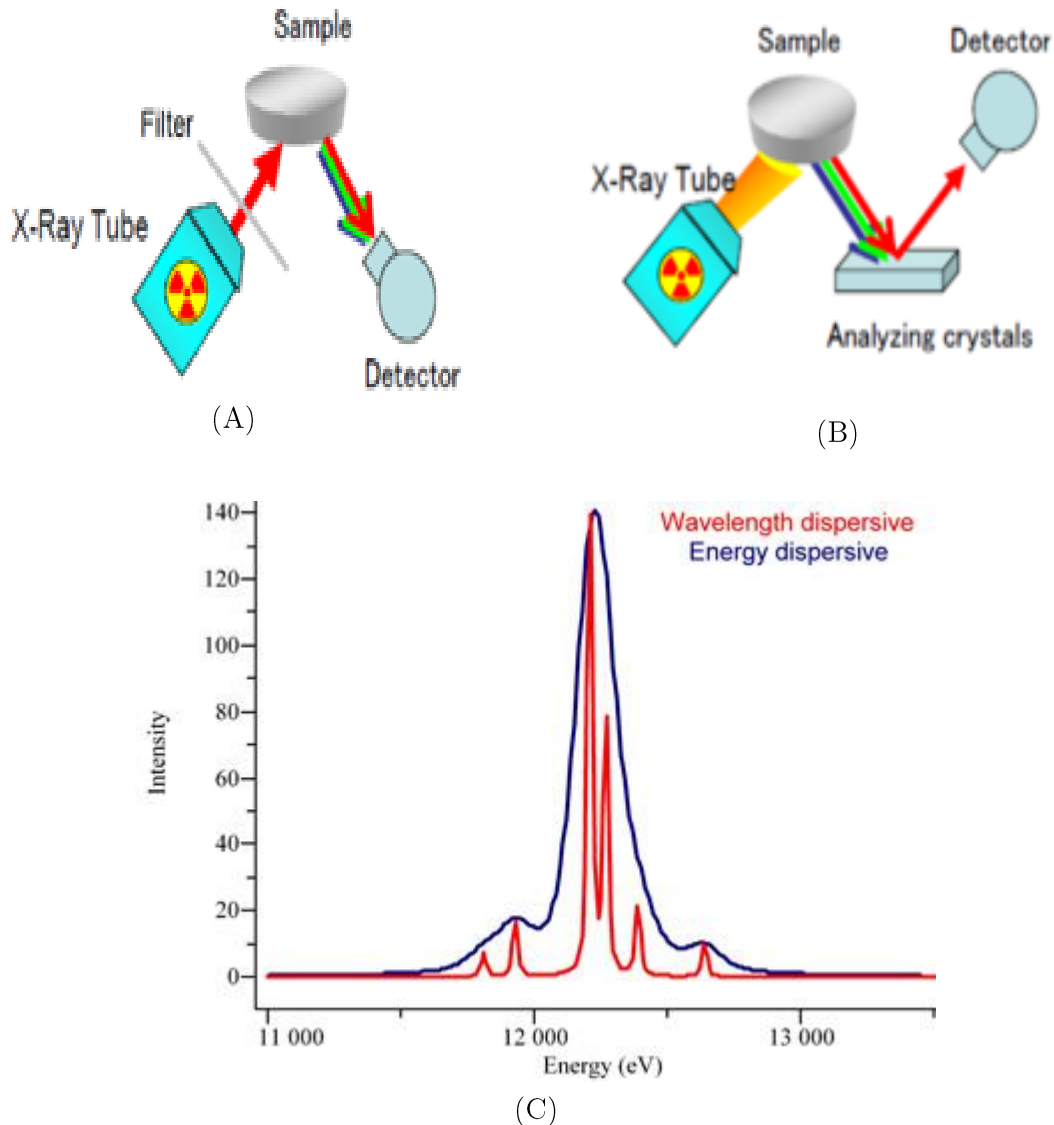


FIGURE IV-8*: Comparison between EDXRF and WDXRF work principle

A and B: equipment comparison, C: intensity (wave length) vs energy curves' comparison. We can see peaks are thinner in the wave dispersive curve then in the energy dispersive one which translates into higher accuracy. Also, many peaks are seen only on the WD-curve but remain undetectable on the ED-curve.

b) T[O] and T[N] determination

Total oxygen and total nitrogen in steel are determined using an ELTRA O-N 900 machinery.

In order to run the analysis on the samples, they must be put into a graphite crucible which has been placed on the lower electrode and then elevated to make contact with the upper electrode of the impulse furnace. A high current pass through the crucible to create a high temperature (up to 2000°C). The gasses extracted during fusion are directly analyzed after the dust filter. The oxygen present in those steel samples is then turned into CO and CO₂, while the nitrogen transforms into N₂.

(1) NDIR:

The quantity of oxygen is directly determined and deduced from the quantity of CO and CO₂ gasses, which is calculated by a *non-dispersive infra-red* principle. The method is quite similar to the XRF test, with the main difference remaining on the type of the light we use, as this time it is infrared-light beams.

The light is sent from a source and passes through a chamber containing the gasses resulting from the heating. In this method, we are more interested by the wave number γ instead of the wave length. The two of them are simply linked with the formula:

$$\gamma = \frac{1}{\lambda}$$

(3.2)

Experience shows that if we send a definite number of waves into the gas, some of them pass through while the rest are absorbed (**FIGURE IV-9-A**). A physical amount of transmittance is then defined and plotted in function of wave number (**FIGURE IV-9-B**). The computer system will then analyze the plots and define the quantity of the corresponding CO and CO₂ and deduce the corresponding total oxygen.

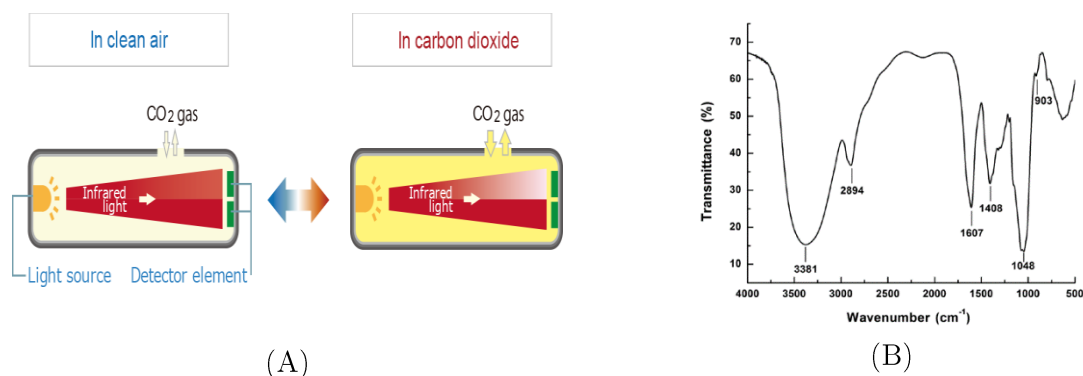


FIGURE IV-9*: NDIR working principle

In figure A, we can see that the infrared-light intensity hitting the detector in clean air medium is way bolder than in the CO medium where it is nearly transparent. Actually, transmittance in function of wave number is characteristic to the species of the medium and gives the possibility of quantifying the percentage of the oxygen in it.

(2) TCD:

A thermal conductivity detector (TCD) operates on the principle of measuring the thermal conductivity of a gas sample compared to a reference gas. The detector consists of an electrically heated filament, typically made of tungsten or platinum, placed in a flow cell through which the gas sample and reference gas pass. The thermal conductivity of the gas affects the rate at which heat is dissipated from the filament. When the sample gas, which has a different thermal conductivity than the reference gas (usually a carrier

gas like helium or nitrogen), flows over the filament, it causes a change in the filament's temperature. This temperature change alters the electrical resistance of the filament. By measuring the change in resistance, the TCD can determine the difference in thermal conductivity between the sample gas and the reference gas. The magnitude of this change is proportional to the concentration of the target gas in the sample. The TCD is known for its simplicity, sensitivity to a wide range of gases, and ability to provide continuous measurements, making it useful in applications such as gas chromatography and monitoring of industrial processes [4:7].

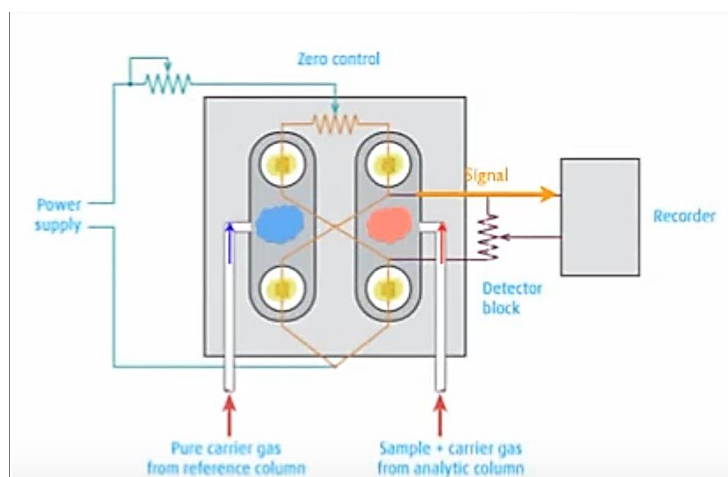


FIGURE IV-10*: TCD working principle

c) Experimental operating

(1) XRF test:

With the advanced technology available today, especially in such a big steelmaking leader as AQS, the XRF characterization test require little sample preparation with only mechanical grinding being indispensable.

Step 1. Samples obtained from the CCM mold in form of medallions receive firstly a quick grinding at 80 paper grade silicon carbide paper.

The objective of this step is to delete the calamine layer that covers the sample when it cools down from the molding temperature. In fact, calamine is a form of metallic oxides that precipitate on the interface of the sample when it is heated to temperatures above 500°C, and cooled in an oxidating atmosphere. If it is let unremoved, it will prevent the XR beams from reaching the interior parts of the sample, which will lead automatically to a miss calculation of the composition.



FIGURE IV-11: *XRF test sample*

On the left: in its as obtained state, directly cooled from the CCM mold, covered with calamine;

On the right: the sample after mechanical grinding at 80 grade Si C paper

Step 2. A quick cleaning of the sample holder must be applied.

Sometimes, dust and residues from previous tests can fall into the sample holder and create a form of a boundary between them. If this happens, the test can't be done, and the machine is directed to maintenance.

Step 3. If cleaning is done, and the sample is grinded, then the test is ready to be run. The sample is placed in the holder, and a signal is sent by the operator from the computer to start the amplification.

Step 4. After few seconds, the chemical composition is directly presented on the computers screen.

At this step, the obtained chemical composition is compared to the steel grade requirements tables determined by the standards. If the composition is in the good range, then testing is successful. If not, there must be a problem either from the machine or the heat is simply unconfirm, in which case it needs to be re-melt in the EAF and to be reproduced again. This judgement is taken by calibration of machine, as we use a certified sample and run the test on it. If results are good in this case, then previously, the problem was in the heat. Else, then if the test works wrong even with the calibrating sample, then there is a problem with the machine and it is put to maintenance.

(2) Total oxygen and nitrogen determination test:

The equipment ELTRA ON 900 available at the Quality Control lab of AQS has the ability to run simultaneously both the NDIR and TCD tests.

Step 1. The machine must be calibrated using certified steel before running the experience.

The calibration is important before every use of this experience for two principal reasons: the first is because the nitrogen and oxygen quantities are generally very small (in order of just few ppm) so calibration is done to adjust the sensibility of the machine. The second reason is because this test isn't done for every heat since the XRF results are usually enough for the quality control.

Step 2. Using a drill, we make a hole in the sample taking away some steel of it in form of steel fillings.



FIGURE IV-12: *Sample preparation for ELTRA ON 900 tests*

Step 2. Fillings are placed into the machine.

Step 3. Calibrating gas in form of helium is introduced, and the command of starting the test is given from the computer.

Step 4. After a while, the computer receives the test results, analyzes them and gives them to the operator in form of numerical values.

IV.2.2 Structural characterization

The structural characterization is done in order to check the effects of the aluminum and those of heat treatments and deformation on the structure of the steel, as this latter will have some direct effects on the mechanical properties. For this purpose, optical microscopy will be used for qualitative and quantitative characterization of the structure, while the scanning electronic microscopy will be used for inclusions analysis, in terms of shape and composition.

a) Optical Microscopy for phase determination

Optical microscopy is the main experience we firstly apply in order to characterize the steel samples metallographically. This is typically due to many reasons, such as:

- The relatively cheap cost of such equipment (compared to other equipment for more advanced and specialized use),
- The easy manipulation and operating process, as well as the interpretation of the obtained images,
- The non-complexity of its working principle.

b) OM working principle and operating

In order to generate the microscopy (microscope photography), a light will be created from a source (a lamp) in order to be projected on the studied specimen. The light intensity can be controlled thanks to the condenser lens. When it hits the sample, some regions will appear as bright, while other regions will look obscure and dark, due to the effect of the contrast we created before (during the chemical etching step). The observation of the image is then done as the reflected light travels through the magnification objective we are using, and then it will pass through the ocular (which has also its own magnification) ending the path by being caught by the operator's eye. Some optical microscopes have an integrated camera; thus, micrographs can be seen on an attached computer and pictures can be taken (**FIGURE IV-13**).

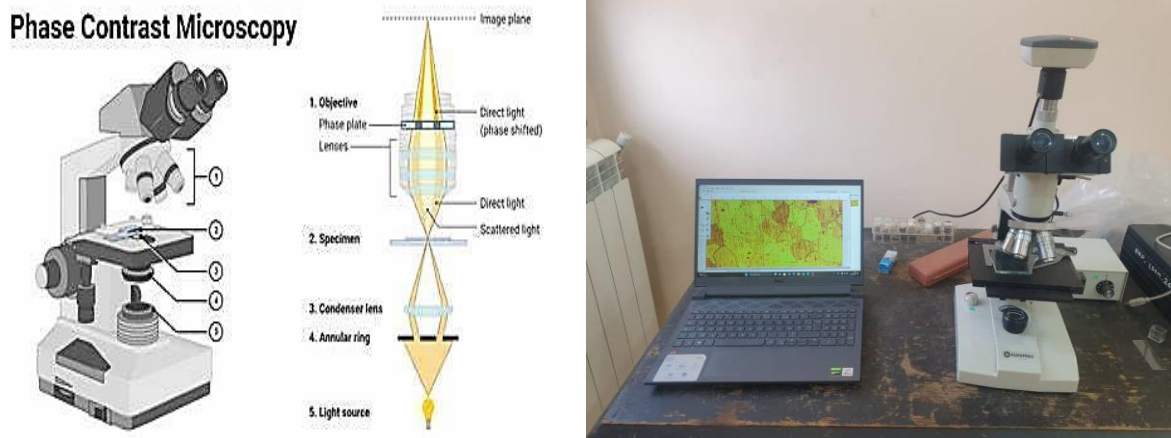


FIGURE IV-13: *Optical microscope components*

With this in mind, the operating process of the optical microscope will follow the following steps:

Step 1. Sample preparation: grinding, polishing and etching.

Step 2. Sample is placed in its dedicated localization. Light intensity and coherent magnification through the objectives are selected.

Light intensity can be controlled from the side panel on a scale from 1 (most obscure) to 10 (brightest). Otherwise, five different objectives with varied magnifications are available on the used microscope, as shown on the *following table*:

TABLE IV-3: *Magnifications available on the laboratory microscope*

Ocular magnification	Objectives magnification	Overall magnification
10	4	40
10	10	100
10	20	200
10	40	400
10	100	1000

Step 3. Using the camera attached to the microscope and the image we see on the computer's screen, we scan the surface of the sample to check over and select the areas with the fewest (or preferably with none) of the stripes left, and we picture it.

Many pictures must be taken for the same sample in order to get a well representative micrography, and the interpretation will be correct.

Step 4. Scales are introduced into the figures and pictures are saved into well-organized files on the computer.

c) Methodology of micrographs analysis

Micrographs provide many valuable information about the grains and the treatments applied on specific sample. Data are extracted from them through qualitative analysis, where we describe only the aspect of the pictures, and through quantitative analysis as we do some calculations and give some numerical values to confirm our constatations (**TABLE IV-4**).

TABLE IV-4: *Methodology of micrographs analysis*

Type of analysis	Deduced information	Methodology
Qualitative	Present phases	Comparison of the grains' colors and shapes
	Phase and heterogeneities distribution	Visual evaluation of the grains and inclusions positioning
	Effect of heat treatment	Visual estimation of the variation of the steel grains' size
	Effect of deformation (hot rolling)	Observation of the directions of the steel grains on the structure

Quantitative	Effect of heat treatment	Calculation of the grains' sizes and areas
	Effect of deformation (hot rolling)	manually (based on the norm: ASTM E112) and numerically using ImageJ
	Effect of composition	software.

☞ ASTM E112 specifications [4:8]

In order to determine the grain size and area manually, we use the interception method indicated on the standard specifications. The method consists briefly on five steps:

Step 1. Draw three co-centric circles with different (and known) radiuses on any spot of the micrography (**FIGURE IV-14**).

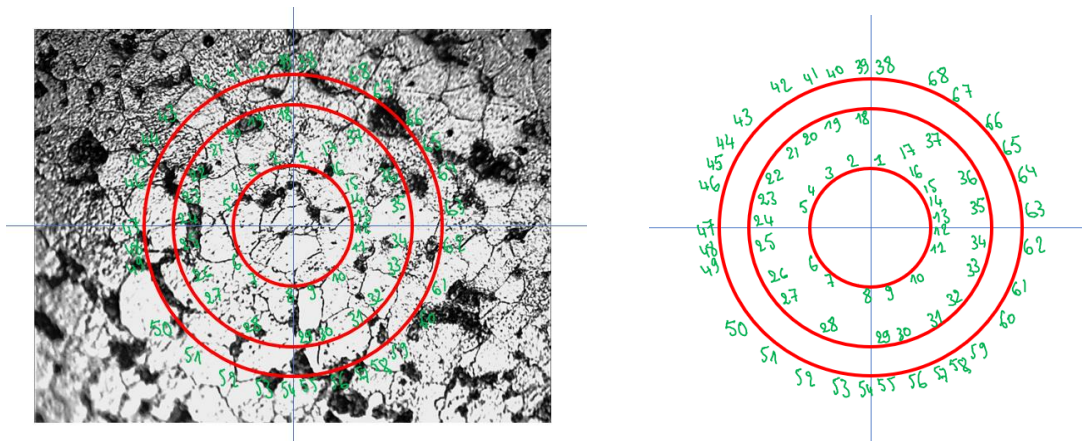


FIGURE IV-14: *Example of application of manual grain size determination*

On the left: three concentric circles with diameters 4cm, 8cm and 10cm have been drawn on the microstructure.

On the right: count of intersections displayed on a tracing paper.

Step 2. Sum the circumferences of all three circles together (L)

For our example:

$$L = \pi(d_1 + d_2 + d_3) \approx 69.08cm \quad (3.4)$$

Step 3. Count the total number of the intersections between the circles and the grain boundaries (N).

For our example, 68 intersections have been found.

Step 4. Use the ASTM formula to calculate the grain size number G:

$$G = -10 + 6.64 \log\left(\frac{NM}{L}\right)$$

(3.5)

Where M is the corresponding magnification.

In this micrography, the magnification we used is M=400 times. Thus, the corresponding size number would be evaluated as: G=7.23.

Step 5. Use the conversion table given by the norm to estimate the grain size and area.

TABLE IV-5: Grain size equivalence by the ASTM E112 norm [4:8]

Grain Size No. G	\bar{N}_A Grains/Unit Area		\bar{A} Average Grain Area		\bar{d} Average Diameter		\bar{l} Mean Intercept		\bar{N}_L No./mm
	No./in. ² at 100X	No./mm ² at 1X	mm ²	μm ²	mm	μm	mm	μm	
00	0.25	3.88	0.2581	258064	0.5080	508.0	0.4525	452.5	2.21
0	0.50	7.75	0.1290	129032	0.3592	359.2	0.3200	320.0	3.12
0.5	0.71	10.96	0.0912	91239	0.3021	302.1	0.2691	269.1	3.72
1.0	1.00	15.50	0.0645	64516	0.2540	254.0	0.2263	226.3	4.42
1.5	1.41	21.92	0.0456	45620	0.2136	213.6	0.1903	190.3	5.26
2.0	2.00	31.00	0.0323	32258	0.1796	179.6	0.1600	160.0	6.25
2.5	2.83	43.84	0.0228	22810	0.1510	151.0	0.1345	134.5	7.43
3.0	4.00	62.00	0.0161	16129	0.1270	127.0	0.1131	113.1	8.84
3.5	5.66	87.68	0.0114	11405	0.1068	106.8	0.0951	95.1	10.51
4.0	8.00	124.00	0.00806	8065	0.0898	89.8	0.0800	80.0	12.50
4.5	11.31	175.36	0.00570	5703	0.0755	75.5	0.0673	67.3	14.87
5.0	16.00	248.00	0.00403	4032	0.0635	63.5	0.0566	56.6	17.68
5.5	22.63	350.73	0.00285	2851	0.0534	53.4	0.0476	47.6	21.02
6.0	32.00	496.00	0.00202	2016	0.0449	44.9	0.0400	40.0	25.00
6.5	45.25	701.45	0.00143	1426	0.0378	37.8	0.0336	33.6	29.73
7.0	64.00	992.00	0.00101	1008	0.0318	31.8	0.0283	28.3	35.36
7.5	90.51	1402.9	0.00071	713	0.0267	26.7	0.0238	23.8	42.04
8.0	128.00	1984.0	0.00050	504	0.0225	22.5	0.0200	20.0	50.00
8.5	181.02	2805.8	0.00036	356	0.0189	18.9	0.0168	16.8	59.46
9.0	256.00	3968.0	0.00025	252	0.0159	15.9	0.0141	14.1	70.71
9.5	362.04	5611.6	0.00018	178	0.0133	13.3	0.0119	11.9	84.09
10.0	512.00	7936.0	0.00013	126	0.0112	11.2	0.0100	10.0	100.0
10.5	724.08	11223.2	0.000089	89.1	0.0094	9.4	0.0084	8.4	118.9
11.0	1024.00	15872.0	0.000063	63.0	0.0079	7.9	0.0071	7.1	141.4
11.5	1448.15	22446.4	0.000045	44.6	0.0067	6.7	0.0060	5.9	168.2
12.0	2048.00	31744.1	0.000032	31.5	0.0056	5.6	0.0050	5.0	200.0
12.5	2896.31	44892.9	0.000022	22.3	0.0047	4.7	0.0042	4.2	237.8
13.0	4096.00	63488.1	0.000016	15.8	0.0040	4.0	0.0035	3.5	282.8
13.5	5792.62	89785.8	0.000011	11.1	0.0033	3.3	0.0030	3.0	336.4
14.0	8192.00	126976.3	0.000008	7.9	0.0028	2.8	0.0025	2.5	400.0

The closest value of the previous grain number found on the bibliographic table is 7.5, which gives a grain size of 26.7μm and an area of around 713μm².

☞ Semi-automatic (numerical) process for measurements

For this purpose, we use ImageJ software. We follow these steps:

Step 1. We first upload the corresponding microscopy. Once it is displayed on the screen, we set the scale of the figure.

In order to set the scale, we can choose one of two possible ways:

- (i) Go to **Analyze > Set Scale...** and then we introduce our values. For this method, the scale must give the corresponding pixels for 100 microns.

On the scale attached to the micrograph, it was displayed that for X400 magnification, 100 μm correspond to 893 pixels, so we introduce these values (**FIGURE IV-15**).

- (ii) The scale is set directly from the figure. We draw a line on the figure's scale, and go to **Analyze > Set Scale...** and we introduce directly the corresponding distance (100 μm).

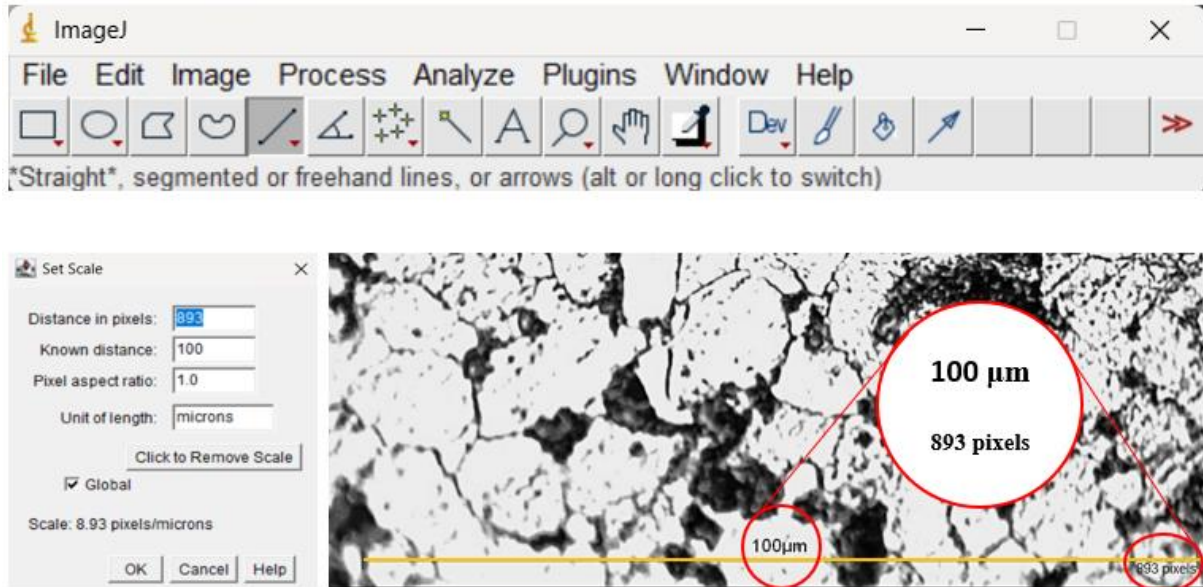


FIGURE IV-15: *ImageJ software manipulation*

Step 2. Measure the grain size using the “straight” option, and the grain area using the “free hand selection” option.

For the grain size, we draw several lines between the borders of the grains. Many measures should be applied for each grain, and saved using the command **ctrl+M**. As we collect measures for all the grains of the micrograph, we go to **Results > Summarize**. The mean value will be displayed. For the area, we hover the perimeter of the grain and save the result.

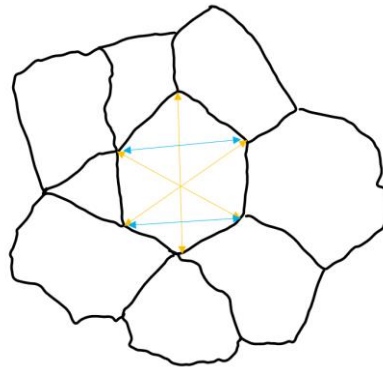


Figure IV-16: *Measurements taken on typical equiaxial structure (sketch)*

For the previous micrography as well as others for the same sample in the same conditions, average dimension was measured for $19.72\mu\text{m}$ and the area for $624.25\mu\text{m}^2$.

The table attached on the next chapter giving the calculating results displays the average value between the numerically and manually calculated values.

d) Inclusions analysis using SEM/EDX

When we apply the optical microscopy on the etched steel samples, a lot of heterogeneities will appear on the screen. Using only the OM images, one cannot distinguish their types, as they could be:

(1) Some kinds of Non-Metallic Inclusions (NMI):

When present on the steel microstructure, the NMIs absorb more of the etching solution for the reaction, which makes them look like some dark areas and spots on the image. Our study aims for following the evolution of this type of heterogeneities regarding the applied annealing conditions. Normally, we expect that their form should be spherical or rounded shaped in our case, as we added the Ca-Si wire during the steelmaking process to reduce the impact of aluminum inclusions on the continuous casting machine as indicated on chapter II.

(2) Porosities:

A sort of some surface defects that form consequently to the internal strains that result from the solidification. They are like some sorts of cavities distributed all along the microstructure. The density of the porosities is generally measured during the quality control of the billet using a method consisting on an immersion in a hydrochloric acid solution, where some spots will appear clearly on the surface. In our project we also aim to optimize the coherent heat treatment that helps us reduce their amounts as much as possible, since the real objective is to fully clean the surface and the structure.

With this in mind, the SEM test will give us the opportunity to get a magnification on the structure up to much greater levels, making it possible to analyze more consistently the structure. Nevertheless, a full and complete quantitative study will require more than just an SEM, but it also requires some additional characterization experiments. In our case, as we also want to determine the types of inclusions we are dealing with, yet, the EDX analysis is the best option to be selected for this purpose. The obtained results can also be interpreted both qualitatively by comparing the shapes and the distribution of the aluminum inclusions on the structure, and quantitatively by the determination of the composition of the inclusions.

IV.2.3 Mechanical characterization

As we mentioned previously in anterior chapters, the mechanical properties of materials are highly dependent on their structure phases and on their grain size; as samples with smaller grain sizes are supposed to have better mechanical properties (higher resistance and hardness).

In order to check over the effects of aluminum, heat treatment and plastic deformation (rolling) on the mechanical properties of the steel, two common mechanical with an extreme importance for the usage of wire rods were applied: tensile test and hardness test.

a) Tensile test

The tensile test consists principally on applying an increasing load on the specimen and measure its corresponding deformation.

At a first glance, the specimen will receive an elastic elongation, meaning that the deformation is reversible, and the suppression of the load will lead to a reestablishment of the initial form of the sample. At a defined point afterward, the deformation will no longer be reversible, but becomes however permanent and the sample will no longer be able to retrieve its initial form, we call this as the plastic deformation.

The continuation of the load increase will finally end up by cutting the specimen, the rupture. The overall process is described by the stress-strain curves (**FIGURE IV-17**).

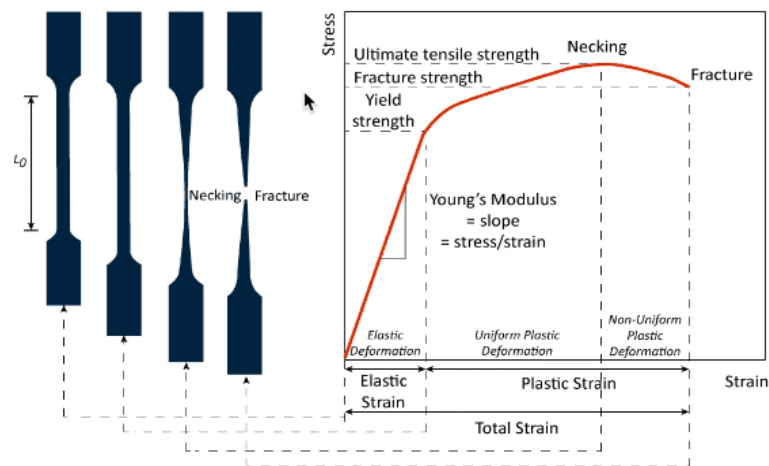


FIGURE IV-17*: *Stress-strain tensile test curve interpretation*

From such a curve, many practical characteristics can be defined, as:

- **Elastic limit R_e :** The maximum load the sample can hold within its elastic domain.
- **Young Modulus E :** Represents the ability of the specimen to absorb the load while maintaining its ability to return to its initial form. It is often linked to the sample's ductility.

- **Mechanical resistance R_m :** The maximal load the specimen can hold.
- **Final elongation $A\%$:** The total deformation of the sample calculated by the formula:

$$A\% = 100 \cdot \frac{L - L_0}{L_0} \quad (3.6)$$

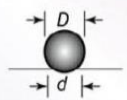



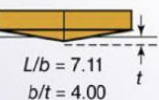

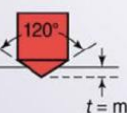



This test was only applied on the rolled samples at their final stage of the production (after 24 passes of hot rolling). Wire rod samples were directly put on the testing machine, which realized the test automatically, giving as an output the three tensile curves as well as the previously defined characteristics.

b) Hardness test

Hardness test consist on applying a specific load using an indenter to press the testing sample. The indenter will then leave a mark on the specimen's surface, of which dimensions and deepness will express the samples hardness.

Most common indenters shapes are shown on the *following table*:

TABLE IV-6*: Most common indenters shape

Test	Indenter	Shape of indentation		Load, P	Hardness number
		Side view	Top view		
Brinell	10-mm steel or tungsten carbide ball			500 kg 1500 kg 3000 kg	$HB = \frac{2P}{(\pi D)(D - \sqrt{D^2 - d^2})}$
Vickers	Diamond pyramid			1-120 kg	$HV = \frac{1.854P}{L^2}$
Knoop	Diamond pyramid			25 g-5 kg	$HK = \frac{14.2P}{L^2}$
Rockwell					
A } C } D }	Diamond cone			60 kg	HRA
				150 kg	HRC
				100 kg	HRD
B } F } G }	$\frac{1}{16}$ - in. diameter steel ball			100 kg	HRB
				60 kg	HRF
				150 kg	HRG
E	$\frac{1}{8}$ - in. diameter steel ball			100 kg	HRE

For our tests, a Brinell spherical indenter was used on all the samples at a press of 125kgf/m². the machine is equipped with a microscope to examine the scar left by the test, and a ruler to measure the mark's dimensions and introduce them into the system which will calculate then the hardness.



FIGURE IV-18: *Brinell indentation hardness test*

References

- [4:1] Mohamed Shidar. Metallography: Sample preparation and examination
- [4:2] Enes Akca. Erwin Trgo. Metallographic Procedures and Analysis – A review. 2015
- [4:3] ASM Handbook. 9th ed. Volume 9, Materials Park, OH: ASM International; 1985. p 279–296.
- [4:4] Walker p, Tarn WH, editors. CRC Handbook of Metal Etchants. Boca Raton, FL: CRC press; 1991. p 1188–1199
- [4:5] Mabrouk Bouabdallah. XRF analysis. ENP. 2023
- [4:6] Mohammed A. Al-Elsheikh. Ahmed Kadachi. Elemental analysis of steel products using X-ray fluorescence (XRF) technique. King Saud University. 2010
- [4:7] Fulton G. Kitson et al. Chapter I: What is GC/MS in Gas Chromatography and Mass Spectroscopy a practical guide. 1996. P: 3-23
- [4:8] ASTM. Standard Test Methods for Determining Average Grain Size

Note: All the pictures and tables with a (*) mark are taken from open sources found on the internet.

Results, Interpretation and Analysis

“Research is creating new knowledge.

*Neil Armstrong; an American astronaut
famed for being the first man to walk on the
Moon.*

Introduction to the chapter:

In This chapter, we present the findings results derived from the methodologies detailed in chapter III. where we aim to provide a comprehensive analysis of the data collected, offering insights into the research questions posed at the beginning of this study. The results are systematically presented and critically analyzed, allowing us to interpret their significance in the context of existing literature and theoretical frameworks.

This chapter is structured first to present the raw data and observations, followed by a detailed discussion, that examines the implications of these findings. We will explore how the results align with or diverge from previous research, highlight any unexpected outcomes, and discuss the potential reasons behind these patterns. In Addition, we address the limitations encountered during the research and suggest areas for future investigation.

Our aim through this analysis is therefore to provide a clear and concise understanding of the study’s contributions to the field, reinforcing the importance of the research and its potential impact on future work.

V.1 Chemical composition of the test specimens

In order to prepare the samples, the process of steelmaking starts from the point of the use of CDRI at the EAF furnace as raw and source material. The chemical quality control of this substance showed that although being purified during the direct iron reduction, it stills not perfectly formed of iron, and contains always some leftover oxides in it.

Titration of the CDRI specimens taken from the quantity used for the elaboration of steel of the three studied heats led to the following results:

TABLE V-1: *Oxides determination on the raw material*

Oxide	SiO ₂	Al ₂ O ₃	CaO	MgO	P ₂ O ₅
Ratio (%)	3.15	1.20	0.98	0.15	0.04

Results shown on the *previous table* mean that initially, the aluminum is present on the steel structure before even the start of the elaboration process. However, it isn't present in form of a pure metal but in form of alumina oxide which cannot be removed.

A direct conclusion of this is that basically, aluminum and alumina inclusions that we would find later on as we proceed into further interpretations are provided from two main sources:

- (1) **Natural sources:** In form of alumina oxide which is always present in the composition and cannot be avoided.
- (2) **Industrial sources:** In form of aluminum metallic bars that we add to hot steel mixture during the elaboration process, in order to reduce the oxygen amount present in it. The process of alumina inclusions formation has been detailed previously on chapter I.

In fact, even though being deoxidized, the steel still has a quantity of oxygen and nitrogen in it. The quantity that's kept in the hot steel mixture will react with alloying elements and form other oxides, as most of them rise up into slag, and leftovers are trapped in form of inclusions. Thus, total oxygen and total nitrogen (T[O] and T[N] respectively) are directly linked to the inclusions density the we could find later as we carry on with the structural characterization.

That's why we need to run a determination test through the NDIR and TCD machine. Results are shown, besides the chemical composition obtained from the XRF test, applied on the three studied samples are shown in the *following table*.

TABLE V-2: *Chemical composition of the studied steel samples*

Element (%)	C	Si	Mn	P	S	Ni	Cr	Al	N ppm	O ppm
Steel A	0.0777	0.0767	0.359	0.0039	0.0067	0.0032	0.0123	0.0029	17.51	4.07
Steel B	0.0773	0.0715	0.368	0.004	0.0071	0.0033	0.0136	0.0011	16.89	4.11
Steel C	0.0780	0.0766	0.367	0.0039	0.0068	0.0028	0.0128	0.0019	21.17	4.08

Considering the fluctuations on the proportions of the alloying elements other than Al, one could argue that variations on the properties might be due to them, and thus the effect of aluminum would be covered.

First, it is important to clarify that technically as well as theoretically, it is very hard (almost impossible) to adjust the three heats with exactly the same chemical composition. This difficulty is mainly caused by the fact that when present in the steel structure, alloying elements tend to take oxide forms, however, these oxides enter in an equilibrium two-sided state, as most of them rise into the slag while the rest is dissolved in the liquid steel. Thermodynamics suggest multiple methods in order to estimate the coherent quantities, but no method has actually reached perfect accuracy.

Moreover, theoretical formulas in bibliography show that aluminum proportions for these steels have an effective influence on many critical equilibrium values that are directly linked to the properties of the final material, such as the liquidus temperature, recrystallization temperature and martensite starting temperature. When comparing the effect of the variation of the proportion of each alloying element, we could notice that the variation of aluminum affects these values (according to the theoretical empirical equations) as much as, or even more than the fluctuations of the alloying elements. In order to show this by calculation, we present bellow calculations of theoretical recrystallization temperature as well as the contribution of Al into its modification compared to the other alloying elements.

TABLE V-3: *Theoretical calculation of the Al-contribution on recrystallization temperature*

Empirical formula	Grades	Theoretical value	Al contribution*
$T_{rec} = 887 + 464C + 890Ti + 363Al$ $- 357Si + 6445Nb$ $- 644\sqrt{Nb} + 732V$ $- 230\sqrt{V}$ (4.1) ; [5:1]	Steel A	844.86	49.19%
	Steel B	884.70	17.36%
	Steel C	883.86	21.96%

☞ Al contribution calculation method:

When we look to the empirical formulas of the equilibrium temperatures, we usually see that the equations start with constants, and then additions are introduced into the equations in form of a factor multiplied by the proportion of the respective alloying element. As we see, each term is preceded by a (+) or a (-) sign according to its influence on this theoretical value. The first constant represents then the theoretical value for pure iron with no addition introduced. Then, the aluminum contribution is calculated from the ratio between the term representing the aluminum influence and the difference between the theoretical value calculated, and the pure iron constant (as this difference will then represent the overall influence of the additions):

$$Al\ influence = \frac{K.(\%Al)}{T_{pure\ iron} - T_{theoretical}} \quad (4.2)$$

Where K is the coherent factor of Al in the corresponding equation. In the example of recrystallization temperature above, $K=363$ and $T_{pure\ iron} = 887^{\circ}C$.

Underneath are some formulas that we found for liquidus temperature and martensite start temperature, as given in bibliography for further estimation of the Al influence on the equilibrium values of steel [5:2,3]:

$$T_{liq} = 1536 - 251C - 12.3Si - 6.8Mn - 123.4P - 183.9S - 3.3Ni - 1.4Cr - 3.1Cu - 3.6Al \quad (4.3)$$

$$M_s = 525 - 350(C - 0.005) - 45Mn - 35V(Nb + Zr + Ti) - 30Cr - 20Ni - 16Mo - 8W + 6Co + 15Al \quad (4.4)$$

Even with this approach taken, the effectiveness of the aluminum may still be obscure and cannot be reliable for some clear and obvious reasons:

- The calculation method of aluminum contribution isn't very accurate with some gaps within its logic that can be argued. A clear example is the result of the aluminum contribution on the recrystallization temperature for the steel A where it was calculated to be around 50% which is clearly far from being a logical result.
- The theoretical formulas shown above are different from a bibliographic reference to another, because they are empirical, thus unprecise and not really representative. For example, the same reference we mentioned for the liquidus temperature we gave stated nine other equations, each of them being completely different from the other.

However, we still took this approach just to show that theoretically, aluminum is proven to be impactful even at such low proportions, especially when we look on the amounts of the other additions. The theory is indeed insufficient to give a full demonstration but the SEM/EDX test results support it strongly as we will carry on a little bit further in this chapter.

V.2 Structural analysis

During testing phase, the studied steels were submitted into heat treatment and into hot rolling. The revelation of the microstructures of billet samples as well as heat treated and hot rolled samples will indicate the effects brought by these modifications besides those of the aluminum composition. Microstructures are analyzed as it was shown in the **TABLE IV-4** of the previous chapter. Before we start the interpretation, we present the *following table* that gives all the results of grain sizes and areas calculations:

TABLE V-4: *Grains sizes and areas calculations*

State	Specimen	Size (μm)	Area (μm^2)	
Bulk state	A	72.951	12132.231	
	B	171.657	30426.172	
	C	140.214	23006.071	
Conditions				
Heat treated	800, 3h	A	125.955	10930.948
		B	238.263	26425.979
		C	196.951	20234.255
	1000, 3h	A	87.477	8289.175
		B	134.246	15517.562
		C	97.368	9966.324
	1100, 3h	A	81.483	7549.565
		B	111.284	11235.078
		C	91.771	10791.337
1100, 6h	A	145.835	23601.754	
	B	145.321	22087.000	
	C	144.253	23381.227	
Direction				
Rolled	Parallel	A	10.739	139.335
		B	11.332	150.401
		C	11.099	146.292
	Perpendicular	A	9.874	126.983
		B	10.890	147.384
		C	10.061	145.828

V.2.1 Observation before etching

Between each step of mechanical grinding, a microscopic observation needs to be taken in order to verify the success of the operation for the current silicon carbide paper grade. After the final paper grade, and the final polishing, and as no stripes are left on the sample, the observation will show in this case many dark points (even when no etching is applied).

Before we run the SEM testing, the nature of these points is still unknown. However, bibliographic research suggests one of two possible options:

- The dark points can be porosities, small spherical shaped cavities that are formed as defects resulting from the steelmaking process. Their presence in high amounts can lead to serious deteriorating influence on the steel properties.
- They can also be non-metallic inclusions that didn't rise into slag, and that slid past the CCM's nozzles.

For the specific applications and uses of the steel we are studying, the cleanliness of the surface is highly required, and so both, porosities and inclusions are considered as impurities that need to be eliminated. The perfect method to do so, is by applying heat treatments on the samples and verify the perfect conditions to completely delete them.

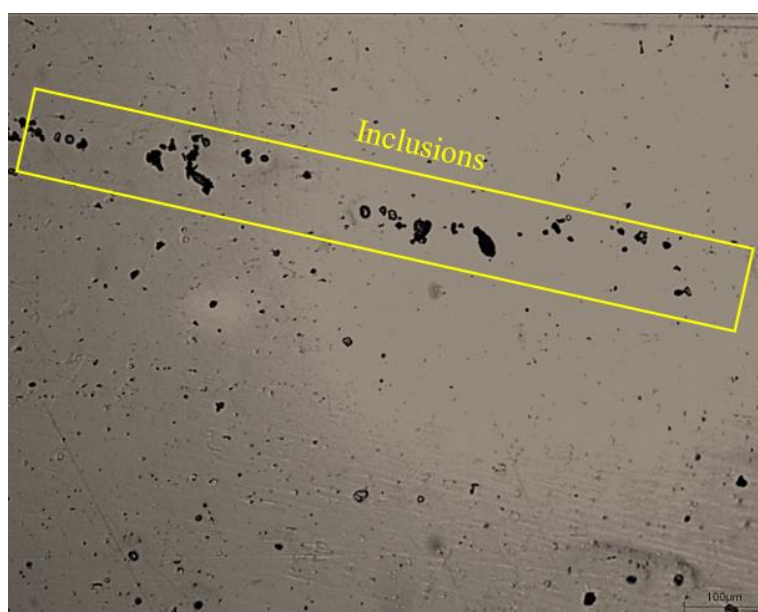


FIGURE V-1: *Microscopic observation before chemical etching, sample taken from billet (X100)*

Porosities are observed all around the surface. Inclusions are arrayed in a direct straight line

V.2.2 Structure revelation

When they are issued from the CCM's molds, are after being heat treated, specimens receive a relatively slow cooling, either in ambient air for the first case, or inside the treating furnace for the second one. Here, some might suggest that according to what we said before, when the billets are being casted at the machine, they are submitted to a water jet for cooling. We stated this in the chapter about the steelmaking process and elaboration of specimens. However, we answer them saying that the water serves only to cool the surface to soften the surface a little bit, so the billet could slide in the arc shaped part of the machine. The cooling hits only the external surface which will be removed later on in form of calamine.

So, after all, the studied surfaces received slow cooling, which means that the phases formed during their solidification follow the equilibrium phase diagram (**FIGURE V-2**).

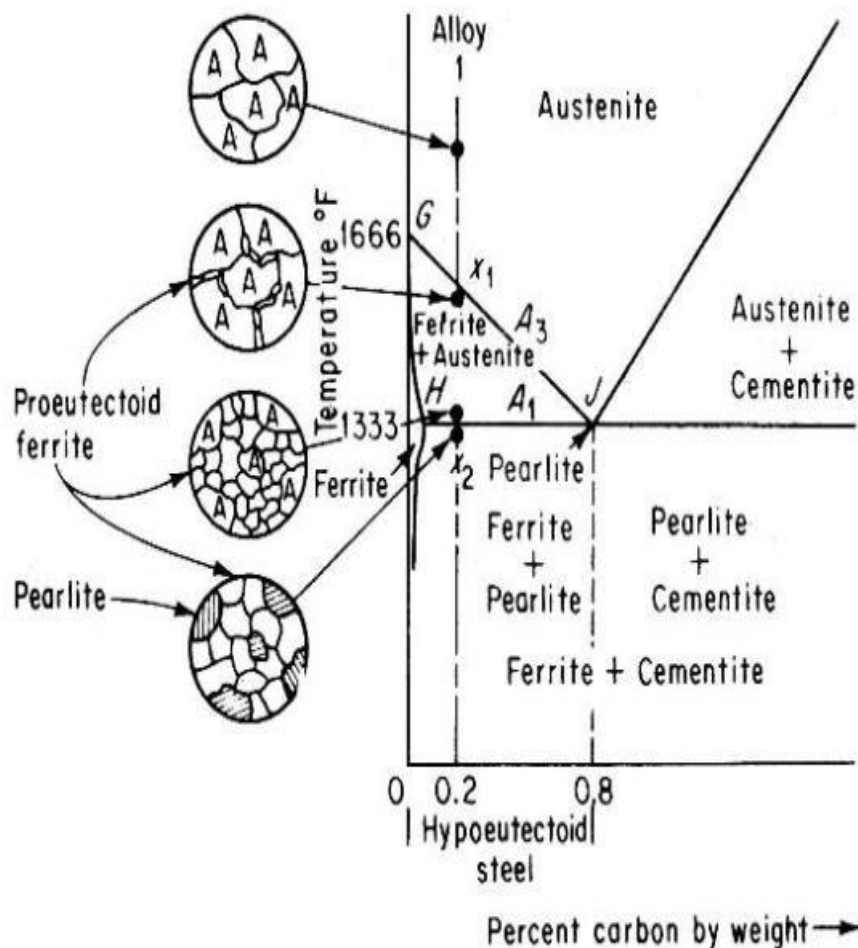


FIGURE V-2: Phase evolution during cooling of hypoeutectoid steel [5:4]

As shown in the *figure above*, we can see that the estimated structure of our steel will be ferritic with (and regarding its low carbon content) very little pearlite at grain boundaries.

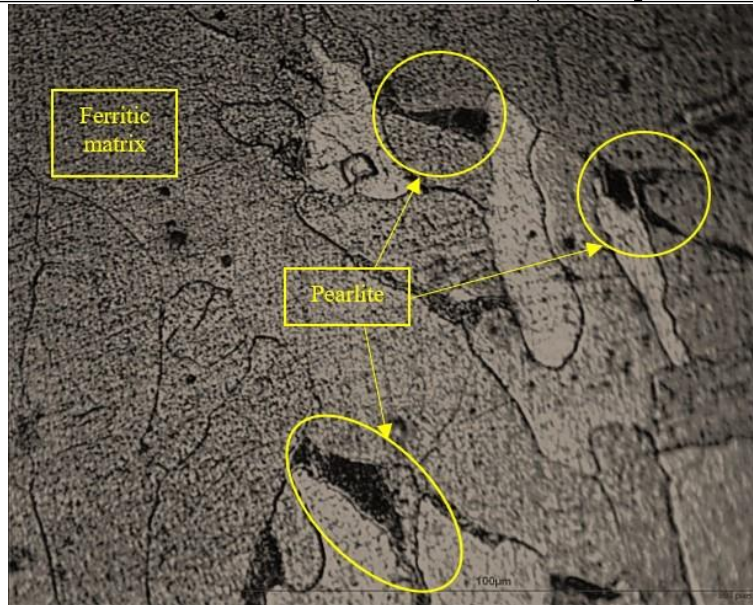


FIGURE V-3: *Microstructure of billet sample before heat treating or rolling (X400)*

In fact, it is a little bit hard to determine the quantity of the pearlite present on the structure through the analysis of the optical micrography pictures only. A theoretical linear approach can help this time to give an approximation to its content. For this, we consider, according to equilibrium diagram, that when the steel has a 0.022% carbon content, there is no pearlite on the structure, but when the carbon content is at 0.8%, which means for a eutectoid steel, the full structure is pearlitic and contain no ferrite and no cementite. Thus, if we consider a linear variation, we will have and expression:

$$\text{pearlite (\%)} = a(\%C) + b \quad (4.5)$$

With:

$$a = \frac{100 - 0}{0.8 - 0.022} = 128.53 \quad ; \quad b = -2.68$$

$$\Rightarrow \text{pearlite(\%)} = 128.53(\%C) - 2.68 \quad (4.6)$$

So, the pearlite content can be calculated theoretically as shown in the *following table*:

TABLE V-5: *Theoretical calculation of pearlite amount in steel*

Steel	Carbon content (%)	Pearlite content (%)
A	0.0777	7.31
B	0.0773	7.26
C	0.0780	7.35

V.2.3 Heat treatment effect on steel microstructure

a) Effect of heating temperature

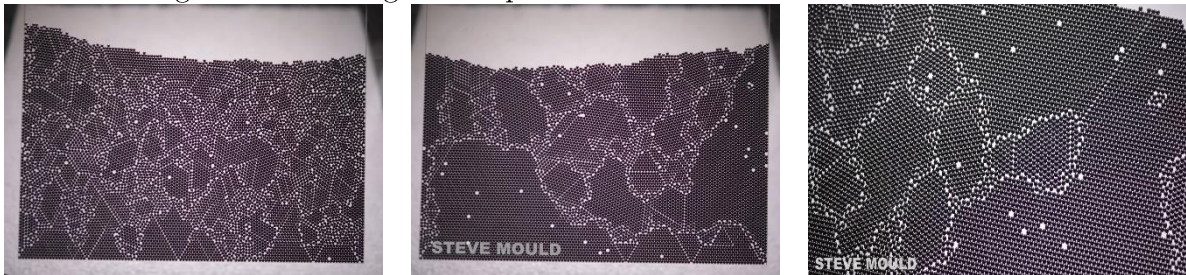
When we check the bibliography, it is largely documented that heat treatments usually serve for the augmentation of grain sizes. A mechanical simulation that imitates the phenomena that happen during the operation, suggested by Steve Mould [5:5] uses around 3000 small steel ball-bearings trapped between two layers of acrylic. First, when we put the equipment on a vertical position, we can notice that the balls will take random positions, in some directions that are not the same, leaving in between them some boundaries. The analogy links between the mechanical behavior of steel balls and what really happens during the thermodynamic phenomena as:

Steel balls represent atoms

Groups formed by the balls represent grains

And the limits between these groups represent the grain boundaries

Thermodynamically, temperature is usually defined as atomic scale vibrations, and thus can be simulated in the previous equipment using a vibrating machine. Heating temperatures in this model is analogic to the vibrating frequency. As we run the test, we can see that the balls will rearrange, pushing away the limits between them as the number of balls with the same direction increases. This means that heat treatment actually increases the grain size. A higher temperature will increase it even more.



(a) *Initial position without mechanic vibration (non-heat-treated sample)*

(b) *System after being vibrated at 50Hz frequency: limits between steel balls arrangements have moved (analogic to more grown grains at the metal)*

(c) *System after being vibrated at 100Hz frequency: arrangements have moved even further (more grown grains)*

Figure V-4: *Mechanical analogy for heat treatment effect on the structure [5:5]*

Meanwhile this model serves for giving a general overview about the heat treatment effects, in the other hand, it is noteworthy to keep in mind that it oversimplifies the process for educational purpose only, as not all heat treatments, and even not all annealing treats affect the grain size equally, results of calculations represented in the curves bellow serve for showing this fact.

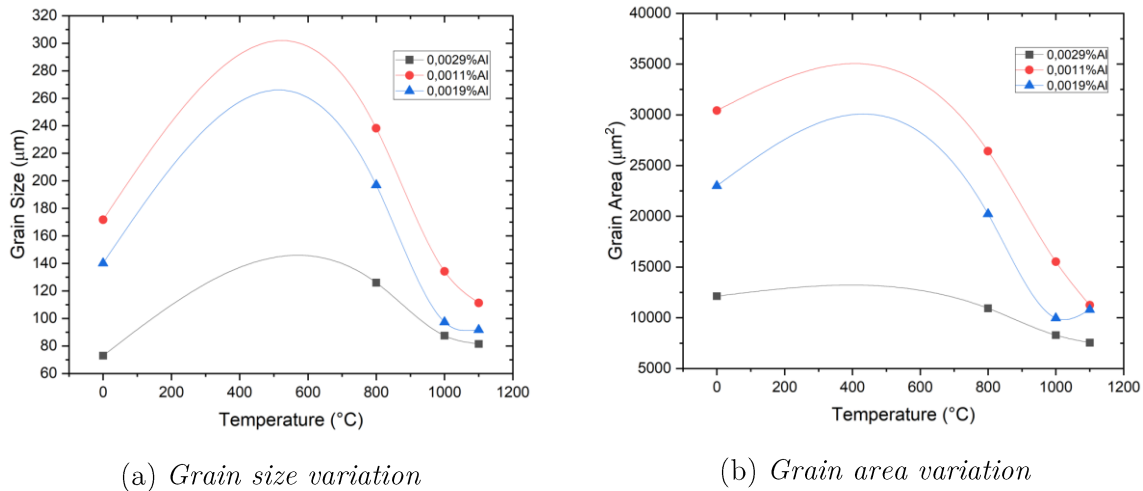


FIGURE V-5: Evolution of grain dimension depending on heating temperature (the curve)

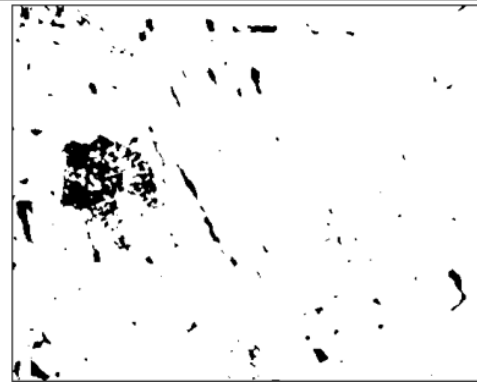
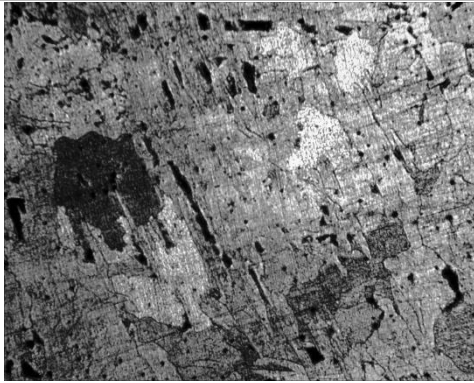
Holding time for all annealing treatments is 3 hours long

Looking at the numerical values presented on **TABLE V-4**, we can see that calculations express a grain size grow compared to non-heat-treated samples, yet following the previous simple constatation about the heat treatment effect on the microstructure. However, surprisingly, we start noticing a decrease on the grain dimensions starting from this temperature, which is contradictory to the intuition one could have regarding the previously mentioned approach. This is conclusive evidence that the anterior conclusion (heating samples increases grain size) isn't definitive, as in some cases the opposite could happen.

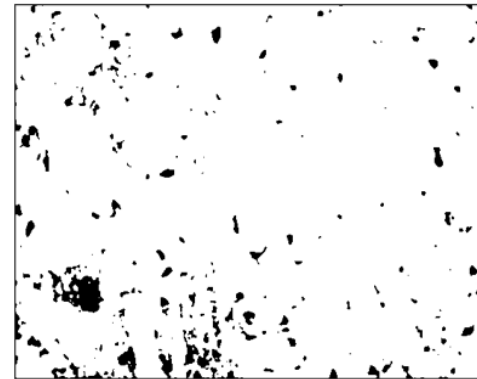
Polynomial interpolation represented on the graphics above (**FIGURE V-5**) shows that despite 800°C heat treated samples have higher dimensions then the untreated ones, but these dimensions aren't the highest we could reach, as maximal values would have been reached at temperatures between 550 to 600°C, and so we constate that the size evolution passes through two steps of evolution:

- (i) From $0 \leq T \leq 550^\circ\text{C}$: A grow on grain dimensions is noted, with significant increase on both size and area.
- (ii) From $550^\circ\text{C} \leq T \leq 1100^\circ\text{C}$: Grain dimensions decrease to very low values. The decrease slope is significant at the beginning of this domain, but slightly falls to even be null for temperatures above 1000°C.

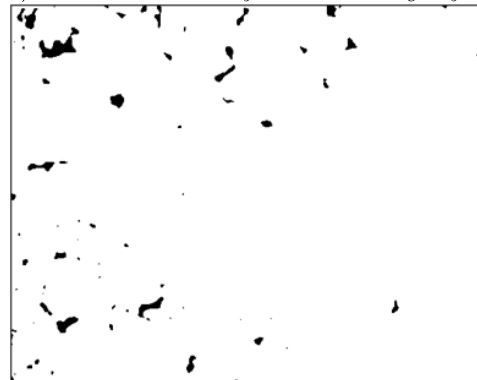
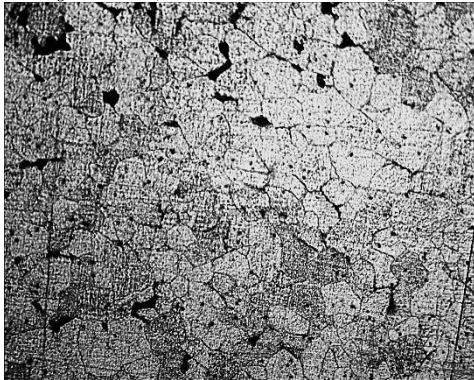
The variation of the grain size of the sample as function of heat treatment temperature leads us to ask a question about the justification of such results. To answer this, we must use photographs observed by an optical microscope (**FIGURE V-6**).



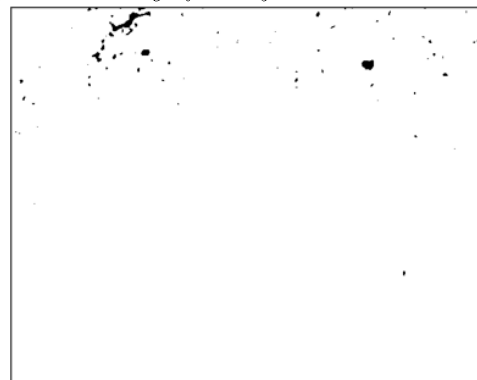
(a) Sample taken at bulk state (no heat treatment applied). We can see big longitudinal grains leaning toward a direction due to rolling at CCM. A high density of the inclusions and impurities is remarked



(b) Sample taken after an 800°C, 3h heat treatment. Bigger grains are observed (most of them still longitudinal, with some smaller grains between them). Inclusions density decreased slightly.



(c) Sample taken after a 1000°C, 3h heat treatment. Grains became much smaller and retrieved their equiaxial form. Inclusions density decreased significantly



(d) Samples taken after a 1100°C, 3h heat treatment. Grains have nearly the same size as those of the previous treatment. Inclusions are nearly disappeared.

FIGURE V-6: Evolution of grain dimension depending on heating temperature (micrography X100)

In fact, during heat treatments, two different types of annealing are applied on the samples, according to the temperature, those are: recrystallization and homogenization of the steel structure.

To understand how these two types of annealing treatments affect the samples properties, we need to match the information collected from qualitative and quantitative analysis (micrographs and curves respectively) together.

Looking at the micrograph of the bulk state samples, we can see that grains have a longitudinal form. Grains are directed into a specific direction, which is the one of the rolling that the steel billet received when being casted through the CCM. This means that grains don't have the equiaxial form with dimensions equally distributed, but they rather have a structure that has a higher length than width (this is better seen on **FIGURE V-3**, where the microstructure is shown at higher magnification).

For treatments that could have been done at temperatures around 550°C, interpolation shown on the curves show that grain size is just increasing. At this level, it is the same effect we checked at the head of this subsection, which means that atoms are subjected to increasing vibration frequency, letting them to rearrange and regroup with more similar grain directions, and thus, the microstructure has bigger grains.

Now, after reaching the maximum size that grains could have under those conditions, recrystallization begins at levels. This means that new grains begin to split from the previous ones. These new grains tend to retrieve the equiaxial form, but with a smaller dimension. They begin to appear from the grain boundaries and grow slowly. At the same time, the longitudinal grains are decreasing in size, since matter is diffusing from them to the newly formed grains. In this case, longitudinal grains will have smaller dimensions, while small new grains are forming. The overall average decreases, making the slope of the graph become negative. This is perfectly seen on the microstructure presented on **FIGURE V-6, b**.

The grain size continues to decrease until it reaches the temperature of complete recrystallized system. Theoretical values of respective temperatures of this phenomenon have been calculated on **TABLE V-3**. Calculations gave results near to 890°C, which explains the reason why the system isn't completely recrystallized at 800°C heat treatment. For treatments at temperatures above 900°C, microstructures should be in form of completely recrystallized equiaxial grains, which is perfectly seen when we applied a heat treatment at 1000°C, as represented on **FIGURE V-6, c**, as well as for the 1100°C heat treatment at **FIGURE V-6, d**. The two last microstructures present a full equiaxial structure, with evenly distributed dimensions on the grains, which explains why the graphics show a nearly constant level between these two heating temperatures.

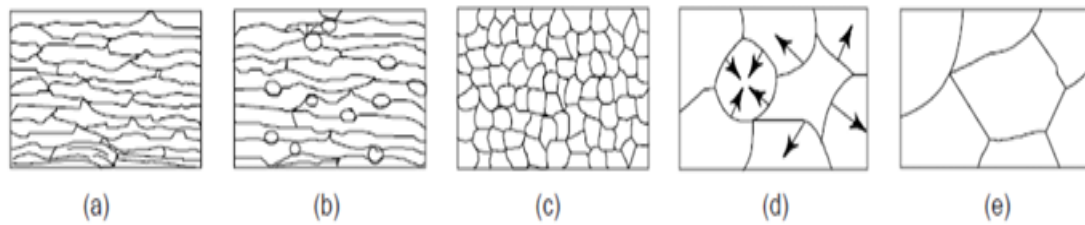


FIGURE V-7*: Sketch for grain size evolution during the heat treatments

Besides the study of the evolution of grain size in function of heating temperature, two more constatactions can be taken from the figures:

(1) Heterogeneities and inclusions

Firstly, we need to notice the decreasing density of the heterogeneities present on the structure with the increase of the annealing heating temperature. At the beginning, the density of the black spots, representing the heterogeneities, is very high as they can be observed all around the microstructure. When the final heat treatment is applied, the structure reveals very few of them that are hardly detected. After heat treatment of 1000°C, the density increased significantly and remarkably (FIGURE V-8)³.

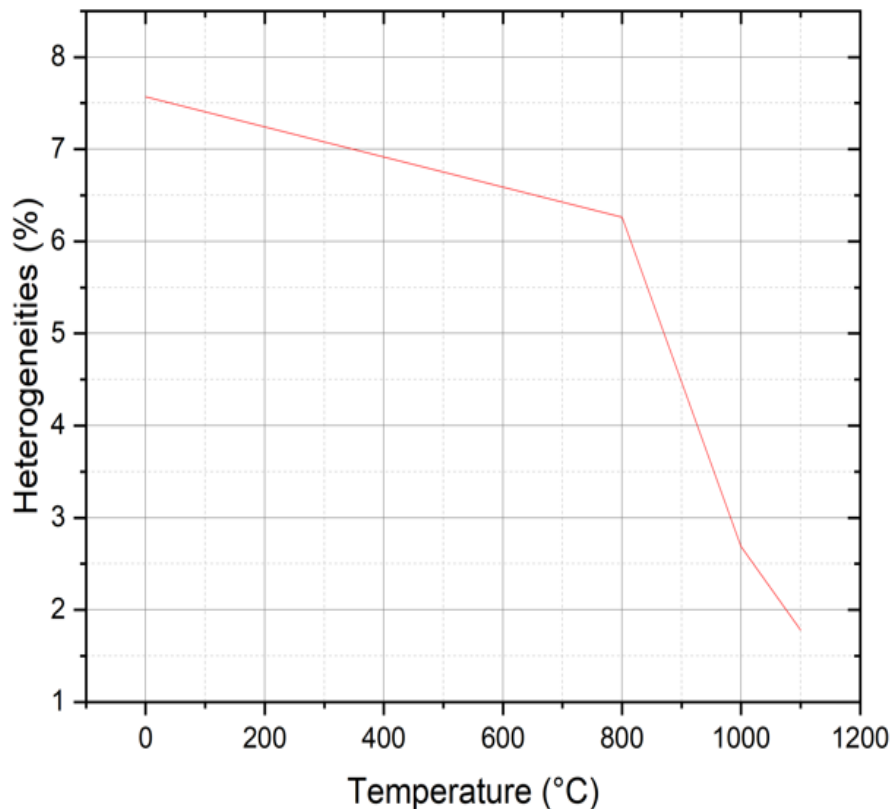
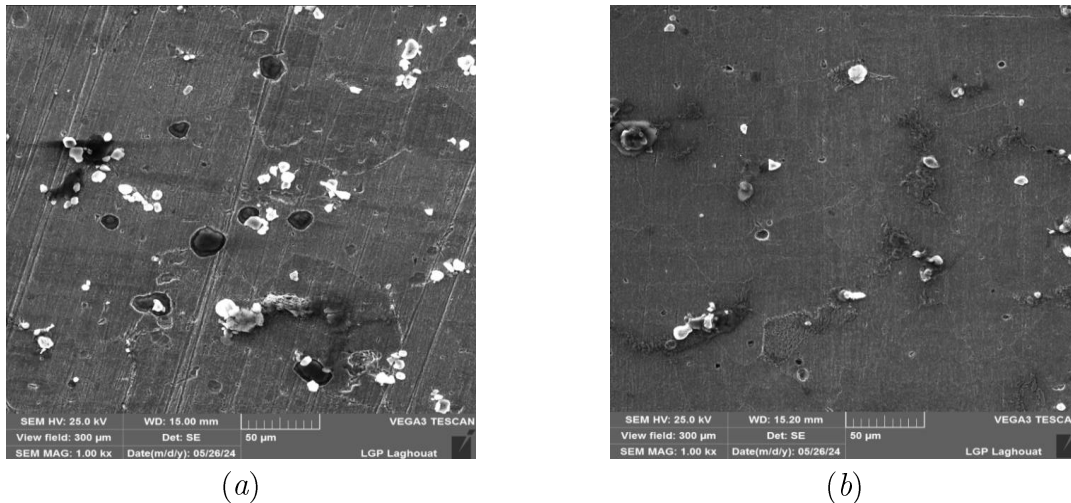


FIGURE V-8: Evolution of heterogeneities density in function of heat treatment

³ Measures have been taken by numerically calculating the area percentage of the black pixels out of the total area of the figure, using a python code. The calculation code is presented at index C.

This decrease of density is a part of the homogenization annealing theory. As its name may suggest, the homogenization is mainly about deleting all types of heterogeneities. Porosities will be closed under the effect of the expansion of the grains as they grow in size (as shown before), meanwhile the inclusions are dissociated into their base elements under the effect of the high temperature (for example, alumina is dissociated to aluminum and oxygen). The gaseous part will spread in the atmosphere while the metallic part will integrate the lattice of the steel structure.

This effect on the inclusions can be seen better by comparing the inclusions using the SEM characterization. The obtained comparative pictures are shown on the *figure below*.



(a)

At bulk state

(b)

After annealing at 1100°C for 3h

FIGURE V-9: Comparison between inclusions density and distribution using SEM (X1000; 25kV)

Through the previous pictures, we can see that inclusions at the bulk state are dispersed all around the structure, mainly positioned on the grain boundaries. The same remark can be taken for the sample after receiving an annealing at 1100°C for 3h. Nevertheless, we can easily see that the density decreased significantly meaning that the inclusions dissociated and integrated the lattice.

The EDX test can push the observations a little bit further quantifying and determining the nature of these inclusions, where they were found composed of aluminum, oxygen, iron and carbon as shown on the *following figure*:

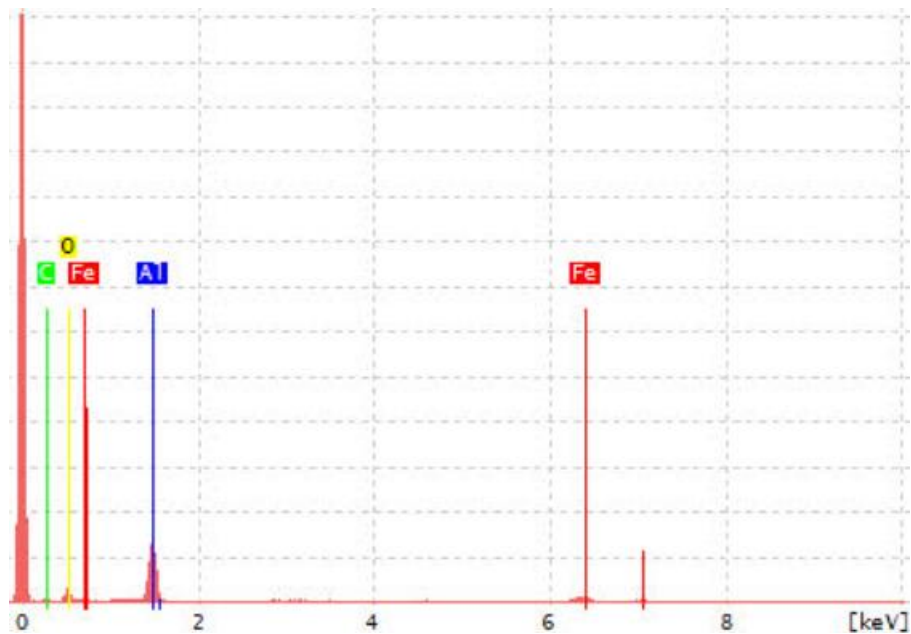
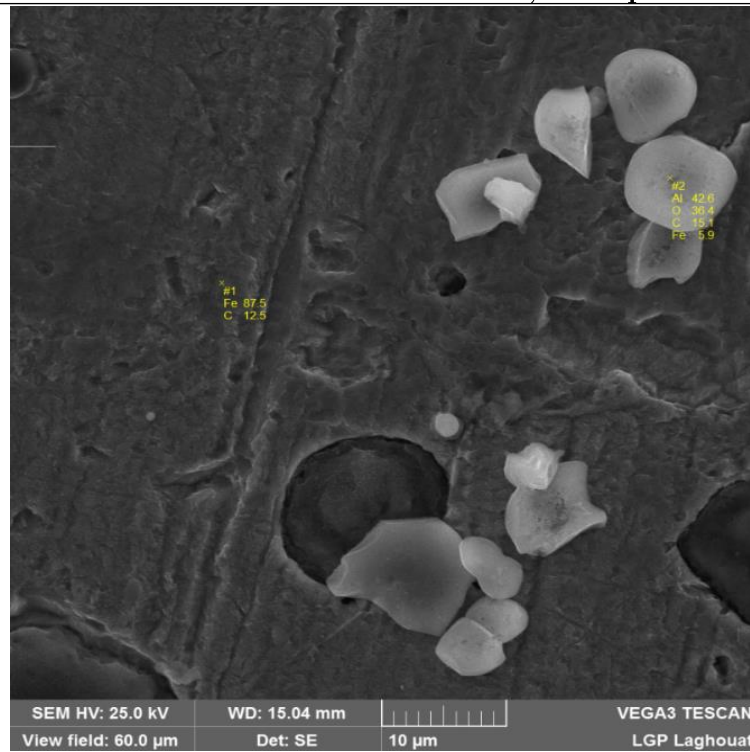


FIGURE V-10: SEM/EDX focus on the composition of inclusions

(2) Effect of aluminum

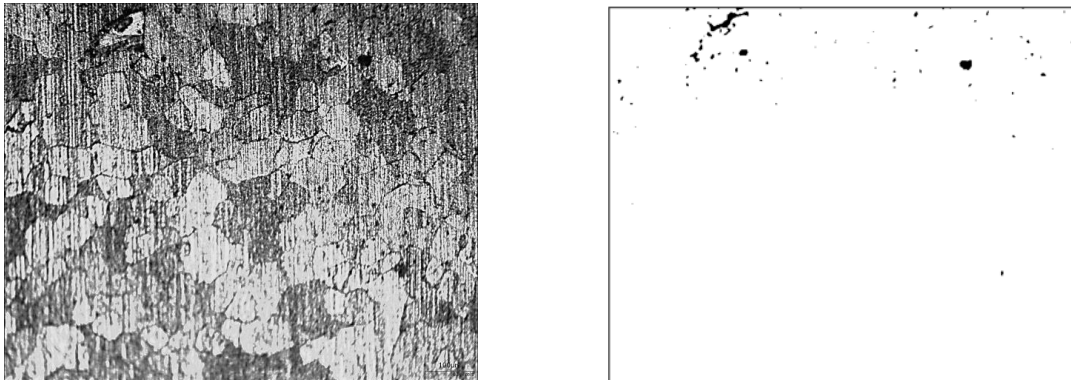
The second and last thing to be observed at this level, is the influence of aluminum on the structure. The graphics show that grain sizes are always higher when the amount of aluminum in the steel is fewer. This indeed matches the bibliography we stated early in this report. During the solidification, aluminum reacts with the dissolved nitrogen on the molten steel and forms aluminum nitrides inclusions that have a hexagonal structure,

and thus cannot precipitate inside the steel grain, yet, they will precipitate at grain boundaries. With this in mind, and regarding the hardness of those inclusions, they will interfere with the ability of the grain to expand when it is heat treated, which explains that higher the amount of aluminum, the smaller the grain will be.

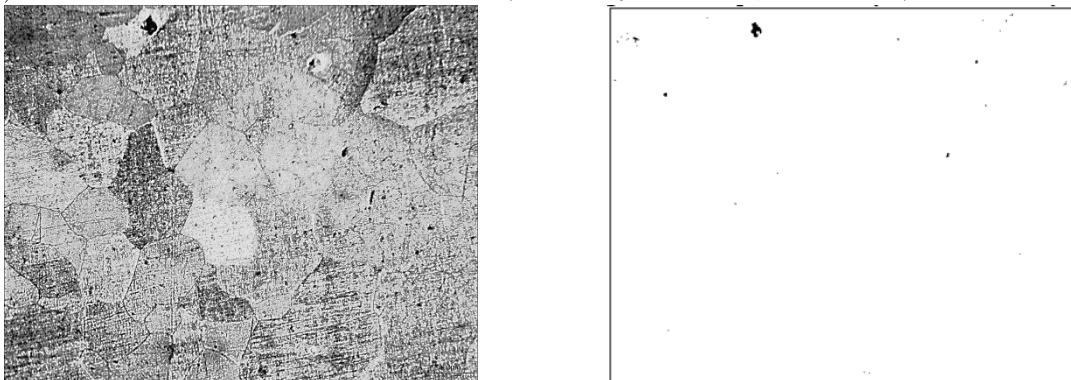
On the figure, steel samples that have 0.0029%Al content have significantly lower grain size than the others for all heat treatments with 3 hours of holding time. However, the numerical values of **TABLE V-4** show that 6 hours holding time at 1100°C will lead to a similar grain size for all the three samples.

b) Effect of holding time

Besides to the effect of the heating temperature, the effect of holding time has also been explored. In the previous analogic model, holding time is linked to the vibrating time. It is logical to assume that in this case, holding time is also directly linked to the grain size, as grains grow more when they have more time to rearrange. Well, this time this assumption isn't wrong, but isn't enough neither. Graphics and micrographs give a representation about what happens inside the microstructure. They will eventually help us to see the things correctly.



(a) *The same microstructure we saw previously, all the grains are equiaxial with few inclusions left*



(b) *Samples taken after a 1100°C, 6h heat treatment. Grains have an equiaxial form with a bigger size than the previous ones. Heterogeneities disappeared completely*

FIGURE V-11: *Evolution of grain dimension depending on holding time (micrography X100)*

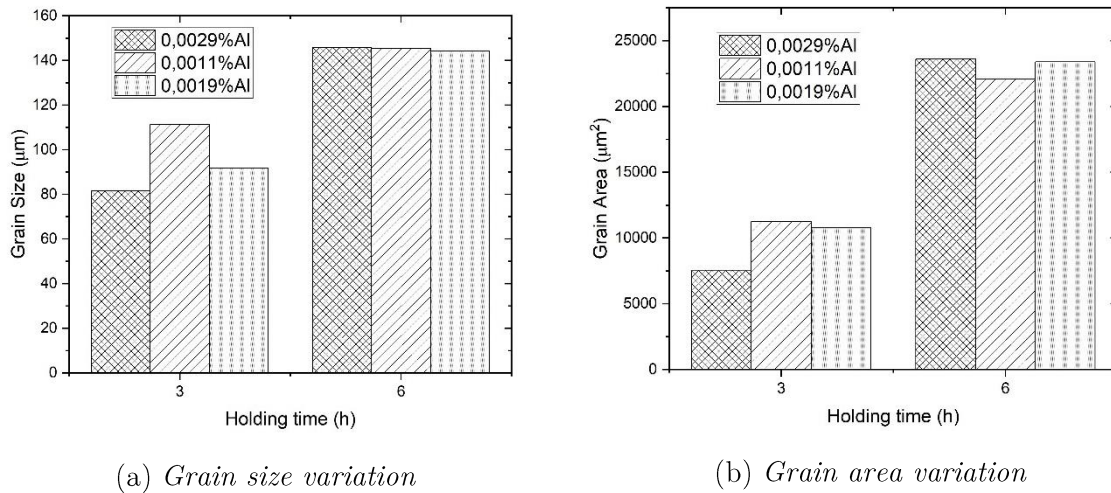


FIGURE V-12: Evolution of grain dimension depending on holding time (the curve)

Heating temperature for the two heat treatments is 1100°C

More than the increase of the grain sizes, data show that after six hours of holding time, all the three steel samples reached the same grain size and area. All the shapes are equiaxial and have nearly the same dimensions. Besides, inclusions and heterogeneities have completely vanished from the structure at this level. The last fact we could observe, is that at six hours of holding time, the aluminum doesn't appear to affect the size anymore.

These three constataions are linked to each other. It looks that when we leave each of the samples inside the furnace as long as six hours, all the inclusions have enough time to dissociate and their metallic atoms can integrate the steel lattice. Thus, the grains expansion will no longer be disturbed and delayed under the effect of those non-metallic inclusions. The structure is then completely homogeneous, yet the atoms can easily grow in size if we treat them longer, or eventually at higher temperatures.

With all this being said, we could summarize all this discussion on the following table:

TABLE V-6: Synthesis of heat treatment effects on the microstructure

Parameter	Variation domain	Mechanism	Effects on microstructure	Effect of Al in response to the HT
Heating temperature	0-550°C	Homogenization	- Grow of grain size - Slight decrease of NMIs density	Decrease the effect of HT
	550°C-900°C]	Recrystallization	- Formation of new equiaxial grains - Reduction of size of old grains	Increase the effect of HT

			- Slight decrease of NMIs density
	>900°C	Homogenization	- Completely recrystallized grain structure - Important decrease of NMIs density - Grow of grain size in all the directions
	[3h, 6h]	Homogenization	- Complete disappearance of NMIs - Improvement of surface cleanliness - Grow of grain size in all the directions
Holding time			

V.2.4 Effect of hot rolling on the microstructure

The theory after the rolling effect on the microstructure has been explored on the bibliographic chapter. In order to hot roll the billets, they must be heated to a temperature around 1150°C. As soon as this temperature is reached, billets are pushed into the rolling train at successive passes. Ultimately, the billets pass through 24 passes with a decreasing distance between the cylinders. The section of the billets at the start has a square form with dimensions of 15x15 cm². At the end, billets are transformed into wire rod that is going to be commercialized. The section becomes round, with a diameter of only 6 mm. The operation happens at around 910°C.

Variations of grain size and microstructure is mainly done on the surface in contact with cylinders as the billets are subjected to stretching deformation. To augment the length of the billet, cylinders apply a vertical force to reduce its section and a horizontal force to expand it. This will result an expansion of grains on the horizontal direction (parallel to rolling direction), and a reduction of their size on the vertical direction (perpendicular to rolling direction). However, as the work temperature is above the recrystallization value, the grains reestablish the equiaxial form after passing through the gap, with the only difference is that their size become smaller and smaller after each pass.

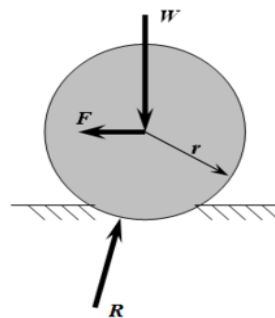
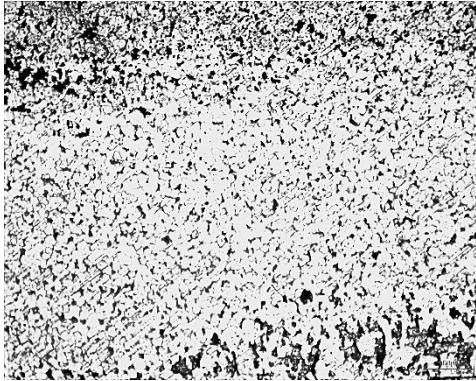


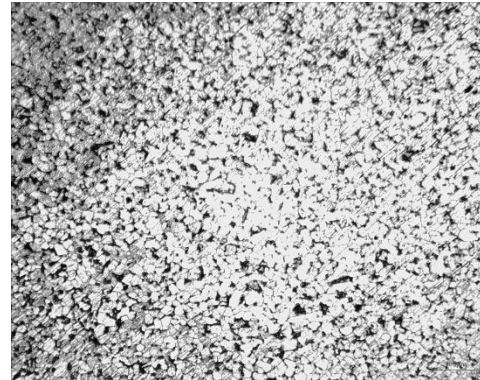
FIGURE V-13*: Forces applied during rolling of materials

Just after the final pass, the wire rod receives water quenching, resulting in a high cooling speed. As a consequence of this, the microstructure of the last pass will freeze and will be kept. The recrystallization will not have enough time to occur, and then we would be able to see how the rolling affects the grain sizes.

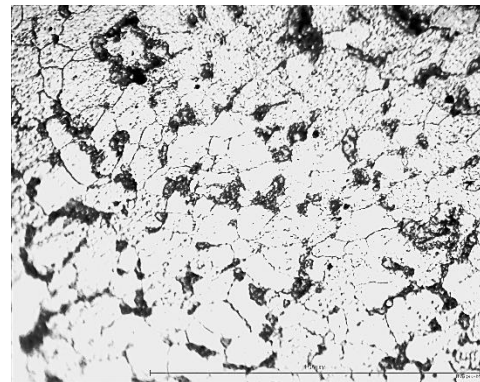
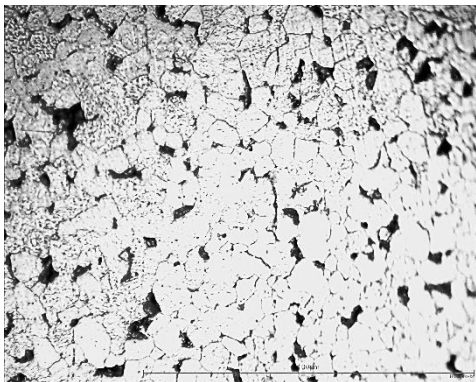
Perpendicular to rolling direction
(Cross section)



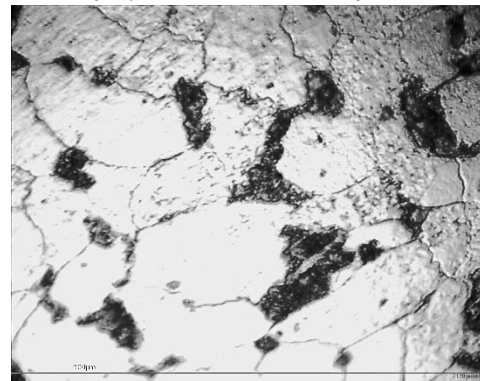
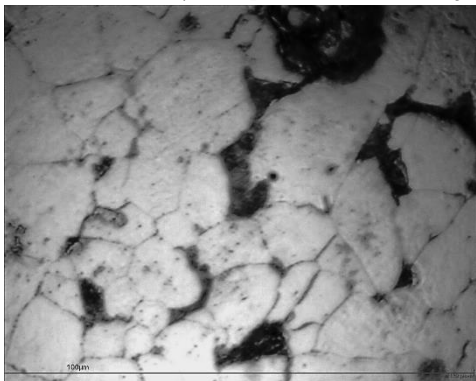
Parallel to rolling direction
(Longitudinal section)



(a) At X100 magnification. Grains are too small that they could hardly be seen. In the opposite, we could easily see the previous microstructures before rolling at this scale of magnification



(b) At X400 magnification. Grains can be seen, we can a slight stretching on the microstructure of the parallel to rolling direction, but magnification isn't enough to be sure



(c) At X1000 magnification. Grains are very clear, we can see the equiaxed form on the picture on the left, and the elongated form on the picture on the right

FIGURE V-14: Microstructure of wire rod after the final pass of the process

On the microstructure we can see at the 1000 magnification figure how the grains are bonded into the rolling direction as their axes are all parallel to each other. Meanwhile, the cross section presents an equiaxial microstructure.

Another interesting point we can see on the microstructure is the phases present. In this specific case, when the samples are quenched with water and are quickly cooled, a bainite structure will appear on the steel instead of pearlite. We can see the bainite on the grain boundaries on the previous picture. Theoretically speaking, bainite is harder than the pearlite, which will affect directly the mechanical properties of the materials as we will see later on.

On the structure, the bainite is represented by those black spots on grain boundaries. We can guess that these are not inclusions because we previously mentioned that before the rolling, billets were heat treated at 1150°C, which is typically above the temperature of total homogenization as we proved before on the previous paragraph.

V.3 Mechanical properties

In order to study the effect of the different variables we are dealing with in our report, and select the optimal combination, we need first to take a closer look at our studied steel and its uses. Basically, the Algerian Qatari Steel complex produces main construction steel in form of rebar and wire rod, as in our example.

The studied wire rod, according to the description of the client, is directed to the fabrication of construction materials, specifically it is used as tie and binding wire, which are used to tie and secure rebar in place. Such applications require a high mechanical resistance, as well as a lower hardness since the material should be ductile enough to be easily twisted and bent without breaking. With this in mind, we run two elemental mechanical tests to evaluate the three studied samples. Those are the tensile test and hardness test.

V.3.1 Harness test

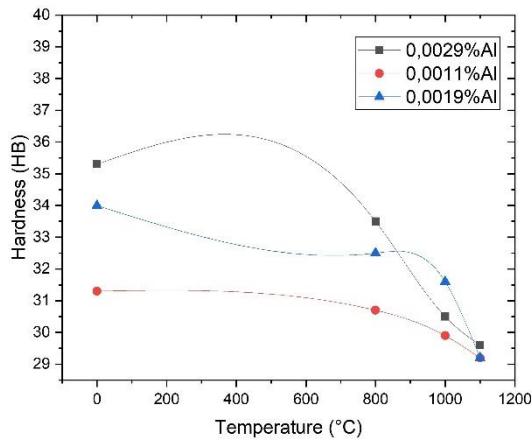
Let's start first with the hardness test. In order to amplify it, we used a Brinell indenter. The working principle is quite easy to understand, and it was already introduced in the previous chapter.

Below are presented the numerical values we got after the amplification of the test:

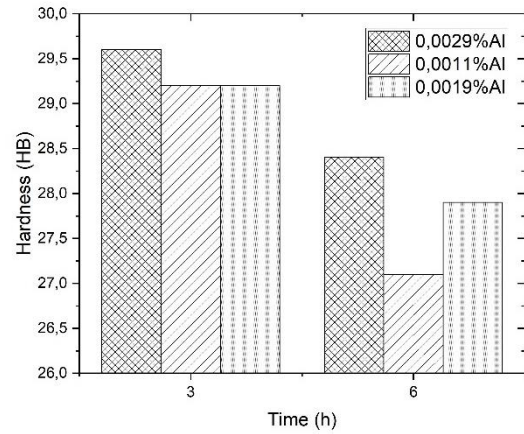
TABLE V-7: Numerical results for the hardness test

State	Bulk		Heat treated			Rolled	
Condition	None	800°C, 3h	1000°C, 3h	1100°C, 3h	1100°C, 6h	⊥	∥
Steel A	35.3	33.5	30.5	29.6	28.4	69.1	42.2
Steel B	31.3	30.7	29.9	29.2	27.1	44.9	39.6
Steel C	34.0	32.5	31.6	29.2	27.9	57.8	40.4

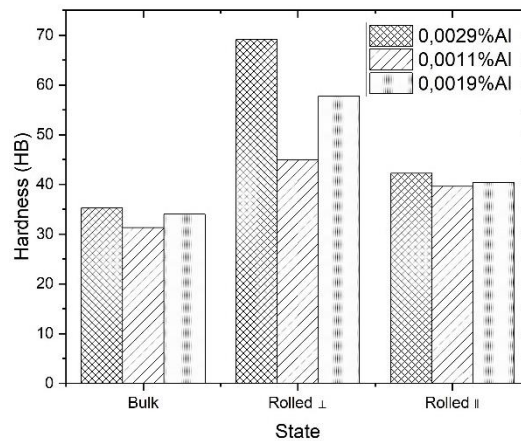
These numerical values can be translated into the following diagrams.



(a) Variation of hardness in function of heating temperature. Holding time is 3 hours



(b) Variation of hardness in function of holding time. Heating temperature is 1100°C



(c) Variation of hardness before and after deformation

FIGURE V-15: Graphic representation of hardness variations

a) Constatations

Direct observation of the graphics can help us to take some assumptions about the parameters that could affect the hardness of materials. Three main relations could be extracted from the curve as presented below:

(1) Relation Hardness – Annealing parameters

Looking into the graphics of FIGURE V-15, a and b, one can quickly establish the constatation about the effect of heat treatment on the hardness of the material.

Ultimately, annealing heating temperature or holding time both reduce the samples hardness. Samples receiving heat treatments at 1100°C for 6h are significantly softer than samples without heat treatment or with annealing at lower temperatures or shorter times.

(2) Relation Hardness – Deformation

The previous curves show that plastic deformation by hot rolling the steel billets increases the hardness of the material. The increase is much more significant at the cross section, perpendicular to rolling direction, than it is at the longitudinal section parallel to rolling direction.

(3) Relation Hardness – Aluminum proportion

Hardness values vary inversely compared to aluminum content in the steel structure. Samples of steel A are the hardest, while samples of steel B with the lowest quantity of Al dissolved (0.0011% compared to 0.0029%, i.e. nearly the triple quantity) are the softest, at all the stages and states.

b) Interpretation of the results

In the theory, hardness results rely mainly on the present phases on the microstructure and their resistance to the plastic deformation. On the studied microstructures the present phases are:

- a- **Ferrite:** Mainly made of pure iron, which is known to be a soft malleable material (see bibliography chapter). Thus, when this phase is present on the microstructure, it will reduce its overall hardness. This phase constitutes the majority of the structure of our material, which explains the reason why their hardness is relatively low.
- b- **Pearlite:** This phase has a little amount of carbon dissolved at it. It has a form of alternative iron-carbon layers. The presence of carbon on the microstructure makes it harder regarding its nature. Pearlite amounts on our samples have been calculated on **TABLE V-5** above. The quantity of this phase on steels A and C are higher than on steel B, which is part of the reason why both of them are harder than it.
- c- **Heterogeneities (NMIs):** The non-metallic inclusions that precipitate on grain boundaries are usually forms of metallic oxides (Al_2O_3 , SiO_2 , ...), nitrides (AlN , ...) or carbides (SiC , WC , ...). The previous forms are ranked with increasing influence on the hardness values.

When we apply annealing on the specimens, we saw previously that they are associated with a homogenization process, which will dissolve all the types of heterogeneities into the structure. This will reduce the amount of NMIs. This explains the reason why the hardness falls down as we apply annealing on a metal. Firstly, it will

reduce the amount of NMIs, and secondly it changes hard structures into soft ones, playing then a softening role.

When we apply rolling on the samples, we are significantly reducing the grains sizes. We saw before that at the final pass of the operation, and as we quench the produced wire rods, the structure is saved. Results and interpretations shown that at this step, grains take a longitudinal shape pointing to the rolling direction on the parallel side, meanwhile they have an equiaxial form on the cross section. Thus, grains are smaller on the cross section than on the longitudinal section, meaning that there are lot of grain boundaries (defects) holding more NMIs and hardening heterogeneities. This, explains the gap between the hardness values of the cross and side sections of the samples.

V.3.2 Tensile test

Unlikely to the hardness test which relies mainly on the phases and substances present on the microstructure, the tensile test (being part of those stress – strain experiences that work with a principle of submitting the specimen onto a load force and measure the resulting deformation) relies rather on the grain boundaries and their compositions.

On microscopic scale, the deformation of a sample depends mainly on the deferent defects that could be found on its crystals. Those defects are classified according to their dimensions into:

- (1) **Unidimensional defects (1D):** in form of empty points in the crystal lattice of the metal. Vacancies are the most known defects of this category.
- (2) **Bidimensional defects (2D):** in form of linear defects. Dislocations are the most common examples of this category.
- (3) **Tridimensional defects (3D):** expend into all the directions of the space, in form of grain boundaries that englobe the grains and separate them form their neighbors.

The last two categories are the ones which affect the most the samples deformation when submitted to tensile test.

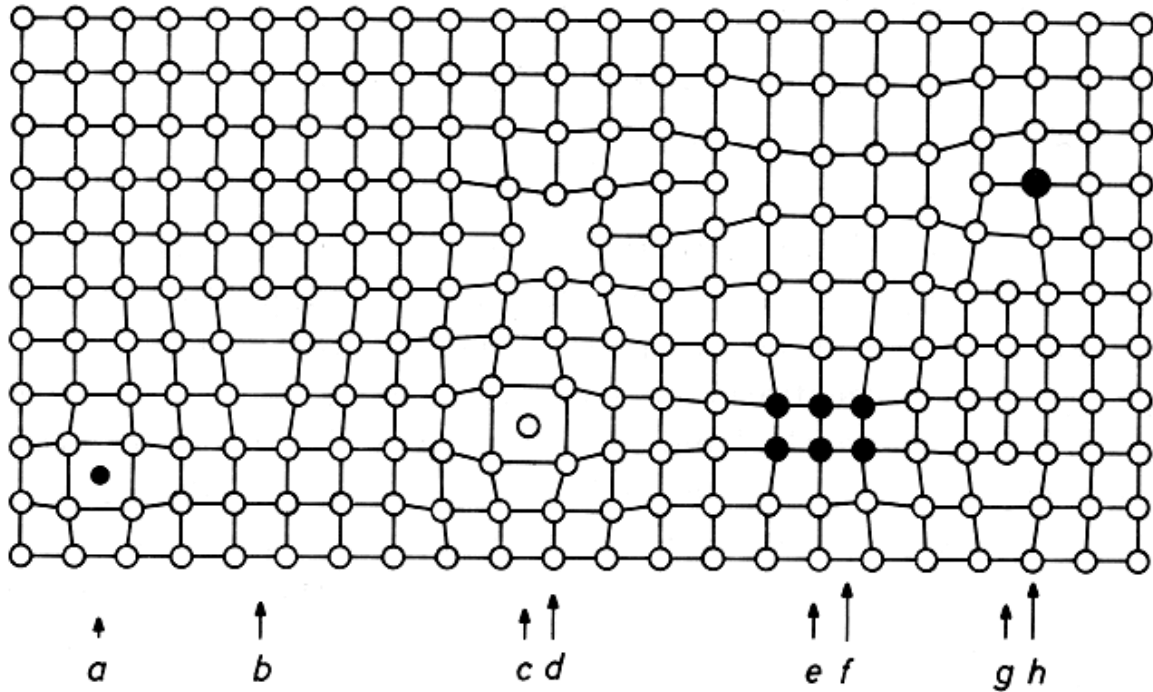


FIGURE V-16: *Most common types of 1 and 2D crystal imperfections [5:6]*

- a) *Interstitial impurity atom, b) Edge dislocation, c) Self interstitial atom, d) Vacancy, e) Precipitate of impurity atoms, f) Vacancy type dislocation loop, g) Interstitial type dislocation loop, h) Substitutional impurity atom*

Basically, a deformation is explained in metallurgy and materials science as the movement of dislocations. When a sample receives a certain load, this will cause it to change its form. For the tensile test example, the change occurs on the length and the section area of the specimen. This elongation is, in fact, due to the movement of the dislocations within the atomic arrangements of the same lattice, then the deformation is possible because when it is in the same lattice, all the atoms are directed in the same way, yet it is easy to move through it.

However, when the dislocation arrives into a grain boundary, it will not be able to move any further for a couple of reasons: first, because in order to pass through a grain boundary, a dislocation needs to have enough energy to break them, the energy is so high compared to the one of the dislocations displacements that it is almost impossible to happen. Grain boundaries are 3-D defects that englobe the grain, and they are rich of all kinds of heterogeneities such as NMIs, increasing its hardness and the energy required to pass through them. The second reason is derived from the definition of grain boundaries themselves. We said earlier on the bibliography chapter that they are considered as limits between grains that have different types grain arrangements, which means that even if the dislocation succeeded to break through boundaries and transport into the next grain, it still needs to change its direction to proceed into moving forward.

The previous theory Implies that when we apply a load on the specimen, the deformation happens within steps:

Step 1. The creation of the dislocations.

As we said, a deformation requires imperatively the presence of those linear defects. Priorly, they always exist in the metal, however not all the grains have them. At a first step, the applied load will start by creating the dislocations in all of the metallic grains. This operation is reversible and corresponds to the elastic deformation zone on the stress – strain curves.

Step 2. The movement of dislocations.

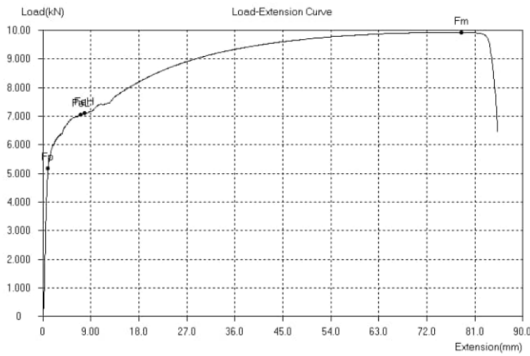
When the applied load continues to increase, the dislocations are next forced to move forward inside the crystals' lattices. This advance will continue until the dislocation arrives into the grain limit. In this case, the dislocation will not be able to go any further nor the system will be able to restore its initial form, and then the deformation will be permanent and irreversible. This corresponds to the elastic zone on the stress – strain curves.

Step 3. Rupture of the material

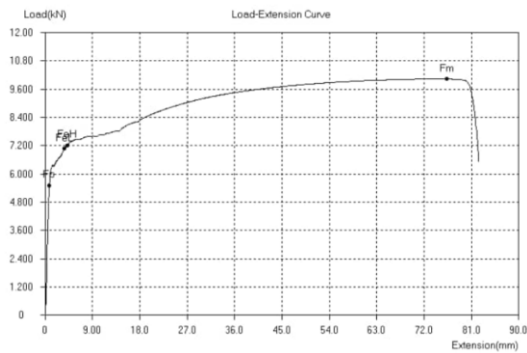
If we continue the application of the load, we will arrive at a certain spot where all the previously formed dislocations reach their respective grain boundaries. We explained that they will try to push forward to move into the next grain, which requires a high amount of energy to break the boundaries and rearrange into the new lattice. The pushing energy is provided by the applied load; however, the material will not be able to support holding it causing it to beak. We call this rupture, and it corresponds to the last measured point in the stress strain curves.

Table 4-8. Numerical results of the tensile test (critical values)

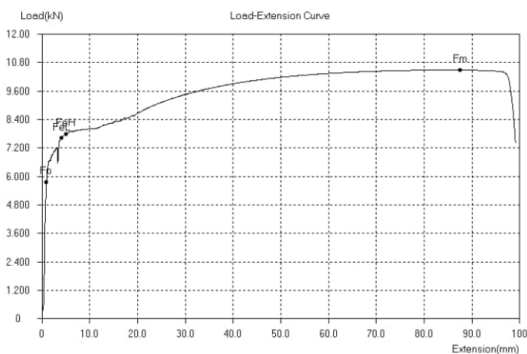
Critical value	Yield strength	Tensile strength	Elongation
Symbol & unit	R_e (Mpa)	R_m (Mpa)	A (%)
Steel A	257	363.5	34.805
Steel B	261.25	363	36.7375
Steel C	270.5	371.25	36.62



Steel A



Steel B

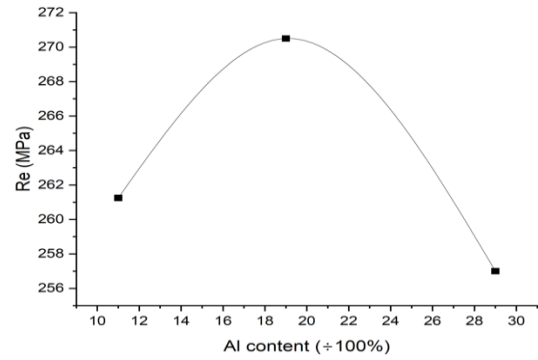


Steel C

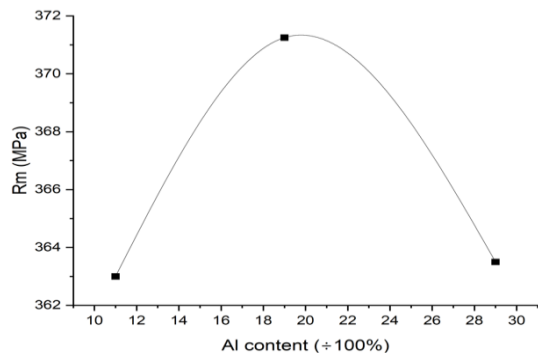
FIGURE V-17: Load-extension curves for the three specimens

The curves can be transformed into stress-strain curves using the laws that link the load (F) to the stress (σ), and the extension (ΔL) to the strain (ϵ) such as:

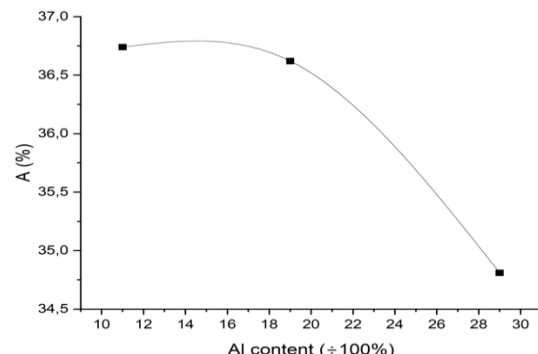
$$\begin{cases} \sigma = \frac{F}{S_0} \\ \epsilon = \frac{\Delta L}{L_0} \end{cases} \quad (4.7)$$



Variations of yield strength



Variation of tensile strength



Variations of elongation

FIGURE V-18: Measured variations of the critical values of the tensile strength in function of Al content

Graphics of **FIGURE V-18** showed a remarkable similarity between the Re and the Rm variations for the three steel samples. Both of these values marked an increase between samples B and C, but also marked a decrease between samples A and B.

Otherwise, we can see also from the last curve that the final elongation of the three specimens decreases when more aluminum content is dissolved into the metal. From what we have seen previously at the microstructure analysis, a clear justification comes to the mind quickly. We have just to link the following facts:

- a- Al forms inclusions at grain boundaries that limit the growth (or even the variations) of the grains' sizes.
- b- Tensile test forms dislocations that transport within the grain lattice until reaching the boundaries.
- c- Elongation is directly linked to the time all dislocations spend in order to reach their respective boundaries (rupture point).

With all this in mind, the idea is that as aluminum participates in the decrease of grain size, it will automatically rise up the quantity of the boundaries, shortening the path of dislocations during the deformation, which finally explains the reason why higher aluminum content reduces the final elongation of the specimens.

References:

[5:1] Ming et al. Effect of trace magnesium addition on the characteristics of mechanical properties in high strength low alloy steel

[5:2] Gryc et al. Determination of the solidus and liquidus temperatures of the real steel grades with DTA methods. 2013

[5:3] Liu et al. A new empirical formula for the calculation of Ms temperatures in pure iron and super-low carbon alloy steels. 2001

[5:4] [Practical Maintenance » Blog Archive » The Iron-Iron Carbide Equilibrium Diagram](#)

[5:5] [Self organising steel balls explain metal heat treatment \(youtube.com\)](#)

[5:6] Pf. Helmut Föll. Crystal defects. University of Kiel; Faculty of Engineering. Link: [Defects in Crystals \(uni-kiel.de\)](#)

Note: All the pictures and tables with a (*) mark are taken from open sources found on the internet.

GENERAL CONCLUSION

In this project, we thoroughly investigated the effects of aluminum content on the structural and mechanical properties of a low-carbon, low-alloy steel intended for wire rod fabrication. The study began with the interpretation of the chemical composition provided by XRF testing. Chemical analysis of the raw material and examination of the steelmaking process revealed two main sources of aluminum (in addition to other alloying elements) that introduce it into the steel lattice. The first source is natural, in the form of non-metallic oxides embedded in the CDRI, while the second is industrial, as aluminum is used for deoxidation during steel production. Upon solidification, aluminum precipitates on the steel surface as aluminum oxide or aluminum nitride inclusions, preferably at the grain boundaries.

Optical microscopy was the next thing we analyzed. Investigations led us to the derivation of the following conclusions:

- (i) Annealing heating temperature can affect the grain size in two separate ways: it can either reduce it within a recrystallization mechanism, or increase it within a homogenization mechanism.
- (ii) In both of the previous cases, inclusions density reduces as they separate into their elemental components, with aluminum entering the lattice in substitutional position, and oxygen freed into the atmosphere.
- (iii) However, the decrease of the inclusions amount is way more significant during homogenization phase than during the recrystallization phase.
- (iv) At advanced stages of homogenization, all aluminum inclusions will disappear from the grain boundaries, so, their effect on the grain size reduction will disappear. Test samples showed equal grain sizes after this spot (corresponding to heating until 1100°C and holding for 6 hours).
- (v) Hot rolling under recrystallization conditions causes the grains size to reduce even more significantly. Quenching the samples led to a freeze of the microstructure after the final pass (24th). Grains were clearly observed only after 1000 times magnification.
- (vi) Microstructures parallel to the rolling direction had a longitudinal form of grains, while the one perpendicular to the rolling direction had an ordinary equiaxial structure.

Theory specifies that the microstructures of steel affect directly its mechanical properties, as the phases influence its hardness while the grain size influence its reaction when submitted to tensile test. The two experiments were amplified on the samples, as we discovered that:

- (vii) The hardness of the three materials variates oppositely to the annealing temperature and holding time, since they reduce the amount of aluminum inclusions which participate into hardening the metal.
- (viii) The wire rod samples exhibit higher hardness than the ones with heat treatments, because they have received quenching, resulting in the formation of a hard bainitic phase.
- (ix) Concerning the tensile test, no relation between the yield and tensile strengths were possibly linked to the aluminum content due to an absurd variation. However, elongation did show an interesting decrease as the quantity of aluminum increase, since it narrows the grains, rising up the density of the three-dimensional defects.

The comparison of the mechanical properties of the three samples (at their wire rod quenched state after rolling, as they are commercialized only in this form), regarding their industrial use made us select the steel C (the one with aluminum content of 0.0019%Al) as the nearest one among the three studied steels to the optimal point. Results show that it has importantly higher yield and tensile strengths with just moderate hardness compared to the others (not too high nor too low), making it the most suitable for the fabrication purpose.

INDEXES

Index A

1. General information about the AQS complex

1.1. Definition of AQS

AQS is a new Economic Public Enterprise that was established in December 2013. Operating and commercial activities began in 2017, as an Algerian-Qatari joint venture created to execute the new Bellara steel complex. The capital of the complex is held 46% by the SIDER company, 5% by the National Investment Fund (FNI), and 49% by Qatar International. [A:1].

SIDER and QATAR STEEL, the main partners of AQS, are companies with extensive experience in the steel industry, responsible for managing and operating Algeria's two major steel complexes (El Hadjar Complex in Annaba) and Qatar's (MIC Complex near Doha), respectively. The technology implemented at Qatar Steel's MIC Complex and that of Direct Reduction are similar to the technology chosen for the Bellara Complex.

The steel complex has two main installations:

- An installation in the industrial zone of Bellara in the municipality of El Milia, wilaya of Jijel, covering an area of 216 hectares.
- A plot of 10 hectares at the port of Djendjen in the municipality of Taher, for import and export purposes.
- The two areas, 40 km apart, are connected by a railway line on which the ore will be transported and by the road transport corridor formed by National Road 43 (RN43), the most important regional road axis, with two lanes in both directions [A:2].

Thus, it is noted that the complex engages in economic exchanges directly linked to the national economy; it imports raw materials as needed in the form of CDRI and exports its various finished or semi-finished products, which will be presented later in this chapter.

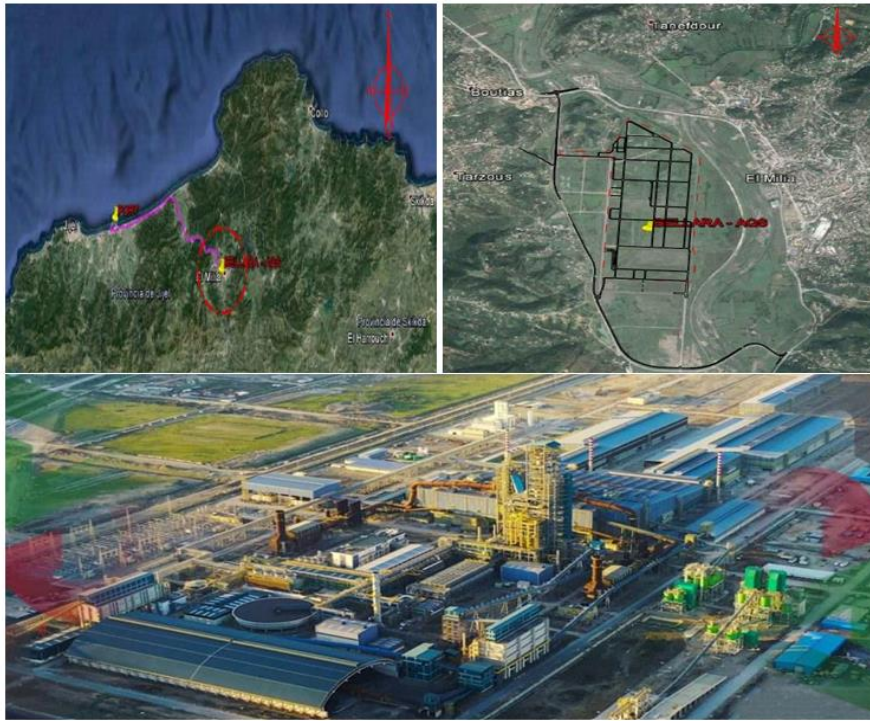


Figure A-1*. *Geographic localization and an aerial view on the complex*

1.2. Phases of development

The construction of a steel complex, as desired by both parties of the agreement, cannot be carried out directly; rather, it is planned to proceed through two phases of development. The first phase began its work from 2017 until the present time. It involves the development of various main and auxiliary units that can currently be found in the complex.

Currently, this phase has reached over 90% of its production capacity, and planning for the start of the second phase of development has begun. The partners owning the plant plan to build another iron reduction unit, another steel melt shop, and three additional rolling machines. This is intended to double the steel production rate, with a wider and more varied range of products. [A:2]

1.3. AQS in numbers

1.3.1. Economy [A:1]

The AQS steel mill plays a crucial role in the national economy, as evidenced by its impressive statistics. With a capital value of **58 billion Algerian dinars**, AQS represents a significant investment in the country's steel industry. In addition to its intrinsic economic value, AQS also generates substantial employment. With over **2600 direct employees** during the operation phase of the complex, the company directly contributes to the creation of stable and rewarding job positions. However, its impact

doesn't stop there, as AQS also has a multiplier effect on employment, generating approximately **10,000 indirect jobs** through its supply chain and related activities. By supporting both direct and indirect employment, AQS stimulates local economic growth, strengthens the financial security of families, and contributes to the broader socio-economic development of Algeria. As a driver of the national steel industry, AQS is a vital pillar of the economy, fostering prosperity and progress across the country.

1.3.2. Productivity

AQS holds a significant position in the landscape of the steel industry in Algeria, making a substantial contribution to steel production. Each year, AQS efficiently processes **2.5 million tons of iron ore** through direct reduction using pellets and other raw materials, which accounts for a significant portion of the national steel production. In terms of output, AQS annually produces **2.1 million tons of steel in the form of billets**.

Approximately **0.1 million tons** are directly allocated for local sale or export as semi-finished products, while the remaining 2 million tons are sent to rolling mills to produce **1.5 million tons of concrete reinforcing bars** and **0.5 million tons of wire rod**, thus meeting the demand of both national and international markets (*Figure 2*) [A:2]. It is noteworthy that these statistics will double as soon as the second phase commences its production sequence.

Thanks to its diversified production and efficient processes, AQS contributes to supporting various economic sectors in Algeria. Its role in providing quality steel for construction and other essential industries is undeniable, thereby promoting economic growth and industrial development in the country.

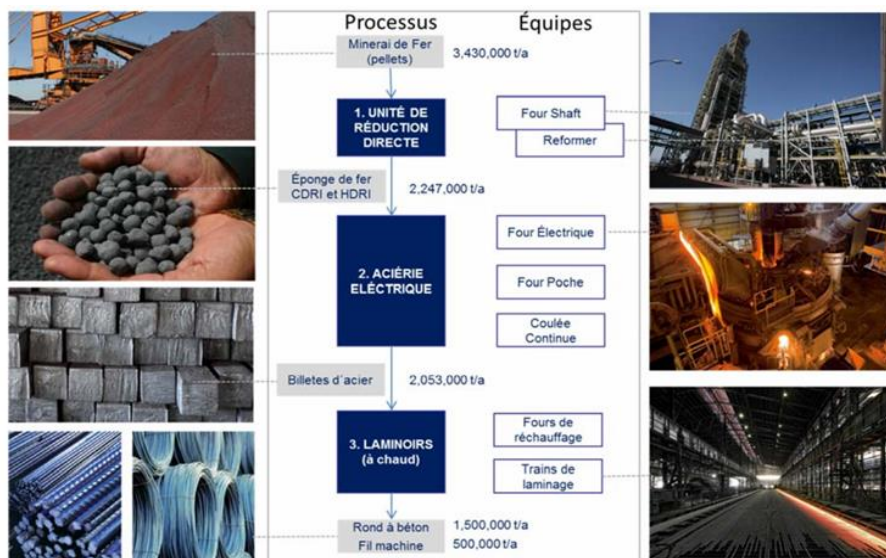


Figure A-2. Material balance for steel produced at various stages of the manufacturing process [A:2]

1.4. Normalization and sustainable development

1.4.1. Normalization

International standards define quality, safety, and performance requirements for products and services, ensuring better satisfaction of clients and reducing risks for consumers. The AQS steel complex benefits from certifications adhering to several national and international standards for quality, including:

- **ISO 9001:** A globally recognized quality management standard, it assists organizations of all sizes, across various sectors, in enhancing their performance, meeting customer expectations, and demonstrating their commitment to quality. Its requirements define how to establish, implement, maintain, and continually improve a quality management system (QMS).
- **ISO 14001:** An internationally recognized standard for Environmental Management Systems (EMS). It provides a framework for organizations to design and implement an EMS and continually improve their environmental performance. By adopting this standard, organizations can ensure they take proactive measures to reduce their environmental footprint, comply with current legal requirements, and achieve their environmental objectives. The framework provided by this standard encompasses various aspects, from resource usage and waste management to monitoring environmental performance and involving stakeholders in environmental commitments.
- **ISO 45001:** An international standard that specifies the requirements for a Occupational Health and Safety Management System (OHSMS). It provides a framework for organizations to manage risks and improve their performance in occupational health and safety. [A:3]

1.4.2. Sustainable development

Despite the various industrial risks that can be found in a steel manufacturing environment, such as emissions of toxic gases or hazardous dust, the AQS complex is working to obtain accreditation to an international standard for sustainable development preservation. Indeed, when comparing it to an ordinary steel mill, it is easy to see that AQS stands out for several important qualities, such as:

- **Greenhouse gas reduction:** By avoiding the use of coal and replacing it with natural gas. It is known in chemistry that gas is more combustible than coal, resulting in a complete reaction producing carbon dioxide instead of carbon monoxide (CO₂ instead of CO), which is the most important agent of greenhouse gas and climate warming.

- **Waste management and recycling:** AQS significantly reduces the waste it emits, and the majority of waste is recycled. The following *table 1* presents the different waste products produced by AQS and the treatment method used:

Table A-1. *AQS waste management system*

Waste type	Source	Re-use method
Steel, iron	Scrap, non-conform products	Melted again in the electric arc furnace
Slag*	Steel making process	Rich in metal oxides that can improve soil quality, it can be used as fertilizer in agriculture.
Refractory stones*	Furnace walls (EAF and LRF)	Intended for tar production.
Organic waste*	Food	Fertilizers in agriculture.
Dangerous chemicals*	Quality control laboratories	Can't be reused, they are sent to specialized authorities for destruction.
Wastewater	Cooling systems for equipment	Intended for the water treatment unit for purification and reuse.

* Re-use is not done in AQS; instead, the waste is sold as a product to other companies specialized in recycling or treatment.

- **Preservation of raw materials:** As mentioned, AQS reduces its consumption of raw materials by using scrap as a source of iron. However, it should be noted that the quantity used must be controlled, as excessive amounts can lead to significant quality issues, since controlling the composition in this case is challenging.
- **Community engagement:** AQS engages with local communities to understand their concerns and needs, and works in partnership with them to create local employment, provide training, and contribute to the economic and social development of the region. In this regard, the efforts of AQS can be summarized as follows:
 - ✓ 3,000 workers during the construction phase and 2,600 direct jobs and 10,000 indirect jobs during the operational phase.
 - ✓ Annually, a minimum distribution of \$23 million in wages, and \$27 million in maintenance fees, most of which would have a direct impact on the local economy.
 - ✓ Positive effect of the project on Algeria's external trade balance, resulting in a significant reduction in the import bill and dependence.
 - ✓ Positive effect on public finances through tax payments.

- ✓ Retention of economic value added and technical knowledge in the country.

2. Units and divisions

2.1. Production units

In the Algerian Qatari Steel complex, the main work is carried out by the production units responsible of making the billets, wire rods or the rebar. The process passes through three main units that work in collaboration with each other forming a sequence.

2.1.1. Direct Reduction of Iron (DRI)

In this unit, the raw material in the form of iron oxide is reduced (deoxidized) with the aim of purifying it. Iron oxide is obtained or imported in the form of pellets, then transformed through direct reduction to obtain CDRI.

The direct reduction of iron oxide is achieved through a chemical reaction of hydrogen and carbon monoxide with iron oxide. The pre-reduced product is metallic iron. The chemical and thermal aspects of the reduction process are more efficient in a counter-current reduction reactor with a uniform descent of solids and an ascent of gases, such as the MIDREX reduction reactor shaft, where oxygen is removed in a reduction furnace by reducing gases such as CO and H₂. An external view of the unit is presented in *fig 3-a* below.

2.1.2. Steel Melt Shop (SMS)

This unit (*fig. 3-b*) is considered as the second and the most important step in the steelmaking sequence. At this stage, CDRI, HDRI and scrap are used for the production of billets. The work passes through three important stages: The electric arc furnace, the ladle refining furnace and the continuous casting machine.

(a)



(b)



Figure A-3. *Some production units in AQS*

2.1.3. Rolling Machines (RM)

Most of the steel billets (semi-product) obtained from the SMS are transported to the rolling machines unit, in order to transform them into wire rod or rebar (final product). In the complex, we find three rolling machines:

- (i) **RM.1:** Production of rebar with a diameter between 16 and 32.40mm.
- (ii) **RM.2:** Production of wire rod with a diameter between 5.5 and 12mm.
- (iii) **RM.3:** Production of wire rod with a diameter between 8 and 14mm.

2.2. Auxiliary units

Although the production units (DRI, SMS and RM) constitute the main body of the AQS complex, it is necessary to know that their works are supported by other auxiliary units whose objective is providing some essential resources, some energy for the production line, or simply recycling and reutilizing materials when possible. In this paragraph we note the most important ones of those auxiliary units.

2.2.1. Air separation unit

During the steel making process, inert gases, such as Argon and Nitrogen, are needed to mix the contents in the different furnaces at different stages. AQS provides the necessary gases through its own air separation unit, in order to minimize the cost of the production.

The process of separating the main gases that compose air through fractional distillation aims to remove impurities like dust and moisture. The gases are introduced into a fractional distillation column where the temperature gradually decreases until

components begin to separate into liquid form through a physical reaction of condensation. At this stage, the temperature will be holding constant until the gas with the highest boiling point is liquefied and separated first. This process continues until all constituent gases are obtained in liquid form. The resulting liquefied gases exhibit a high degree of purity. Please note that prior removal of carbon dioxide from the air is necessary as it can solidify and block the system. [A:4]

In the process of air separation, one or all of the main gases that compose air are extracted, and the three primary components are nitrogen, oxygen, and argon. The residual gases in the air exist in trace amounts and are generally not recovered. In Very Large Air Units (ASUs), neon, xenon, and krypton are recovered in small quantities.

Table A-2. *Air components and their boiling points, obtained in large ASUs* [A:5]

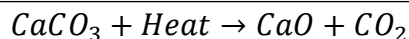
Gas	Molar Mass (mole)	Volume (%)	Boiling Point (K)
Nitrogen	28.01	78.084	77.35
Oxygen	32.00	20.946	90.19
Argon	39.95	0.934	87.27
Hydrogen	1.01	0.00005	20.27
Neon	20.18	0.001921	27.09
Helium	4.00	0.0005239	4.22
Krypton	83.80	0.0001139	119.81
Xenon	131.29	0.0000087	165.04
Carbon dioxide	44.01	0.02-0.04	194.68

2.2.2. Lime and dololime unit

AQS produce high-grade Calcined lime and Dololime for captive consumption with a combined annual production capacity of 280.000 metric tons both. Both high grade Lime and Dololime are used extensively as a flux in the refining of the steel.

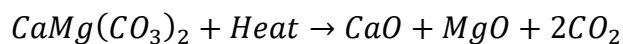
In the Electric Arc Furnace, Lime is particularly useful in removing phosphorous, Sulphur, silica, and a insignificant amount of manganese. And they are also used to perform other critical functions such as fine-tuning steel chemistry, lowering oxygen content, and reducing the inclusions trapped by the slag.

Lime is produced by calcining calcium carbonate (or magnesium) at temperatures above 800°C, causing the decarbonation of the raw material to produce calcium oxide (CaO or quicklime). The lime is then maintained at temperatures between 1200°C and 1300°C to adjust its reactivity. Lightly calcined lime is the most reactive and commonly used in metallurgy. The calcination equipment consists of banks of straight furnaces equipped with filters. The following chemical reaction explains its production process:



(A.1)

High-quality dolomitic lime is produced from deposits of high-grade dolomitic limestone, meaning limestone containing between 40 and 44% magnesium carbonate (MgCO₃). It follows the following reaction:



(A.2)

2.2.3. Other units

In addition to the previous two auxiliary units which served for production, AQS has many other units, such as:

- Industrial water treatment: for purification and reuse of water in the industrial process.
- Electrical substation: providing and distributing the necessary electrical energy to the complex.
- Generator sets: convert energy produced by fuel burning to electrical energy in order to supply the complex in case of electrical substation failure.
- Gas pressure reducing station.

3. AQS productions

3.1. Types of products

The AQS commercializes a wide range of steel products in quantity and quality, at competitive prices and with superior reliability in compliance with customer requirements, regulatory standards, and legal requirements. Its products are manufactured with state-of-the-art fully automated technology, with a high production capacity and storage of finished products of various dimensions.

Figure 4 bellow shows the main commercialized products by the steel complex, while *table 3* gives some specifications for each one of them.



Figure A-4. AQS' products range [A:1]

Table A-3. General information about AQS products [A:1]

Product	Form & Geometry	Some Notes
(a) Lime and Dololime (280 T/y)	White crystalline solid stones easy to crash, giving granular powder.	Chemical compositions: * Lime: CaO 94%, MgO 1.5%, LOI 5%, SiO ₂ 2%, CO ₂ 5%, H ₂ O 0.5% Dololime: CaO 57-60%, MgO 35-40%, SiO ₂ 2.4%, S 0.2%, CO ₂ 5%; H ₂ O 0.5%
(b) CDRI** (2.5M T/y)	Grey colored spheric pellets. Types vs diameters: Over size (5%) >18mm, average size (90%) 6.3-18mm, under size (5%) <6.3 mm.	Chemical composition: Fe 95%, C 2%, S <0.01%, P <0.05, Gangue (SiO ₂ +MgO+CaO+Al ₂ O ₃) 3%.
(c) Billet	Cuboid form with a length of 12m and a section of 150*150 mm ² .	Specifications: Free from internal and surface defects. Obtention steps:

(2.2M T/y)		Electric arc furnace Ladle furnace Continuous casting. Use: Production of rebar and wire rods.
(d) Rebar (1.5M T/y)	Long deformed reinforcing steel bars, that come in bundles. Available diameters (mm): 8, 10, 12, 14, 16, 20, 25, 32, 40. Length (m): Standard 12, but can reach 18 at customer request.	Bundle weight: 2.0 T Obtention: by hot rolling, in concordance to the ministry department in charge of the quality standard published on 8 march 1997. Use: High adhesion construction.
(e) Wire Rod (0.5M T/y)	Thin and long steel wires in a coiled shape. Available diameters (mm): 5.5, 6, 6.5, 7, 8, 9, 10, 11, 12, 14. Coil dimensions (mm): Inner diameter 800-850. Outer diameter 1200-1250. Height 2000 max.	Coil weight: 2.0 T Obtention: by hot rolling in concordance with the Algerian standard NA8634 and international standards. Some uses: Welded mesh, nail, galvanized wire, spring wire, paperclips, welding wire.

Table remarks:

*Percentages may exceed 100% in the given chemical compositions because the given values indicate maximal values of components. Actual value might be different according to raw materials' composition.

**Short for: Cold Directly Reduced Iron.

3.2. Produced steel grades

Steel billets, rebars and wire rods produced in Algerian Qatari Steel complex at Bellara can have various chemical compositions, covering a large variety of steel grades, according to customer request, which helps the factory to expand its cliental range, helping it to deal with international market, and cover most of the local needs at the same time.

Being a fundamental element in steel production, AQS complex adds carbon with percentages up to 0.4%, which is ideal for making construction materials. According to the Carbon percentage that has to be added during the production process, the steel grades are classified into low and high carbon, containing less or more than 0.2% respectively.

In the *tables 4 and 5* below, we show all steel grades produced at the AQS complex (valid until the day of the reduction of this report. Please note that as the complex enters its second phase, more grades will be produced, as we mentioned previously).

Table A-4. Low carbon steel grades

	Element	C%	Si%	Mn %	P%	S%	Ni%	Cr%	Mo%	Cu %	V%	Pb%	N ppm
C5D2 (1006)	Min	-	-	0.3	-	-	-	-	-	-	-	-	-
	Max	0.07	0.3	0.5	0.02	0.025	0.1	0.1	0.05	0.1	0.05	0.05	70
	Aim	0.06	0.2	0.4	<0.02	<0.025	<0.05	<0.05	<0.05	<0.1	10ppm	0.005	<50
C8D2 (1008)	Min	0.07	-	0.3	-	-	-	-	-	-	-	-	-
	Max	0.1	0.3	0.5	0.02	0.025	0.1	0.1	0.05	0.15	10ppm	0.005	70
	Aim	0.08	0.2	0.4	<0.02	<0.025	<0.05	<0.05	<0.05	<0.1	10ppm	0.005	<50
C10D2 (1010)	Min	0.09	-	0.3	-	-	-	-	-	-	-	-	-
	Max	0.12	0.3	0.5	0.02	0.025	0.1	0.1	0.05	0.15	10ppm	0.05	70
	Aim	0.1	0.2	0.4	<0.02	<0.025	<0.05	<0.05	<0.05	<0.1	10ppm	0.005	<50
C12D2	Min	0.1	-	0.3	-	-	-	-	-	-	-	-	-
	Max	0.14	0.3	0.5	0.02	0.025	0.1	0.1	0.05	0.1	0.001	0.005	70
	Aim	-	-	-	-	-	-	-	-	-	-	-	-
C18D2 (1018)	Min	0.16	-	0.3	-	-	-	-	-	-	-	-	-
	Max	0.2	0.3	0.5	0.02	0.025	0.1	0.1	0.05	0.1	0.001	0.005	70
	Aim	-	-	-	-	-	-	-	-	-	-	-	-
C20D2 (1020)	Min	0.18	-	0.3	-	-	-	-	-	-	-	-	-
	Max	0.23	0.3	0.5	0.02	0.025	0.1	0.1	0.05	0.1	0.001	0.005	70
	Aim	-	-	-	-	-	-	-	-	-	-	-	-
1022	Min	0.18	-	0.7	-	-	-	-	-	-	-	-	-
	Max	0.23	0.3	1	0.04	0.05	0.1	0.1	0.05	0.1	0.001	0.005	70
	Aim	-	-	-	-	-	-	-	-	-	-	-	-
3sp	Min	0.14	0.15	0.4	-	-	-	-	-	-	-	-	-

	Max	0.2 2	0.3	0.65	0.04	0.05	0.3	0.3	-	0.3	-	-	120
	Aim	-	-	-	-	-	-	-	-	-	-	-	-
4sp	Min	0.1 8	0.1 5	0.4	-	-	-	-	-	-	-	-	-
	Max	0.2 7	0.3	0.7	0.04	0.05	0.3	0.3	-	0.3	-	-	120
	Aim	-	-	-	-	-	-	-	-	-	-	-	-

Table A-5. High carbon steel grades

	Element	C%	Si%	Mn%	P%	S%	Ni%	Cr%	Mo%	Cu%	V%	Pb%	N ppm
B500	Min	0.22	0.15	0.6	-	-	-	-	-	-	-	-	-
	Max	0.3	0.3	0.9	0.04	0.04	0.3	0.3	0.1	0.3	-	0.05	120
	Aim	-	-	-	-	-	-	-	-	-	-	-	-
B500B	Min	0.2	0.15	1.2	-	-	-	-	-	-	-	-	-
	Max	0.22	0.3	1.6	0.03	0.03	0.15	0.25	0.08	0.2	0.001	0.05	120
	Aim	0.21	0.2	-	<0.02	<0.02	0.05	0.1	0.01	0.1	0.0005	<50ppm	<90
B500W	Min	0.19	0.15	0.6	-	-	-	-	-	-	-	-	-
	Max	0.22	0.3	0.8	0.03	0.03	0.15	0.25	0.08	0.2	0.001	0.05	120
	Aim	0.2	0.2	0.66	<0.02	<0.02	0.05	0.1	0.005	0.1	0.0005	<50ppm	-
E500	Min	0.22	0.15	0.55	-	-	-	-	-	-	-	-	-
	Max	0.27	0.3	0.65	0.06	0.06	-	0.1	0.04	-	-	-	120
	Aim	0.25	0.2	0.6	-	-	-	-	-	-	-	-	-
5sp	Min	0.28	0.15	0.5	-	-	-	-	-	-	-	-	-
	Max	0.37	0.3	0.8	0.04	0.05	0.3	0.3	-	0.3	-	-	120
	Aim	-	-	-	-	-	-	-	-	-	-	-	-
C40	Min	0.38	0.1	0.6	-	-	-	-	-	-	-	-	-
	Max	0.42	0.3	0.7	0.025	0.025	0.1	0.1	0.03	0.1	0.001	-	70

References

[A:1] Official website of AQS

[A:2] Algerian Qatari Steel. Etude de danger.

[A:3] ISO official website. Link: [ISO - Organisation internationale de normalisation](#)

[A:4] Air Separation: Materials, Methods, Principles and Applications - An Overview. D Hazel and N Gobi. p- 856-859

[A:5] Univ. of Petoria. Chap. 2: Cryogenic air Separation p.5

Note: All the pictures and tables with a (*) mark are taken from open sources found on the internet.

Index B

1. Introduction

In the following annex, we will try to give a demonstration for the formula that links between the homogenous and heterogenous nucleation models (equations 1.13 and 1.14) using some common mathematical concepts seen in calculus 3 classes. Moreover, we will show the hypotheses and the different steps adapted to obtain the Johnson-Mehl-Avrami formula (equation 1.20) and give the physical meanings of the constants (n , K) present in the equation.

2. Heterogenous nucleation formula

2.1. Demonstration:

2.1.1. Recall to the nucleation model

In order to transform from an oversaturated phase into an equilibrium phase, materials proceed with a nucleation mechanism. In order to check the possibility of the processing, a model based on the determination of Gibbs free energy is adopted. In this model, it is supposed that in order to have a nucleation (homogenous or heterogenous), two types of energies interfere: Volume energy, and Surface energy, and thus the overall energy is given by (the general form of equation 1.10):

$$\Delta G_{het} = V \cdot \Delta G_v + S \cdot \gamma$$

(B.1)

So, the remaining work to do in order to reach the equation (1.13) is to determine in the volume (V) and the surface (S) of the nucleus created by this mechanism.

2.1.2. Young-Dupree equation

As stated in the chapter I, nucleation favors to proceed within a heterogenous process, which happens preferably near the impurities and the bordures of the sites. Figure 1-8-B shown before (and repeated bellow) describes the form of the obtained nucleus in this case:

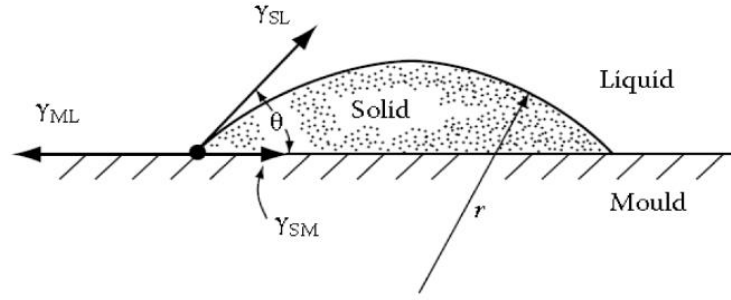


Figure B-1. *Schematic representation of the formed nucleus and the superficial tensions present*

In such composition, three phases (or substances) are present, while each pair of them are in contact with each other. Thus, three superficial tensions are created between them, which we will denote as: γ_{LS} , γ_{SM} and γ_{LM} for the tensions between the liquid-solid steel, solid steel-solid metal and liquid steel-solid metal respectively. The last two tensions are situated within the same line, called the contact line.

Since this contact line is fixed at its initial position, this means that the three superficial tensions are at an equilibrium state, and thus their vectorial sum is null, i.e.:

$$\vec{\gamma}_{SL} + \vec{\gamma}_{SM} + \vec{\gamma}_{LM} = \vec{0}$$

(B.2)

The projection of this vectorial equation on the x-axes will give us simply the Young-Dupree equation:

$$\gamma_{SL} \cdot \cos(\theta) + \gamma_{SM} = \gamma_{LM}$$

(B.3)

In this case, the overall equation of nucleation (B.1) can be rewritten as:

$$\Delta G_{het} = V \cdot \Delta G_v + S \cdot \gamma = V \cdot \Delta G_v + S_{SL} \cdot \gamma_{SL} + S_{SM} \cdot (\gamma_{SM} - \gamma_{LM})$$

(B.4)

Which will become, according to (B.3), as:

$$\Delta G_{het} = V \cdot \Delta G_v + S_{SL} \cdot \gamma_{SL} - S_{SM} \cdot \gamma_{SL} \cdot \cos(\theta) = V \cdot \Delta G_v + \gamma_{SL} \cdot (S_{SL} - S_{SM} \cdot \cos(\theta))$$

(B.5)

2.1.3. Mathematics:

All the remaining work that's left in order to achieve the demonstration is to do some mathematics to calculate the volume V and the surfaces S_{SL} and S_{SM} . For this purpose, a hypothesis was the nucleus formed within a heterogenous way is a cut made

by the metallic surface plan on the nucleus that must have been created within the homogenous way (figure).

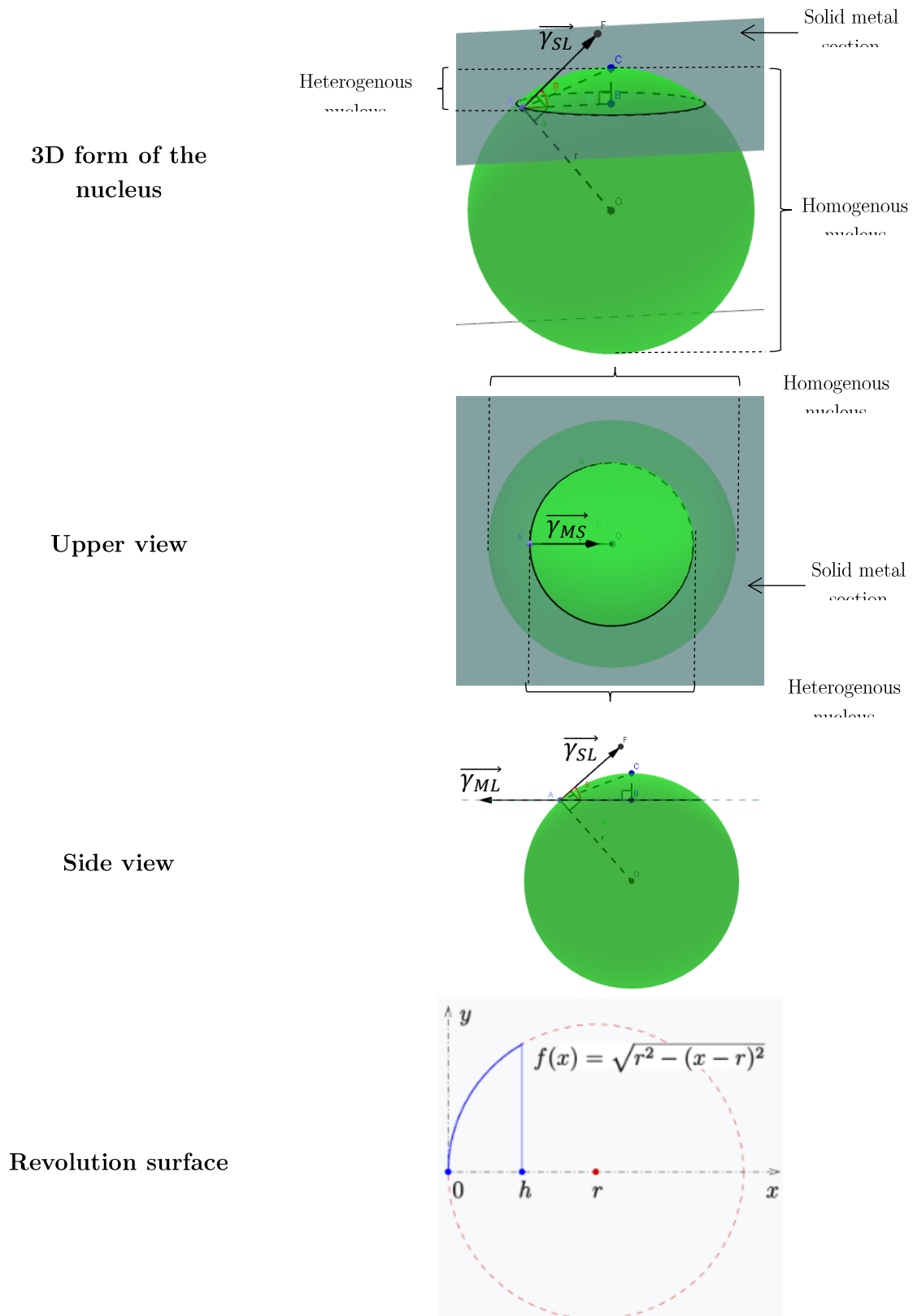


Figure B-2. Schematic comparison between nucleus formed by homogenous and heterogenous nucleation

In this case, the calculation of the surface S_{SM} of the contact between the metal and the solid phase nucleus is easy if we know the radius of the heterogenous nucleus, which is easy using some geometry. From the side view image, we can see that the vector \vec{V}_{SL} tangent to the sphere of the homogenous nucleus, and thus the angle \widehat{OAF} is a right angle, and so we will have: $\widehat{OAB} = \pi - \theta$. And so, the radius of the circle representing the surface S_{SM} is given by:

$$AB = r \cdot \cos(\widehat{OAB}) = r \cdot \cos(\pi - \theta) = r \cdot \sin(\theta)$$

(B.6)

Which will lead us to the result:

$$S_{SM} = \pi \cdot AB^2 = \pi \cdot r^2 \cdot \sin^2(\theta) = \pi \cdot r^2 \cdot (1 - \cos^2(\theta))$$

(B.7)

The lateral surface S_{SL} and the volume of the spherical cap can be calculated easily as we consider the heterogenous nucleus geometrically formed as a revolving surface around the x-axes as shown in the previous figure.

As stated in the figure, the revolving surface is delimited by the function:

$$y = f(x) = \sqrt{r^2 - (x - r)^2} = \sqrt{x(2r - x)}$$

$$D = \{0 \leq x \leq h; 0 \leq \varphi \leq 2\pi\}$$

(B.8)

Where: φ is the angle of revolve

The revolving surface formula is then given by:

$$S_{SL} = \int_0^{2\pi} \left(\int_0^h f(x) \sqrt{1 + \left(\frac{df}{dx}\right)^2} dx \right) d\varphi = 2\pi \int_0^h \sqrt{2rx - x^2} \cdot \sqrt{1 + \left(\frac{2r - 2x}{2\sqrt{2rx - x^2}}\right)^2} dx$$

$$= 2\pi \int_0^h \sqrt{2rx - x^2} \cdot \sqrt{\frac{r^2}{2rx - x^2}} dx = 2\pi \int_0^h r dx = 2\pi r [x]_0^h$$

$$= 2\pi r h$$

(B.9)

The value of h is then shown in the figure as the width of the cap, hence the segment [BC] in the figure we have:

$$OC = r; OB = r \cdot \sin(\pi - \theta) = r \cdot \cos(\theta) \Rightarrow h = BC = OC - OB = r - r \cdot \cos(\theta)$$

$$\Rightarrow h = r \cdot (1 - \cos(\theta))$$

(B.10)

By replacing the value found for h in the S_{SL} equation, we will find:

$$S_{SL} = 2\pi r^2(1 - \cos(\theta))$$

(B.11)

In order to obtain the volume, we use the formula:

$$V = \pi \int_0^h [f(x)]^2 dx = \pi \int_0^h (2rx - x^2) dx = \pi \left[rx^2 - \frac{x^3}{3} \right]_0^h = \pi h^2 \left(r - \frac{h}{3} \right)$$

(B.12)

Using the formula of h given above, we can deduce the expression of the volume, given as:

$$V = \pi r^2(1 - \cos(\theta))^2 \left(r - \frac{r(1 - \cos(\theta))}{3} \right) = \pi r^3(1 - \cos(\theta))^2 \left(1 - \frac{1 - \cos(\theta)}{3} \right)$$

$$= \frac{1}{3} \pi r^3(2 + \cos(\theta))(1 - \cos(\theta))^2$$

(B.13)

With this work all done, we can replace the coherent values of the volume and the surfaces in the equation (B.5) to obtain:

$$\Delta G_{het} = V \cdot \Delta G_v + \gamma_{SL}(S_{SL} - S_{SM} \cdot \cos(\theta))$$

$$= \left[\frac{1}{3} \pi r^3(2 + \cos(\theta))(1 - \cos(\theta))^2 \right] \Delta G_v$$

$$+ \gamma_{SL} \left[(2\pi r^2(1 - \cos(\theta))) - \pi r^2(1 - \cos^2(\theta)) \cdot \cos(\theta) \right]$$

$$= \left[\frac{1}{3} \pi r^3(2 + \cos(\theta))(1 - \cos(\theta))^2 \right] \Delta G_v$$

$$+ \gamma_{SL} \cdot \pi r^2 \left[(2(1 - \cos(\theta))) - (1 - \cos^2(\theta)) \cdot \cos(\theta) \right]$$

$$= \left[\frac{1}{3} \pi r^3(2 + \cos(\theta))(1 - \cos(\theta))^2 \right] \Delta G_v$$

$$+ \gamma_{SL} \cdot \pi r^2 [2 - 3 \cos(\theta) + \cos^3(\theta)]$$

$$= \left[\frac{1}{3} \pi r^3(2 + \cos(\theta))(1 - \cos(\theta))^2 \right] \Delta G_v$$

$$+ \gamma_{SL} \cdot \pi r^2(2 + \cos(\theta))(1 - \cos(\theta))^2$$

Replace each of these terms with its corresponding expression

Factorize by the term: πr^2

Expand and develop the factors on the parenthesis

Factorize this term. Use the change of variable: $x = \cos(\theta)$ and use Euclidean division of the obtained polynomial on the term $(x+2)$

Factorize by this one fourth of this term. We use one fourth to show

$$\begin{aligned}
 &= \frac{1}{4}(2 + \cos(\theta))(1 - \cos(\theta))^2 \left\{ \frac{4}{3}\pi r^3 \cdot \Delta G_v + 4\pi r^2 \cdot \gamma_{SL} \right\} \\
 &= f(\theta) \cdot \Delta G_{hom} \\
 &\quad (B.14)
 \end{aligned}$$

the number 4 on the volume and surface terms.

Identify these terms with those given on equation 1.10

Same equation as (1.13)

2.2. Discussion

With this demonstration, we shown that the heterogenous nucleation model consist (from a mathematical perspective) of a factor multiplied by the homogenous model. Since this factor is only function of the angle θ and is independent from the nucleus radius, then the same critical radius (r^*) is needed for the embryo to develop into a nucleus, this is shown graphically in figure 1-9 where both critical values of energy are reached for the same r^* . However, the factor $f(\theta)$ affects the amplitude of the energy causing it to decrease in the heterogenous model compared to the homogenous model (since it is lesser than 1).

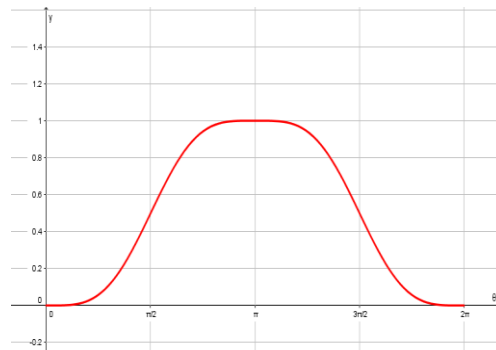


Figure B-3. Variations of $f(\theta)$

Besides all of this, and as the reader can easily notice, even this model of heterogenous nucleation (which is supposed to represent the real mechanism) needed some hypothesis that aren't always verified to be built (we supposed that the heterogenous nucleus has a form of a cap of a sphere that itself was approached to the homogenous nucleus, we supposed also that the only energies that interfere in this case are those for the formation of volume and surface). However, in the real models, more energies can interfere in addition of the previous ones. According to the studied cases, we can have one or both of the following energies along with the surface and the volume ones:

- Energy due to the deformation of the structure (example of alumina inclusions). It disadvantages the nucleation since in order to precipitate, the inclusions need to push away the existing crystals to provide enough space for themselves: $\Delta G_{def} > 0$.

- Energy due to the precipitation on the dislocation sites and the grain boundaries (example of aluminum nitrides inclusions). It favors the nucleation since it contains too many of defects and vacancies: $\Delta G_{dis} < 0$.

Thus, the overall equation becomes:

$$\Delta G_{het} = \Delta g_v + \Delta g_s + \Delta g_{def} + \Delta g_{dis}$$

(B.15)

3. Johnson-Mehl-Avrami formula

3.1. Demonstration

3.1.1. Hypothesis

The equation of Johnson-Mehl-Avrami that represents a model for the growth of the nucleus lies primarily on some simplifying hypothesis, where we consider that:

- Nucleation is mainly made through homogenous model, and thus embryos and nuclei have all perfect spherical shapes.
- Nucleation is done uniformly in the untransformed part of the material.
- The growth mechanism is isotropic (similar in all the directions), constant and independent from the already transformed matter.

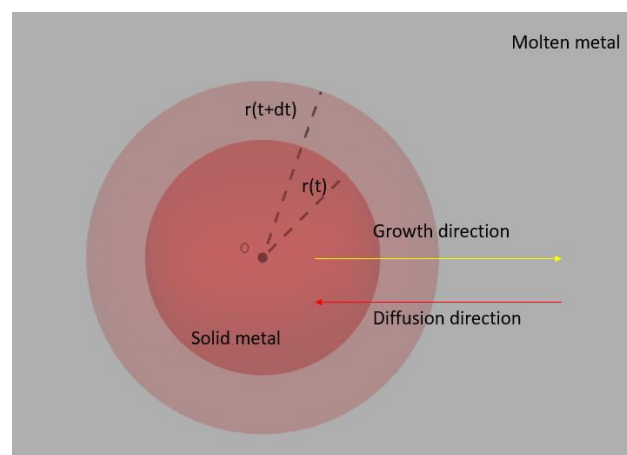


Figure B-4. *Growth mechanism*

3.1.2. Mathematics

When these conditions are verified, we consider that the transformation of the matter from α to β phases, is done with a nucleation speed per volume unit \dot{N} causing the radius of the nucleus to grow with a rate of \dot{r} , such as:

$$\dot{N} = \frac{dN}{dt} = Cte \quad ; \quad \dot{r} = \frac{dr}{dt} = Cte$$

(B.16)

To solve the problem of the growth, we adapt the model of the extended volume of the nucleus, i.e. we try to determine the volume that would be formed by the β -phase if the rest of the sample isn't yet transformed. For this purpose, we will estimate the extended volume transformed at a time t through the nucleation that happened at an instant τ and the growth that happened in the duration of $t - \tau$.

In this case, the number of nuclei that are produced within the time period $[\tau; \tau + dt]$ is given by:

$$dN = V\dot{N}d\tau$$

(B.17)

And according to the hypothesis considered about the growth, we can consider that the radius of the growing nuclei (present in β -phase) increases in this time interval by a value of:

$$r(t) - r(\tau) = \dot{r} \cdot [t - \tau]$$

(B.18)

If we take into account that all the transformed matter obtained within the nucleation process will integrate into the extended volume of the nucleus, then the variation of this volume will be evaluated as the variation of the already existing β -phase volume multiplied by the number of nuclei formed by nucleation (since the growth is isotropic, all the volume will receive new matter), and thus:

$$dV_{\beta}^{ext} = [V_{\beta}]_{\tau}^t \cdot dN = \frac{4}{3}\pi\dot{r}^3(t - \tau)^3 V\dot{N}d\tau$$

(B.19)

Integration will give:

$$\int_0^{V_{\beta}^{ext}} dV_{\beta}^{ext} = \int_0^t \frac{4}{3}\pi\dot{r}^3(t - \tau)^3 V\dot{N}d\tau \Rightarrow V_{\beta}^{ext} = \frac{\pi}{3}V\dot{N}\dot{r}^3 t^4$$

(B.20)

In the other hand, and in the real case, not all of the extended volume is really produced, but only part of it is. The transformed fraction is given then by:

$$dV_{\beta} = dV_{\beta}^{ext} \left(1 - \frac{V_{\beta}}{V}\right) \Rightarrow \frac{dV_{\beta}}{\left(1 - \frac{V_{\beta}}{V}\right)} = dV_{\beta}^{ext}$$

(B.21)

Integration will give:

$$-\ln\left(1 - \frac{V_{\beta}}{V}\right) = \frac{V_{\beta}^{ext}}{V} = \frac{\pi}{3} \dot{N} \dot{r}^3 t^4$$

(B.22)

And thus:

$$Y = \frac{V_{\beta}}{V} = 1 - \exp[-Kt^n] \quad ; \quad \left\{K = \frac{\pi}{3} \dot{N} \dot{r}^3 ; n = 4\right\}$$

(B.23)

3.2. Discussion

Even though the model of Johnson-Mehl-Avrami adapts many approximative hypothesis, it was shown practically that the curves obtained in real cases are similar to those obtained with this model. The differences are in the values of the constants K and n, where the K reflects the transformation and the nucleation rates which are dependent themselves on the thermodynamics of the mixture, while n is supposed to reflect the nature of the transformation.

References:

- [B.1] Laurent Cormier. La théorie classique de la nucleation. Institut de Minéralogie et Physique des Milieux Condensés Université Pierre et Marie Curie – CNRS, Paris, France
- [B.2] Kamel Abadli. Théorie de la germination. ENP 2022.
- [B.3] Milton Ohring, Lucian Kasprzak. The mathematics of failure and reliability (in. Reliability and Failure of Electronic Materials and Devices (Second Edition)). 2015.

Index C

1. Introduction

In this index, we present some alternative codes to measure the grain sizes and the inclusion density using Python instead of ImageJ.

2. Grain size determination

Sizes calculation

```
import cv2
import numpy as np

def distance(point1, point2):
    return np.sqrt((point2[0] - point1[0])**2 + (point2[1] - point1[1])**2)

def click(event, x, y, flags, params):
    if event == cv2.EVENT_LBUTTONDOWN:
        if len(params['points']) < 2:
            cv2.circle(params['image'], (x, y), 5, (0, 0, 255), -1)
            params['points'].append((x, y))
            if len(params['points']) == 2:
                cv2.line(params['image'], params['points'][0],
params['points'][1], (0, 0, 0), 5)
                dist_pixels = distance(params['points'][0],
params['points'][1])
                dist_micrometers = dist_pixels *
echelle_en_micrometres_par_pixel
                print("Distance between the two points (in pixels):",
dist_pixels)
                print("Distance between the two points (in micrometers):",
dist_micrometers)
                params['distances'].append((dist_pixels, dist_micrometers))
                params['points'] = []

image_path = "test.jpg"
image = cv2.imread(image_path)
clone = image.copy()
distances = []

echelle_en_micrometres_par_pixel = 100 / 893
```

```

cv2.namedWindow('image')
cv2.setMouseCallback('image', click, {'image': clone, 'points': [],
'distances': distances})

while True:
    cv2.imshow('image', clone)
    key = cv2.waitKey(1) & 0xFF
    if key == ord('q'):
        break

cv2.destroyAllWindows()

if distances:
    distances_pixels = [dist[0] for dist in distances]
    distances_micrometers = [dist[1] for dist in distances]
    mean_distance_pixels = np.mean(distances_pixels)
    mean_distance_micrometers = np.mean(distances_micrometers)
    print(f"\nMean distance (pixels): {mean_distance_pixels}")
    print(f"Mean distance (micrometers): {mean_distance_micrometers}")

```

Image sharpening

```

import cv2
import numpy as np
from matplotlib import pyplot as plt

image_path = "etc 1.jpg"
image = cv2.imread(image_path)

kernel = np.array([[0, -1, 0],
                   [-1, 5.1, -1],
                   [0, -1, 0]])
sharpened = cv2.filter2D(image, -1, kernel)

plt.figure(figsize=(10, 5))

plt.subplot(1, 2, 1)
plt.imshow(cv2.cvtColor(image, cv2.COLOR_BGR2RGB))
plt.title('Image originale')
plt.axis('off')
plt.subplot(1, 2, 2)
plt.imshow(cv2.cvtColor(sharpened, cv2.COLOR_BGR2RGB))
plt.title('Image avec sharpening')
plt.axis('off')
plt.show()
import cv2

```

```

import numpy as np

def nothing(x):
    pass
image_path = "etc 1.jpg"
image = cv2.imread(image_path)
image_gray = cv2.cvtColor(image, cv2.COLOR_BGR2GRAY)

cv2.namedWindow('Canny')
cv2.namedWindow('Sobel')
cv2.namedWindow('Laplacian')

cv2.createTrackbar('Low Threshold', 'Canny', 0, 255, nothing)
cv2.createTrackbar('High Threshold', 'Canny', 0, 255, nothing)
cv2.createTrackbar('Kernel Size', 'Sobel', 1, 31, nothing)
cv2.createTrackbar('Kernel Size', 'Laplacian', 1, 31, nothing)

cv2.setTrackbarPos('Low Threshold', 'Canny', 50)
cv2.setTrackbarPos('High Threshold', 'Canny', 150)
cv2.setTrackbarPos('Kernel Size', 'Sobel', 3)
cv2.setTrackbarPos('Kernel Size', 'Laplacian', 3)

while True:
    low_threshold_canny = cv2.getTrackbarPos('Low Threshold', 'Canny')
    high_threshold_canny = cv2.getTrackbarPos('High Threshold', 'Canny')

    sobel_kernel_size = cv2.getTrackbarPos('Kernel Size', 'Sobel')
    laplacian_kernel_size = cv2.getTrackbarPos('Kernel Size', 'Laplacian')

    if sobel_kernel_size % 2 == 0:
        sobel_kernel_size += 1
    if laplacian_kernel_size % 2 == 0:
        laplacian_kernel_size += 1

    canny_edges = cv2.Canny(image_gray, low_threshold_canny,
high_threshold_canny)
    canny_colored = cv2.cvtColor(canny_edges, cv2.COLOR_GRAY2BGR)
    canny_inverted = cv2.bitwise_not(canny_edges)
    sobelx = cv2.Sobel(image_gray, cv2.CV_64F, 1, 0, ksize=sobel_kernel_size)
    sobely = cv2.Sobel(image_gray, cv2.CV_64F, 0, 1, ksize=sobel_kernel_size)
    sobel_edges = cv2.magnitude(sobelx, sobely)
    sobel_edges = np.uint8(np.absolute(sobel_edges))
    sobel_inverted = cv2.bitwise_not(sobel_edges)
    laplacian_edges = cv2.Laplacian(image_gray, cv2.CV_64F,
ksize=laplacian_kernel_size)
    laplacian_edges = np.uint8(np.absolute(laplacian_edges))
    laplacian_inverted = cv2.bitwise_not(laplacian_edges)

    cv2.imshow('Canny', canny_inverted)
    cv2.imshow('Sobel', sobel_inverted)

```

```
cv2.imshow('Laplacian', laplacian_inverted)

if cv2.waitKey(1) & 0xFF == ord('q'):
    break

cv2.destroyAllWindows()
```

3. Heterogeneities density determination

```
import os
import cv2
import numpy as np
import pandas as pd
from matplotlib import pyplot as plt

def binarize_images_in_folder(folder_path, threshold=127,
output_excel='output.xlsx'):
    results = []

    for filename in os.listdir(folder_path):
        if filename.endswith(('png', 'jpg', 'jpeg', 'bmp', 'tif',
'.tiff')):
            image_path = os.path.join(folder_path, filename)
            image = cv2.imread(image_path, cv2.IMREAD_GRAYSCALE)

            if image is None:
                print(f"skip image : {filename} ")
                continue

            ret, binary_image = cv2.threshold(image, threshold, 255,
cv2.THRESH_BINARY)

            nb_pixels_noirs = np.sum(binary_image == 0)
            total_pixels = binary_image.size
            pourcentage_noir = (nb_pixels_noirs / total_pixels) * 100
            results.append((filename, pourcentage_noir))

    plt.figure(figsize=(10, 5))
    plt.subplot(1, 2, 1)
    plt.title('Image Originale')
    plt.imshow(image, cmap='gray')
    plt.axis('off')

    plt.subplot(1, 2, 2)
    plt.title('Image Binarisée')
    plt.imshow(binary_image, cmap='gray')
    plt.axis('off')
```

```
plt.show()

df = pd.DataFrame(results, columns=['image name', 'Proportion of black
pixels'])

df.to_excel(output_excel, index=False)
print(f"results stored in {output_excel}")
```

Credits®:

The previous codes have been produced by Souhil OUCHENE; they all have been tested for calculations, and the obtained results were close enough to those calculated using ImageJ software, yet it is important to notify the users that some modifications must be applied according to the storage location of the figures on your hardware.

We would like to thank our friend again for his support.